NATIONAL TECHNICAL UNIVERSITY OF ATHENS

SCHOOL OF CIVIL ENGINEERING

DEPARTMENT OF WATER RESOURCES AND ENVIRONMENTAL ENGINEERING

Διπλωματική Εργασία

ΣΤΟΧΑΣΤΙΚΗ ΔΙΕΡΕΥΝΗΣΗ ΤΗΣ ΣΥΜΠΕΡΙΦΟΡΑΣ ΤΗΣ ΘΕΡΜΟΚΡΑΣΙΑΣ ΣΤΗΝ ΕΠΙΦΑΝΕΙΑ ΤΗΣ ΓΗΣ ΣΕ ΠΑΓΚΟΣΜΙΑ ΚΛΙΜΑΚΑ

Diploma Thesis

STOCHASTIC INVESTIGATION OF THE BEHAVIOR OF LAND SURFACE AIR TEMPERATURE ON GLOBAL SCALE

KONSTANTINOS-GEORGIOS GLYNIS

Supervisor: Demetris Koutsoyiannis, Professor

Athens, October 2019

NATIONAL TECHNICAL UNIVERSITY OF ATHENS

SCHOOL OF CIVIL ENGINEERING

DEPARTMENT OF WATER RESOURCES AND ENVIRONMENTAL ENGINEERING

Διπλωματική Εργασία

ΣΤΟΧΑΣΤΙΚΗ ΔΙΕΡΕΥΝΗΣΗ ΤΗΣ ΣΥΜΠΕΡΙΦΟΡΑΣ ΤΗΣ ΘΕΡΜΟΚΡΑΣΙΑΣ ΣΤΗΝ ΕΠΙΦΑΝΕΙΑ ΤΗΣ ΓΗΣ ΣΕ ΠΑΓΚΟΣΜΙΑ ΚΛΙΜΑΚΑ

Diploma Thesis

STOCHASTIC INVESTIGATION OF THE BEHAVIOR OF LAND SURFACE AIR TEMPERATURE ON GLOBAL SCALE

Konstantinos-Georgios Glynis

Supervisor: Demetris Koutsoyiannis, Professor

Athens, October 2019

Οὐδέν γε ἄτακτον τῶν φύσει

Αριστοτέλης

Ευχαριστίες / Acknowledgements

Abstract

Land surface air temperature is one of the most important hydroclimatic variables, and its extremes are of paramount importance. For this reason, it is imperative not only to know the exact shape of the temperature tails, but also their temporal evolution. The aim of this work is to investigate the stochastic behavior of land surface air temperature using Knowable (K-)moments. K-moments were chosen for this study, as they enable reliable estimation from samples and effective description of high order statistics, useful for marginal and joint distributions of stochastic processes. Multiple timeseries of the average, maximum and minimum air temperature are standardized with respect to the monthly variability of each record. We generate segments of the whole timeseries using consecutive rolling 30-year periods, from which we extract extreme values corresponding to four specific return period levels. Furthermore, timeseries of each air temperature variable (average, maximum and minimum) are used as input to an aggregated Climacogram, for deriving the Hurst parameter, through optimization of the parameters of a hybrid Hurst-Kolmogorov and Markov model. The Hurst parameter is later employed in a Monte Carlo simulation to produce synthetic records of similar stochastic properties through the Symmetric Moving Average (SMA) scheme. The synthetic records produced are processed in a similar manner as the observed, in order to compare them. Furthermore, the longest single records for each air temperature variable are selected and compared to the ensemble of observations, as well as the synthetic records.

Key words: Stochastics; Air temperature; Extreme temperature; Temperature tails; Standardized records; Symmetric Moving Average; Climacogram; Hurst-Kolmogorov behavior; Monte-Carlo simulation.

Εκτενής Περίληψη / Extended Abstract in Greek

Εισαγωγή

Η θερμοκρασία θεωρείται μία από τις πιο σημαντικές υδρομετεωρολογικές μεταβλητές, και μαζί με τη βροχόπτωση μπορεί να χαρακτηρίσει σε ικανοποιητικό βαθμό το κλίμα μίας περιοχής. Τις τελευταίες δεκαετίες, η κλιματική αλλαγή και οι επιπτώσεις της τόσο στον άνθρωπο όσο και στο φυσικό περιβάλλον έχουν καταστεί σημαντικά ζητήματα στο πολιτικό, οικονομικό και επιστημονικό πεδίο. Εξαιτίας της τρωτότητας των υποδομών, καθώς επίσης και ολόκληρου του συστήματος συγκομιδής και εμπορίου τροφίμων και ενέργειας, μικρές διαταραχές σε πολύ ευαίσθητες κλιματικές συνθήκες μπορεί να προκαλέσουν σημαντικά προβλήματα. Γι' αυτό τον λόγο είναι επιτακτικό να κατανοήσουμε, όχι μόνο την εξέλιξη της μέσης θερμοκρασίας στην επιφάνεια της Γης, αλλά και της ελάχιστης και μέγιστης. Στο επιστημονικό επίπεδο, επιβάλλεται να κατανοούμε ένα πρόβλημα, πριν επιδοθούμε σε προσπάθειες επίλυσής του.

Η κατανόηση της εξέλιξης της θερμοκρασίας στην επιφάνεια της Γης, σε όρους κατανομής, είναι επίσης βοηθητική στην προσπάθειά μας να αναγνωρίσουμε τα βασικά αίτια της κλιματικής αλλαγής, και αν, και με ποιο τρόπο, μπορούμε να μετριάσουμε τις συνέπειές της, με σκοπό την καλύτερη προσαρμογή μας. Υπάρχουν πολλοί συντελεστές του κλίματος, τόσο εσωτερικοί, όσο και εξωτερικοί. Η εσωτερική μεταβλητότητα του κλίματος περιλαμβάνει παράγοντες όπως η μεταβλητότητα ατμόσφαιρας-ωκεανού (Brown et al., 2015; Hasselmann, 1976), καθώς επίσης και τις επιδράσεις της βιόσφαιρας μέσω των κύκλων του νερού και του άνθρακα. Στους εξωγενείς παράγοντες λαμβάνονται υπ' όψιν τα αέρια του θερμοκηπίου (Cronin, 2010), οι τροχιακές μεταβολές, η ηλιακή δραστηριότητα και η ηφαιστειακή δραστηριότητα μεταξύ άλλων. Ο εντοπισμός των ακριβών μεταβολών της θερμοκρασίας στην επιφάνεια της Γης, σε συνδυασμό με διεπιστημονική προσέγγιση, θα συμβάλει στην αποκρυπτογράφηση των μηχανισμών του κλίματος της Γης.

Ο σκοπός της παρούσας διπλωματικής εργασίας είναι να εντοπίσουμε τη χρονική εξέλιξη των γεγονότων ακραίων θερμοκρασιών στην επιφάνεια της Γης, σε συγκεκριμένα επίπεδα περιόδων επαναφοράς, και να αξιολογήσουμε εάν οι προκύπτουσες μεταβολές είναι εντός των ορίων του αναμενόμενου από τη στοχαστική διεργασία που περιγράφει μία φυσική μεταβλητή όπως τη θερμοκρασία. Για το σκοπό αυτό, εξετάζουμε πιθανές τάσεις της θερμοκρασίας στο παρελθόν και το παρόν, και πώς αυτές εντάσσονται στο γενικότερο πλαίσιο των παγκόσμιων κλιματικών μεταβολών.

Πολλαπλές επιστημονικές μελέτες έχουν δείξει ότι η μέση θερμοκρασία του πλανήτη έχει αυξηθεί σημαντικά κατά τον 20ο αιώνα. Σύμφωνα με την 5η Αναφορά Αποτίμησης του IPCC (2018), η δεκαετία 2009-2018 ήταν θερμότερη κατά 0.93 ± 0.07 °C σε σύγκριση με την προβιομηχανική θερμοκρασία βάσης (1850-1900). Παρόλο που υπάρχει μία αποκλίνουσα συμπεριφορά μεταξύ των αστικών και αγροτικών μετεωρολογικών μετρήσεων (Peterson et al. 1999), η γενική τάση φαίνεται να είναι ανοδική, όπως φαίνεται και στο σχήμα 1.
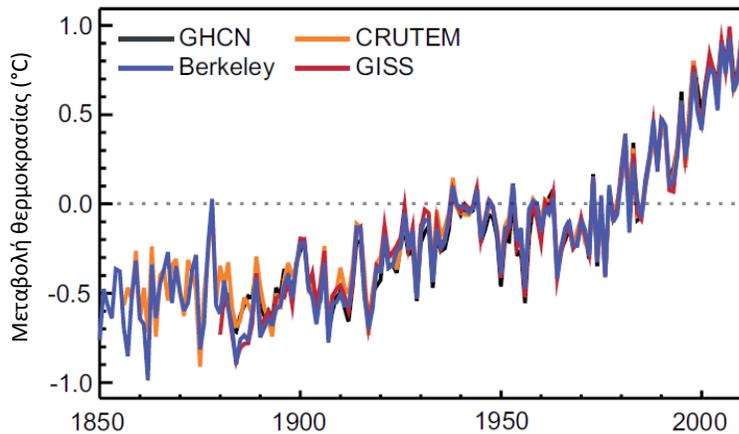
Γράφημα 1: Μεταβολές του παγκόσμιου μέσου όρου της ετήσιας θερμοκρασίας στην επιφάνεια της Γης (LSAT) συγκριτικά με την κλιματολογία του 1961-1990, όπως προκύπτει από τις τελευταίες εκδόσεις τεσσάρων διαφορετικών βάσεων δεδομένων (Berkeley, CRUTEM, GHCN and GISS) | Πηγή: Stocker et al. (2013)

Οι έρευνες, που έχουν γίνει για τη μέγιστη και την ελάχιστη θερμοκρασία δείχνουν ότι η ελάχιστη θερμοκρασία τείνει να αυξάνεται με γρηγορότερο ρυθμό απ' ότι η μέγιστη θερμοκρασία. Αποτέλεσμα αυτής της διαφορετικής συμπεριφοράς είναι το ημερήσιο εύρος της θερμοκρασίας να μειώνεται στις περισσότερες περιοχές του πλανήτη. Συγκεκριμένα, κατά τους Easterling et al. (1997) η ημερήσια διακύμανση της θερμοκρασίας μειώνεται με ρυθμό 0.1 °C/δεκαετία.

Εντούτοις, οι μελέτες της θερμοκρασίας της Γης που έχουν γίνει μέχρι στιγμής έχουν παραλείψει να λάβουν υπ' όψιν την εγγενή εποχική μεταβλητότητα της θερμοκρασίας, η οποία δύναται να συμπεριληφθεί μέσω της τυποποίησης των ημερήσιων καταγραφών της θερμοκρασίας σε σχέση με τον αντίστοιχο μήνα. Σε αυτή την έρευνα θεωρήσαμε την εποχική μεταβλητότητα αναπόσπαστο κομμάτι της μελέτης της θερμοκρασίας, απεμπλέκοντας τα αποτελέσματα από οποιαδήποτε μεροληψία, που πιθανόν επέρχεται από επόμενες, στατιστικά ασήμαντες, καταγραφές.

Επιπλέον, κάναμε χρήση των K-ροπών, οι οποίες είναι ιδιαίτερα εύρωστες στην μελέτη ακραίων δεδομένων (Koutsoyiannis, 2020). Ένα από τα σημαντικότερα πλεονεκτήματά τους είναι ότι είναι γνωστές, με αμερόληπτες εκτιμήτριες, των οποίων η αβεβαιότητα εκτίμησης είναι τάξεις μεγέθους μικρότερη από τις κλασσικές ροπές. Επιπλέον, οι εκτιμήτριες μπορούν να λάβουν υπ' όψιν οποιαδήποτε υπάρχουσα δομή εξάρτησης, ενώ, επίσης, μπορούν να τους αντιστοιχίσουμε άμεσα περιόδους επαναφοράς, όπως και στη χρήση order statistics.

Στοιχεία θεωρίας

Φαινόμενο Hurst

Κλιματικές και υδρολογικές διεργασίες, όπως η θερμοκρασία του αέρα, η βροχόπτωση και η εξάτμιση συχνά εξετάζονται ως στάσιμες στοχαστικές διεργασίες διακριτού χρόνου. Έστω X_i μία διεργασία με $i = 1,2,3, \ldots$ να δηλώνει διακριτό χρόνο (όπως μέρες). Επίσης, έστω ότι έχει μέση τιμή $\mu = \mathrm{E}[X_i]$, αυτοσυνδιακύμανση $\gamma_j = \mathrm{cov}[X_i X_{i+j}]$ και

αυτοσυσχέτιση $\rho_j = \text{corr}[X_i X_{i+j}] = \gamma_j/\gamma_0$, όπου $j = 0, \pm1, \pm2, \pm3, \ldots$. Εάν υποθέσουμε δ να είναι η κλίμακα χρόνου που μας ενδιαφέρει, τότε ο δείκτης i αναπαριστά το συνεχές μεσο-διάστημα χρόνου $[(i-1)\delta, i\delta]$. Έστω $k\delta$ μία κλίμακα χρόνου μεγαλύτερη από τη δ, όπου k είναι θετικός ακέραιος. Η συναθροισμένη στοχαστική διεργασία σε αυτή τη χρονική κλίμακα συμβολίζεται με $Z_i^{(k)}$ και είναι ίση με:

$$Z_i^{(k)} := \sum_{l=(i-1)k+1}^{ik} X_l \tag{1}$$

Από αυτόν τον ορισμό, είναι εύκολο να συνάγουμε ότι για $k = 1$, $Z_i^{(1)} = X_i$, για $k = 2$, $Z_1^{(2)} = X_1 + X_2$, $Z_2^{(2)} = X_3 + X_4$, κ.ο.κ.. Οι στατιστικές ιδιότητες της $Z_i^{(k)}$ μπορούν να εξαχθούν από αυτές της διαδικασίας X_i. Για παράδειγμα, η μέση (αναμενόμενη) τιμή μπορεί να βρεθεί ως:

$$\text{E}\left[Z_i^{(k)}\right] = k\mu \tag{2}$$

ενώ η διακύμανση και η αυτοσυσχέτιση από τις σχέσεις:

$$\gamma_j^{(k)} = \text{cov}\left[Z_i^{(k)}, Z_{i+j}^{(k)}\right] = \sum_{l=1}^{k} \sum_{m=j\cdot k+!}^{(j+1)k} \gamma_{m-l}, \quad j = 0, \pm1, \pm2, \pm3, \ldots \tag{3}$$

Ο Hurst ήταν ο πρώτος που ανακάλυψε την μακροχρόνια εμμονή στις φυσικές διεργασίες (1951), εντούτοις, ο Kolmogorov (1940) ήταν ο πρώτος που την περιέγραψε μαθηματικά, όταν μελετούσε αυτό-όμοιες διεργασίες σε τυρβώδη πεδία (Koutsoyiannis, 2011). Αυτή η συμπεριφορά (δηλαδή η τάση υψηλών ή χαμηλών τιμών να συσσωρεύονται σε μεγάλες χρονικές κλίμακες) είναι γνωστή ως φαινόμενο Hurst, συμπεριφορά Hurst-Kolmogorov (HK), ή δυναμική Hurst-Kolmogorov (HK) (Mandelbrot, 1983; Koutsoyiannis, 2011). Μία στοχαστική διεργασία με συμπεριφορά HK είναι επίσης γνωστή σαν διεργασία Hurst-Kolmogorov ή κλασματικός Gaussian θόρυβος (fGn). Ωστόσο ο fGn προϋποθέτει ότι ο θόρυβος έχει κανονική κατανομή (Gaussian), κάτι το οποίο δεν ισχύει πάντα. Ο fGn μπορεί να οριστεί σε διακριτό χρόνο (που είναι και το

ζητούμενο στην παρούσα εργασία) με τρόπο παρόμοιο με τον συνεχή χρόνο. Συγκεκριμένα, ο fGn ορίζεται ως μία διεργασία, που ικανοποιεί την ακόλουθη συνθήκη:

$$\left(Z_i^{(k)} - k\mu\right) = \left(\frac{k}{l}\right)^H \left(Z_j^{(l)} - l\mu\right) \tag{4}$$

η οποία εφαρμόζεται μόνο σε (πεπερασμένων διαστάσεων κοινή) κατανομή. Η είναι μία θετική σταθερά ($0 < H < 1$) γνωστή και ως συντελεστής Hurst. Η εξίσωση ισχύει για κάθε ακέραια τιμή των i και j (με τη στασιμότητα της διεργασίας να είναι προαπαιτούμενο) και κάθε χρονική κλίμακα k και l (Koutsoyiannis, 2002). Επομένως, για $i = j = l = 1$ προκύπτει ότι:

$$\gamma_0^{(k)} = k^{2H} \gamma_0 \tag{5}$$

Κλιμακόγραμμα

Το κλιμακόγραμμα (Cg) προέρχεται από τις λέξεις «κλίμαξ» και «γράμμα» και είναι ένα δισδιάστατο γράφημα της τυπικής απόκλισης SD(k) της μέσης συναθροισμένης σειράς της τυχαίας μεταβλητής Z στον κατακόρυφο άξονα και της συναθροισμένης κλίμακας k στο οριζόντιο άξονα (Koutsoyiannis, 2010):

$$Z_u^{(k)} = \frac{1}{k} \sum_{i=(u-1)k}^{uk} Z_i \tag{6}$$

όπου οι μεταβλητές Z και Z_u αναπαριστούν το τυχαίο πεδίο ενδιαφέροντος και το μέσο συναθροισμένο πεδίο αντίστοιχα, ενώ u είναι το διάνυσμα-δείκτης του πεδίου, που δείχνει την υστέρηση, δηλαδή τη θέση στο πεδίο.

Το κλιμακόγραμμα χρησιμοποιείται για τον εντοπισμό μακροχρόνιων μεταβολών μίας διεργασίας και την εμμονή (ή εξάρτηση) που αυτή μπορεί να παρουσιάζει. Αυτή η εμμονή μπορεί να ποσοτικοποιηθεί μέσω του συντελεστή Hurst, ο οποίος μπορεί να εξαχθεί από την κλίση του κλιμακογράμματος με λογαριθμικούς άξονες (H=1-κλίση). Για τιμές 0<H<0.5 η διεργασία είναι αντιέμμονη, ενώ για 0.5<H<1 είναι έμμονη (πιο συνήθης συμπεριφορά για φυσικές διεργασίες) και για H=0.5 η διεργασία είναι πλήρως ασυσχέτιστη (λευκός θόρυβος).

Σε κάποιες περιπτώσεις, παρόλ' αυτά, (όπως και στην παρούσα εργασία) η προσαρμογή μίας ευθείας γραμμής στο κλιμακόγραμμα για την εξαγωγή της κλίσης, και άρα της ποσοτικοποίησης της εμμονής δεν είναι η βέλτιστη λύση, λόγω της πιθανής απόκλισης του κλιμακογράμματος από την προσαρμοσμένη «ισοδύναμη» ευθεία για μεγάλες κλίμακες. Για το λόγο αυτό, χρησιμοποιήσαμε ένα ίσης βαρύτητας συνδυασμό διεργασιών Hurst-Kolmogorov και Markov, με σκοπό τη μεγιστοποίηση της παραγωγής εντροπίας, τόσο στις μικρές, όσο και στις μεγάλες χρονικές κλίμακες (Koutsoyiannis et al., 2018).

Η εξίσωση του μοντέλου είναι:

$$\gamma(k) = \frac{\lambda}{2}\left(1 + (k/a)^{2M}\right)^{\frac{H-1}{M}} + \frac{\lambda}{k/a}\left(1 - \frac{1 - e^{-k/a}}{k/a}\right) \qquad (7)$$

όπου H, M και a είναι οι τρεις ανεξάρτητες παράμετροι και λ είναι μία εξαρτημένη παράμετρος, που προκύπτει από την εξίσωση του μοντέλου για κλίμακα $k = 1$. Οι παράμετροι H και M είναι φραγμένες από το 0 και το 1, ενώ η παράμετρος a είναι θετική.

Κ-ροπές

Ας υποθέσουμε ότι η x είναι μία στοχαστική μεταβλητή και $x_1, x_2, \ldots, x_p$ είναι αντίγραφά της, ανεξάρτητα και όμοια κατανεμημένα, αποτελώντας ένα δείγμα. Το μέγιστο όλων, το οποίο ταυτίζεται με το pοστό στοχαστικό, είναι εξ' ορισμού:

$$\underline{x}_{(p)} := \max\left(\underline{x}_1, \underline{x}_2, \ldots, \underline{x}_p\right) \qquad (8)$$

Εαν $F(x)$ είναι η συνάρτηση κατανομής της x και $f(x)$ είναι η συνάρτηση πυκνότητας πιθανότητας, τότε οι αντίστοιχες συναρτήσεις της $x_{(p)}$ είναι:

$$F^{(p)}(x) = (F(x))^p, \quad f^{(p)}(x) = pf(x)\left(F(\underline{x})\right)^{p-1} \qquad (9)$$

όπου η πρώτη είναι το γινόμενο p εμφανίσεων της $F(x)$ (που δικαιολογείται από την υπόθεση ανεξάρτητης και όμοιας κατανομή τους), ενώ η δεύτερη είναι η παράγωγος της $F^{(p)}(x)$ ως προς x.

Για την εξαγωγή των Κ-(knowable, δηλαδή γνωστών) ροπών σε υψηλή δύναμη p, με σκοπό τον ορισμό της pης ροπής, υψώνουμε τον όρο $(x - \mu)$ σε χαμηλότερη δύναμη $q < p$ και για τους υπολειπόμενους πολλαπλασιαστικούς όρους $(p - q)$, αντικαθιστούμε το $(x - \mu)$ με $(2F(x) - 1)$, όπου $F(x)$ είναι η συνάρτηση κατανομής. Αυτό οδηγεί στον ακόλουθο ορισμό της κεντρικής Κ-ροπής τάξης (p, q) (Koutsoyiannis, 2019):

$$K_{pq} := (p - q + 1)\mathrm{E}\left[(2F(\underline{x}) - 1)^{p-q}(\underline{x} - \mu)^q\right], \qquad p \geq q \qquad (10)$$

Αντίστοιχα, η μη-κεντρική Κ-ροπή τάξης (p, q) ορίζεται (Koutsoyiannis, 2019):

$$K'_{pq} := (p - q + 1)\mathrm{E}\left[\left(F(\underline{x})\right)^{p-q}\underline{x}^q\right], \qquad p \geq q \qquad (11)$$

Οι ποσότητες $\left(F(\underline{x})\right)^{p-q}$ και $(2F(\underline{x}) - 1)^{p-q}$ εκτιμώνται από ένα δείγμα, χωρίς τη χρήση των δυνάμεων του x, κάνοντας έτσι την εκτίμηση πολύ πιο αξιόπιστη. Συγκεκριμένα, για το iοστό στοιχείο του δείγματος $x_{(i)}$ μεγέθους n, ταξινομημένο σε αύξουσα σειρά, οι $F(x_{(i)})$ και $(2F(x_{(i)}) - 1)$ υπολογίζονται ως:

$$\hat{F}(x_{(i)}) = \frac{i-1}{n-1}, \quad 2\hat{F}(x_{(i)}) - 1 = \frac{2i-n-1}{n-1} \qquad (12)$$

παίρνοντας τιμές στα διαστήματα [0,1] και [-1,1], αντίστοιχα, ανεξάρτητα από τις τιμές της $x_{(i)}$. Επομένως, οι εκτιμήτριες των Κ-ροπών είναι:

$$\widehat{K}'_{pq} = \frac{p - q + 1}{n}\sum_{i=1}^{n}\left(\frac{i-1}{n-1}\right)^{p-q}\underline{x}_{(i)}^q \qquad (13)$$

$$\widehat{K}_{pq} = \frac{p - q + 1}{n}\sum_{i=1}^{n}\left(\frac{2i-n-1}{n-1}\right)^{p-q}(\underline{x}_{(i)} - \hat{\mu})^q \qquad (14)$$

<u>Περίοδοι επαναφοράς</u>

Όπως είναι κατανοητό, η χρήση των order statistics έχει σημαντικά πλεονεκτήματα έναντι άλλων στατιστικών εργαλείων στο πλαίσιο των περιόδων επαναφοράς, καθώς επίσης και στην αντιστοίχιση μίας ξεχωριστής τιμής συνάρτησης κατανομής σε κάθε μία από αυτές. Αυτό τυχαίνει να ισχύει και με τις Κ-ροπές, καθώς είναι άρρηκτα συνδεδεμένες με τα order statistics.

Γενικά, η περίοδος επαναφοράς μπορεί να εκφραστεί από τη σχέση:

$$\frac{T(K'_{p1})}{D} = \Lambda_p p \qquad (15)$$

όπου D είναι η χρονική αναφορά για την προδιαγραφή της περιόδου επαναφοράς και Λ_p είναι ένας συντελεστής που γενικά εξαρτάται από την συνάρτηση κατανομής και την τάξη p.

Ο ακριβής ορισμός του Λ_p είναι (Koutsoyiannis, 2019):

$$\Lambda_p := \frac{1}{p\left(1 - F(K'_{p1})\right)} \qquad (16)$$

Ελλείψει αναλυτικής λύσης, μία ακριβής σχέση μεταξύ του p και του T έχει καθιερωθεί μέσω της εκτέλεσης αριθμητικών υπολογισμών για διάφορες τιμές του p. Η μικρή διακύμανση του Λ_p με το p μπορεί να υπολογιστεί πολύ καλά εάν είναι γνωστές οι ειδικές τιμές των Λ_1 και Λ_∞. Η τιμή του Λ_1 υπολογίζεται πολύ εύκολα, αφού πρακτικά ταυτίζεται με την περίοδο επαναφοράς της μέσης τιμής:

$$\Lambda_1 = \frac{1}{1 - F(\mu)} = \frac{T(\mu)}{D} \qquad (16)$$

Επιπλέον, σε ένα πλήθος συνηθισμένων κατανομών, ειδικά αυτές που ανήκουν στις Extreme Value Type 1 κατανομές, το Λ_∞ έχει σταθερή τιμή, ανεξάρτητη από την κατανομή. Όπως απέδειξε και ο Koutsoyiannis (2019), η τιμή αυτή είναι:

$$\Lambda_\infty = e^\gamma = 1.781 \qquad (17)$$

όπου γ είναι η σταθερά Euler–Mascheroni.

Για τον υπολογισμό του Λ_p, χρησιμοποιείται η παρακάτω σχέση, η οποία είναι ικανοποιητική για τις περισσότερες κατανομές:

$$\Lambda_p \approx \Lambda_\infty + (\Lambda_1 - \Lambda_\infty)\frac{1}{p} \qquad (18)$$

Αυτό συνεπάγεται μία γραμμική σχέση μεταξύ της περιόδου επαναφοράς T και της τάξης p:

$$\frac{T(K'_{p1})}{D} = p\Lambda_p \approx \Lambda_\infty p + (\Lambda_1 - \Lambda_\infty) \tag{19}$$

Για την κανονική κατανομή, που προσεγγίζει καλύτερα την κατανομή της πραγματικής θερμοκρασίας στην επιφάνεια της Γης, οι προσεγγιστικές τιμές των Λ_1 και Λ_∞. είναι:

$\Lambda_1 = 2$ και $\Lambda_\infty = e^{1/2} = 1.649$.

Δεδομένα

Η GHCN (Global Historical Climatology Network)-Daily είναι η βάση δεδομένων που χρησιμοποιήσαμε στα πλαίσια της παρούσας μελέτης. Περιλαμβάνει χρονοσειρές από πληθώρα μετεωρολογικών σταθμών από όλο τον κόσμο. Για τη θερμοκρασία, περιλαμβάνει δεδομένα από 106.283 σταθμούς από 180 διαφορετικές χώρες. Τόσο το μήκος των καταγραφών, όσο και οι καλυπτόμενες χρονικές περίοδοι, διαφέρουν από σταθμό σε σταθμό, το συνολικό μήκος των οποίων μπορεί να ξεπερνά και τα 175 έτη. Από όλα τα καταγεγραμμένα μεγέθη που περιλαμβάνονται στη συγκεκριμένη βάση δεδομένων, εμείς εξετάσαμε τη μέση, μέγιστη και ελάχιστη θερμοκρασία στην επιφάνεια της Γης.

Τα δεδομένα που χρησιμοποιήσαμε υποβλήθηκαν σε πολυάριθμους ποιοτικούς ελέγχους, τόσο από την Εθνική Υπηρεσία Ατμόσφαιρας και Ωκεανών (NOAA) των Η.Π.Α., η οποία διατηρεί τη βάση, όσο και από εμάς. Οι αυτοματοποιημένοι έλεγχοι, που διενεργήθηκαν από τη NOAA, οδήγησαν στην επισήμανση των προβληματικών τιμών των χρονοσειρών (flagging). Στον πίνακα 1, που ακολουθεί φαίνονται οι επισημάνσεις, που πιθανώς υπήρχαν στις χρονοσειρές της θερμοκρασίας, τις οποίες χρησιμοποιήσαμε.

Για τους σκοπούς της παρούσας εργασίας, χρησιμοποιήσαμε μόνο τις μη επισημασμένες τιμές των χρονοσειρών (με κενή εγγραφή στη θέση της επισήμανσης), καθώς θεωρήθηκε ότι οποιαδήποτε από τις παραπάνω επισημάνσεις υποδήλωνε πρόβλημα στην καταγραφή της πραγματικής θερμοκρασίας.

Επιλέξαμε χρονοσειρές σταθμών, οι οποίες είχαν σημείο εκκίνησης προγενέστερο του 1935, καθώς αυτό επέτρεψε την εξαγωγή παραπάνω από 50 διαδοχικές κυλιόμενες τριακονταετίες. Παρόλο που αυτός ο περιορισμός κατέστησε το δείγμα των χρονοσειρών σαφώς περιορισμένο, εντούτοις, μας επέτρεψε να αναγνωρίσουμε σε μεγάλες χρονικές κλίμακες μοτίβα εμμονής. Αυτό δεν θα ήταν δυνατό με τη χρήση ενός διαρκώς μεταβαλλόμενου δείγματος βραχύβιων χρονοσειρών.

Από τον προαναφερθέντα περιορισμό, ο τελικά χρησιμοποιούμενος αριθμός χρονοσειρών για κάθε μέγεθος είναι:

- Για τη μελέτη της μέσης θερμοκρασίας: 245 χρονοσειρές

- Για τη μελέτη της μέγιστης θερμοκρασίας: 5,006 χρονοσειρές

- Για τη μελέτη της ελάχιστης θερμοκρασίας: 5,006 χρονοσειρές

Μεθοδολογία

Η μεθοδολογία, που ακολουθήσαμε για κάθε παράμετρο της επιφανειακής θερμοκρασίας, συνοψίζεται στο ακόλουθο διάγραμμα ροής. Δηλαδή, οι εικονιζόμενες ενέργειες έγιναν ξεχωριστά για τη μέση, τη μέγιστη και την ελάχιστη θερμοκρασία.

```
┌─────────────┐
│  Συλλογή &  │
│   έλεγχος   │
│  δεδομένων  │
└─────────────┘
       │
       ▼
┌─────────────┐              ┌─────────────┐
│ Τυποποίηση  │─────────────▶│ Κλιμακόγραμμα │
└─────────────┘              └─────────────┘
       │                            │
       ▼                            ▼
┌─────────────┐              ┌─────────────┐
│   K-ροπές   │              │ Παράμετρος H │
└─────────────┘              └─────────────┘
       │                            │
       ▼                            ▼
┌─────────────┐              ┌─────────────┐
│  Απεικόνιση │              │ μοντέλο SMA │
└─────────────┘              └─────────────┘
                                    │
                                    ▼
                             ┌─────────────┐
                             │   K-ροπές   │
                             └─────────────┘
                                    │
                                    ▼
                             ┌─────────────┐
                             │  Απεικόνιση │
                             └─────────────┘
```
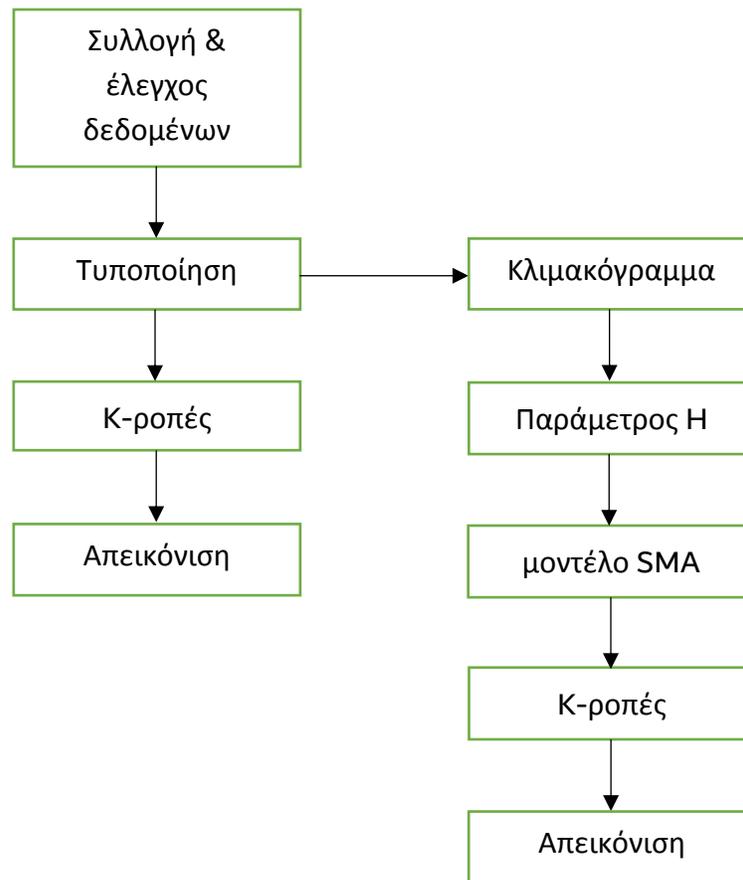
Γράφημα 2: Διάγραμμα ροής εργασιών για κάθε παράμετρο (μέση, μέγιστη, ελάχιστη) της θερμοκρασίας

Τα στάδια που ακολουθήσαμε στην μελέτη της συμπεριφοράς της θερμοκρασίας στην επιφάνεια της Γης σε παγκόσμια κλίμακα συνοψίζονται στο γράφημα 2 που προηγείται. Αξίζει να αναφερθεί, ότι τα βήματα που φαίνονται στο γράφημα, επαναλήφθηκαν για κάθε μία από τις τρεις μεταβλητές της θερμοκρασίας, δηλαδή τη μέση, τη μέγιστη και την ελάχιστη.

Στο πρώτο στάδιο, κατεβάσαμε όλα τα απαραίτητα δεδομένα, σε ημερήσια κλίμακα, από τη βάση GHCNDA, στα οποία κάναμε εκκαθάριση, για να απομονώσουμε τις χρονοσειρές που θα εξετάζαμε περαιτέρω. Στη συνέχεια τυποποιήσαμε τις χρονοσειρές, με βάση τον μήνα της κάθε εγγραφής για τον εκάστοτε μετεωρολογικό σταθμό. Μετά την

τυποποίηση, βρίσκοντας τα χρονικά όρια της κάθε χρονοσειράς, απομονώσαμε συνεχόμενες κυλιόμενες τριακονταετίες.

Για κάθε τριακονταετία, χρησιμοποιήσαμε τις αμερόληπτες εκτιμήτριες των μη-κεντρικών K-ροπών, ώστε σε συγκεκριμένα επίπεδα περιόδων επαναφοράς, που είχαμε προεπιλέξει, να βρούμε το μέγεθος των επεισοδίων υψηλής ή χαμηλής αντίστοιχα θερμοκρασίας. Από το σύνολο των δεδομένων αυτών, που αποκτήθηκαν από κάθε χρονοσειρά, και για κάθε μέγεθος, επιλέξαμε συγκεκριμένα εκατοστημόρια, τα οποία και απεικονίσαμε σε γραφήματα, σε σύγκριση με τη χρονολογία έναρξης των αντίστοιχων κυλιόμενων τριακονταετιών.

Παράλληλα, όμως, με την εξέταση των πραγματικών χρονοσειρών, εξετάσαμε τη στοχαστική δομή τους, με σκοπό την παραγωγή συνθετικών χρονοσειρών. Αυτό επιτεύχθηκε μέσω του συναθροισμένου κλιμακογράμματος. Συγκεκριμένα, μετά την τυποποίηση όλων των πραγματικών χρονοσειρών, υπολογίσαμε τις τιμές του κλιμακογράμματος από την κλίμακα k=1 μέχρι k=n/10, όπου n το μήκος της εκάστοτε χρονοσειράς. Στη συνέχεια, υπολογίσαμε τον μέσο όρο των τιμών των κλιμακογραμμάτων για πλήθος κλιμάκων ίσο με τη μέση τιμή της μέγιστης κλίμακας. Με αυτό τον τρόπο, δημιουργήσαμε ένα συναθροισμένο κλιμακόγραμμα, που εμπεριείχε την στοχαστική συμπεριφορά της θερμοκρασίας όλων των χρονοσειρών.

Στο συναθροισμένο κλιμακόγραμμα εφαρμόσαμε το υβριδικό μοντέλο Hurst-Kolmogorov και Markov, το οποίο είχε τρεις ανεξάρτητες παραμέτρους (H, M και α) και μία εξαρτημένη (λ). Επειδή ο αναλυτικός υπολογισμός των τιμών των ανεξάρτητων μεταβλητών κρίθηκε δύσκολος, επιλέχθηκε η τεχνική της βελτιστοποίησης. Συγκεκριμένα, χρησιμοποιήσαμε τον GRG2-Nonlinear και τον εξελικτικό αλγόριθμο, που προσφέρεται στο πακέτο "Solver" του υπολογιστικού φύλλου "Microsoft Office Excel", με σκοπό την ελαχιστοποίηση του μέσου τετραγωνικού σφάλματος (RMSE) μεταξύ των θεωρητικών και των πραγματικών τιμών του συναθροισμένου κλιμακογράμματος.

Ο συντελεστής Hurst, που προέκυψε από το κλιμακόγραμμα (για κάθε μία από τις τρεις παραμέτρους της θερμοκρασίας) χρησιμοποιήθηκε, για να τροφοδοτήσει την παραγωγή

συνθετικών χρονοσειρών με χρήση του μοντέλου συμμετρικού κυλιόμενου μέσου (SMA). Πέρα από τον συντελεστή Hurst, εισαγάγαμε στο μοντέλο τις τέσσερις πρώτες κλασσικές ροπές της κάθε χρονοσειράς, και το μήκος της, το οποίο το λάβαμε ίσο με τον μέγιστο μήκος των χρονοσειρών.

Αξίζει να αναφερθεί ότι για υπολογιστική οικονομία, αλλά και επιδίωξη της μέγιστης δυνατής μεταβλητότητας του συνθετικού δείγματος των χρονοσειρών, επιλέξαμε να παράξουμε 245 συνθετικές χρονοσειρές με χρήση του μοντέλου SMA για κάθε ένα από τα τρία μεγέθη της θερμοκρασίας (μέση, μέγιστη, ελάχιστη). Για να γίνει όμως αμερόληπτα η επιλογή των χρονοσειρών-δοτών των στατιστικών μεγεθών δημιουργήθηκε ένα βρόγχος τυχαίας προσπέλασης, όπου διάλεξε με τυχαίο τρόπο τους σταθμούς, των οποίων οι 4 πρώτες ροπές χρησιμοποιήθηκαν.

Στο σημείο αυτό, που είχαμε παράξει τις συνθετικές χρονοσειρές, ακολουθήσαμε την ίδια αλληλουχία εργασιών, για τον υπολογισμό των Κ-ροπών σε συγκεκριμένα επίπεδα περιόδων επαναφοράς, τα οποία και απεικονίσαμε σε διαγράμματα.

Θεωρήσαμε επίσης χρήσιμο, από όλους τους σταθμούς, τους οποίους αντιμετωπίσαμε σαν σύνολο, να απομονώσουμε τους μακροβιότερους, και να αποτυπώσουμε τη δική τους συμπεριφορά στη διάρκεια του χρόνου, για να εξετάσουμε με ποιον τρόπο αυτοί οι σταθμοί ταυτίζονται ή όχι με το σύνολο των σταθμών. Ο μακροβιότερος σταθμός καταγραφής της μέσης θερμοκρασίας ήταν της Αγίας Πετρούπολης στη Ρωσία με 136 χρόνια καταγραφών, ενώ καταγραφής τόσο της μέγιστης, όσο και της ελάχιστης, θερμοκρασίας ήταν στο Μιλάνο της Ιταλίας με 146 χρόνια καταγραφών.


Αποτελέσματα

Τα αποτελέσματά της έρευνάς μας φαίνονται στα ακόλουθα διαγράμματα. Με γραμμές μαύρου χρώματος έχουν σχεδιαστεί τα γραφήματα των παρατηρημένων χρονοσειρών, ενώ με μπλε χρώμα, τα γραφήματα των συνθετικών χρονοσειρών. Τέλος, οι μεμονωμένες γραμμές μαύρου χρώματος στα γραφήματα 11-14 αντιστοιχούν σε

περίοδο λειτουργίας των μεμονωμένων σταθμών που ταυτίζεται με το σύνολο των παρατηρήσεων, ενώ με κόκκινη διακεκομμένη γραμμή, απεικονίζεται το χρονικό διάστημα που προηγείται των υπόλοιπων παρατηρήσεων.
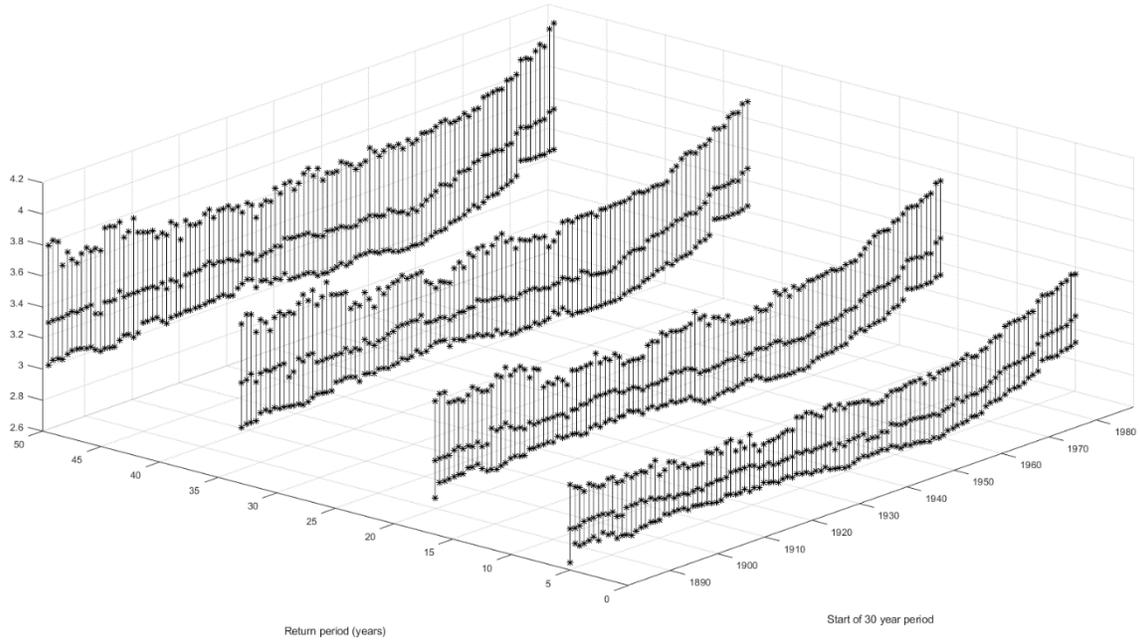

Γράφημα 3: Επάνω ουρά της παρατηρημένης μέσης θερμοκρασίας
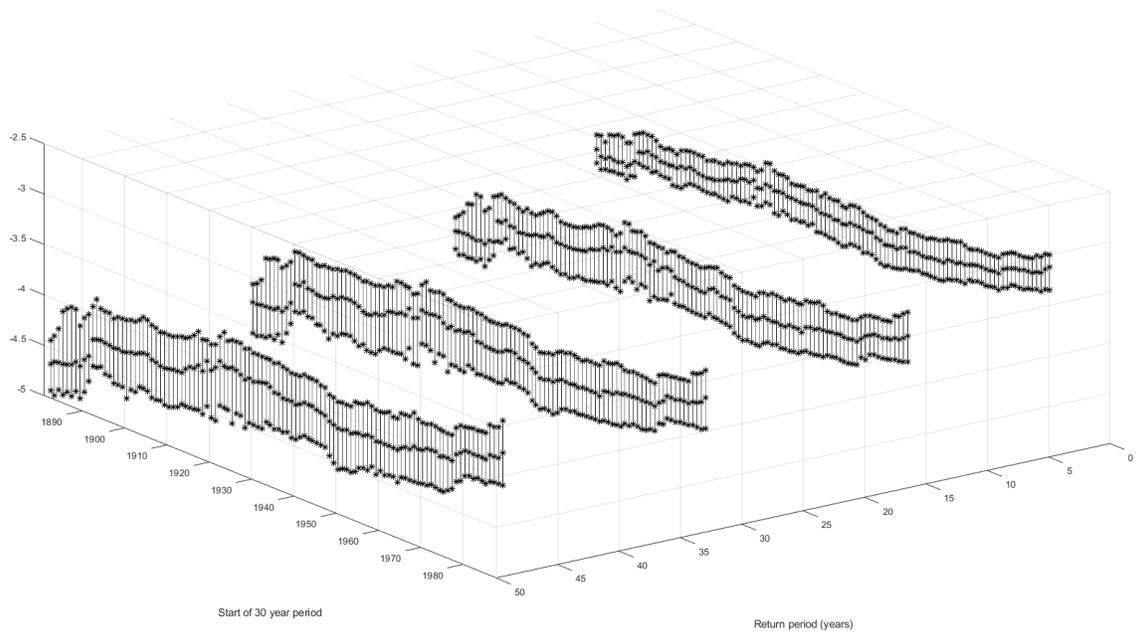
Γράφημα 4: Κάτω ουρά της παρατηρημένης μέσης θερμοκρασίας
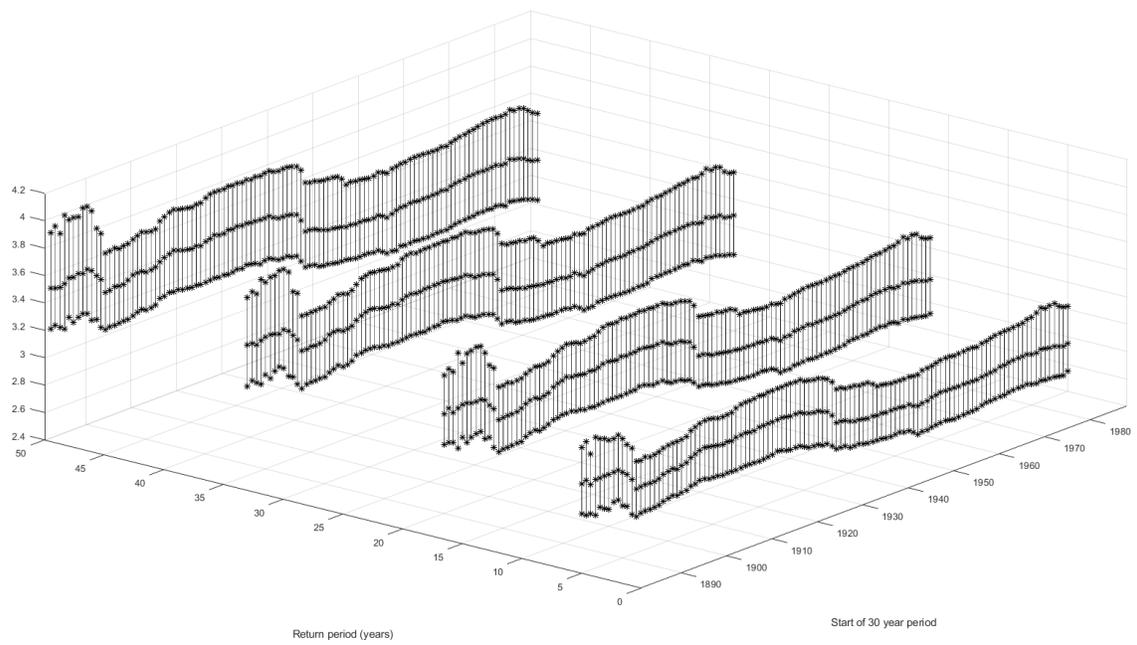
Γράφημα 5: Επάνω ουρά της παρατηρημένης μέγιστης θερμοκρασίας
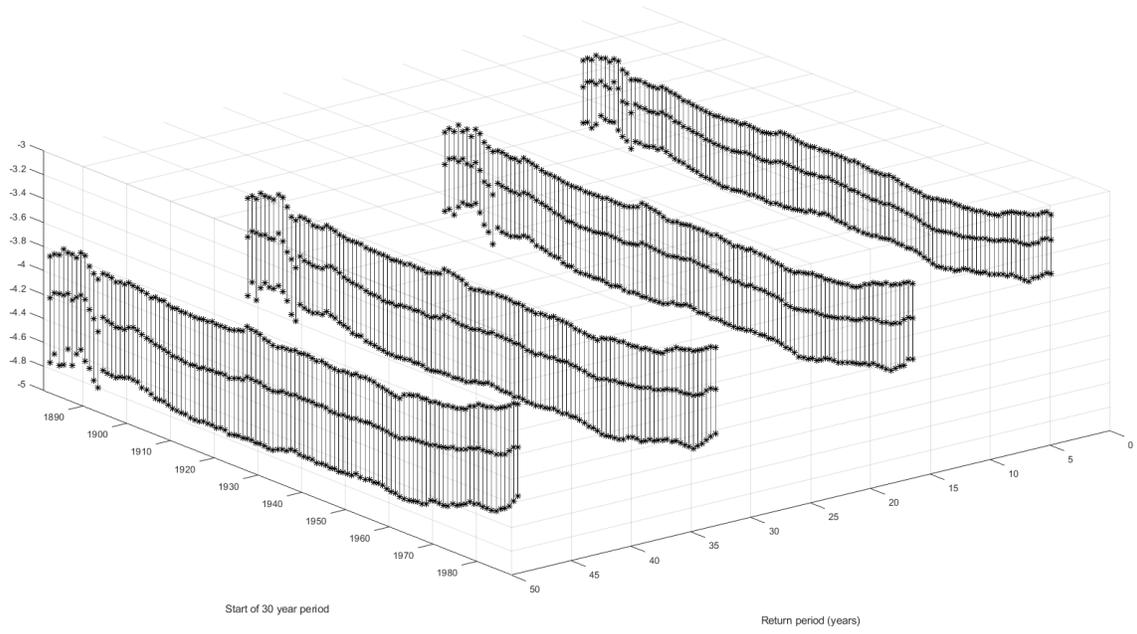
Γράφημα 6: Κάτω ουρά της παρατηρημένης ελάχιστης θερμοκρασίας
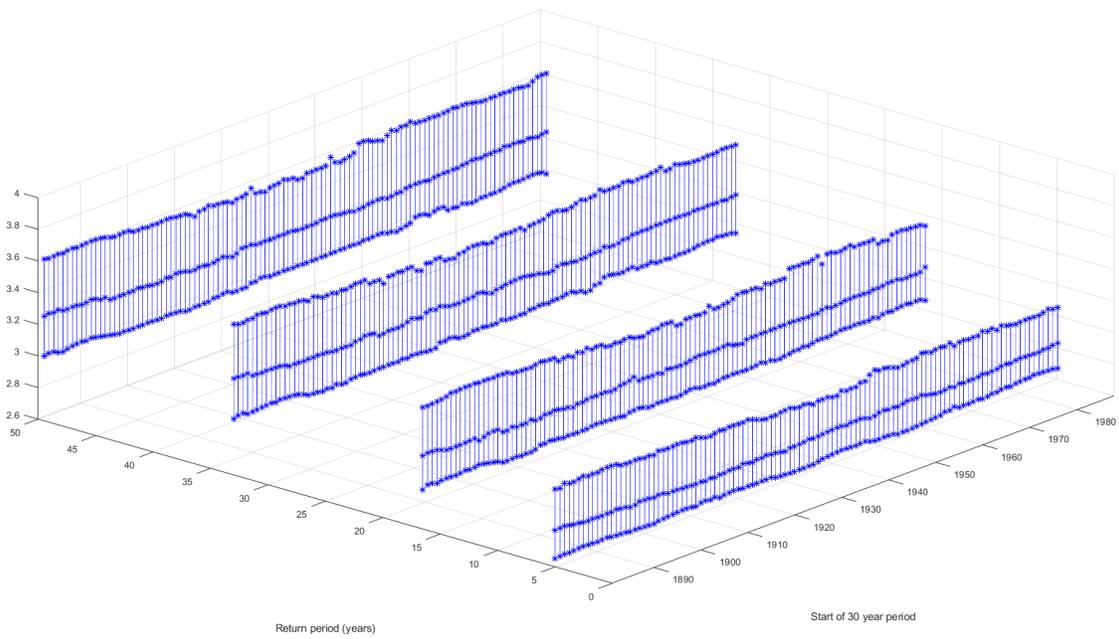
Γράφημα 7: Επάνω ουρά της συνθετικής μέσης θερμοκρασίας
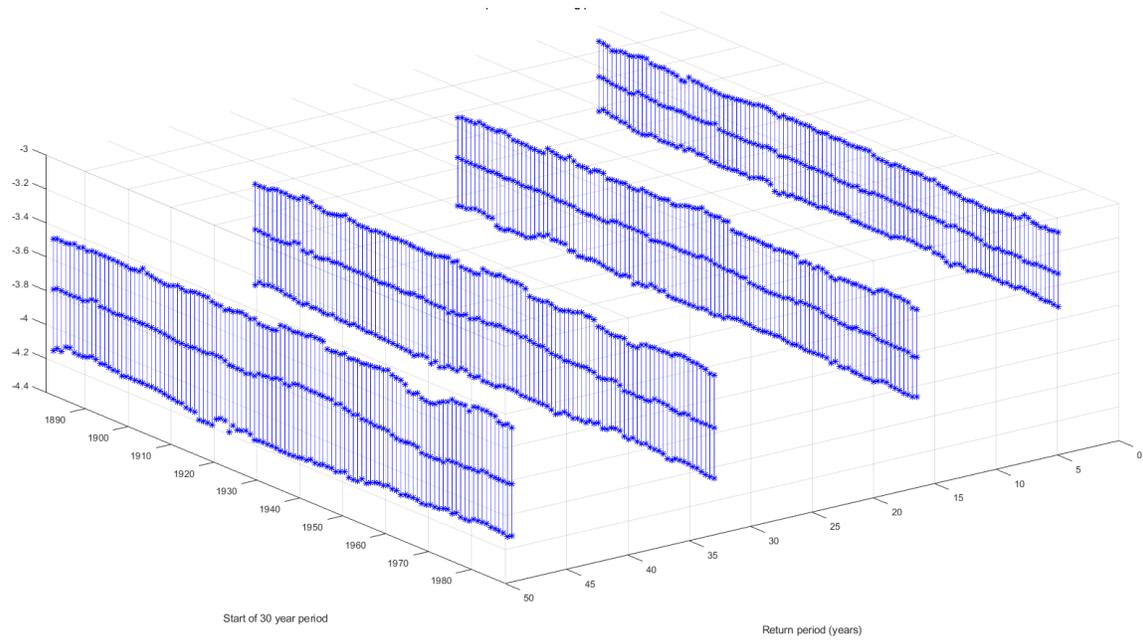
Γράφημα 8: Κάτω ουρά της συνθετικής μέσης θερμοκρασίας
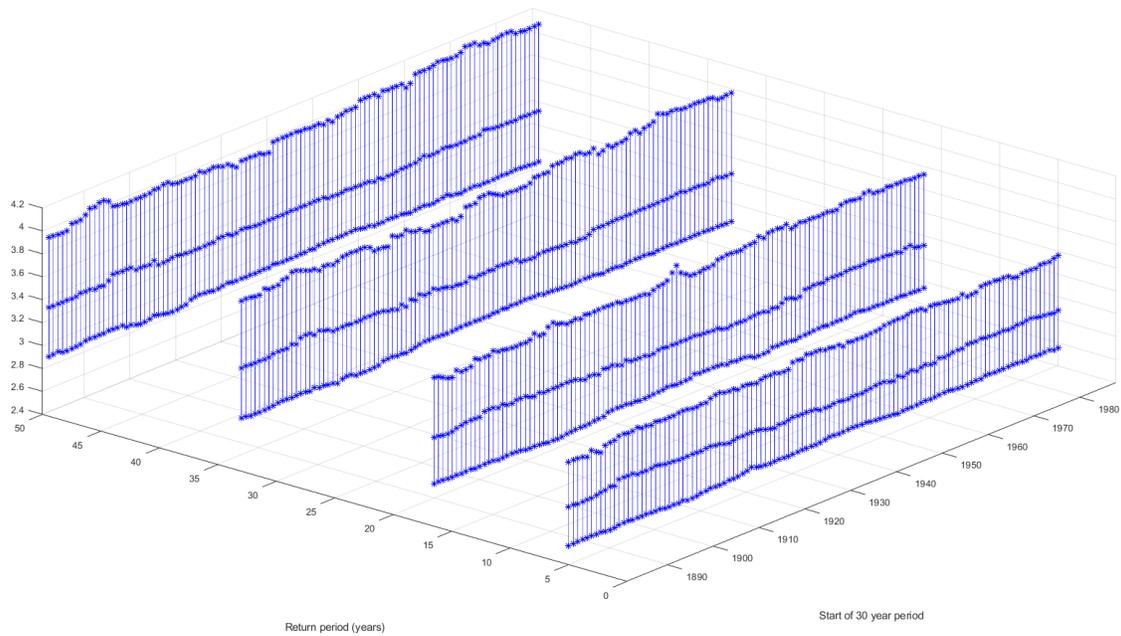
Γράφημα 9: Επάνω ουρά της συνθετικής μέγιστης θερμοκρασίας
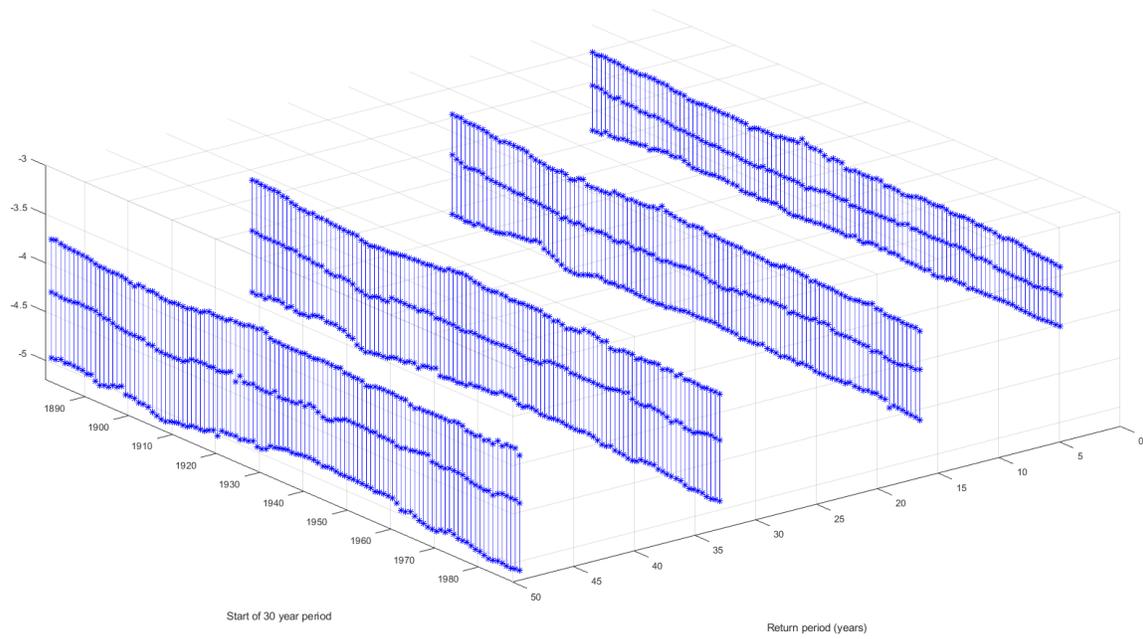
Γράφημα 10: Κάτω ουρά της συνθετικής ελάχιστης θερμοκρασίας
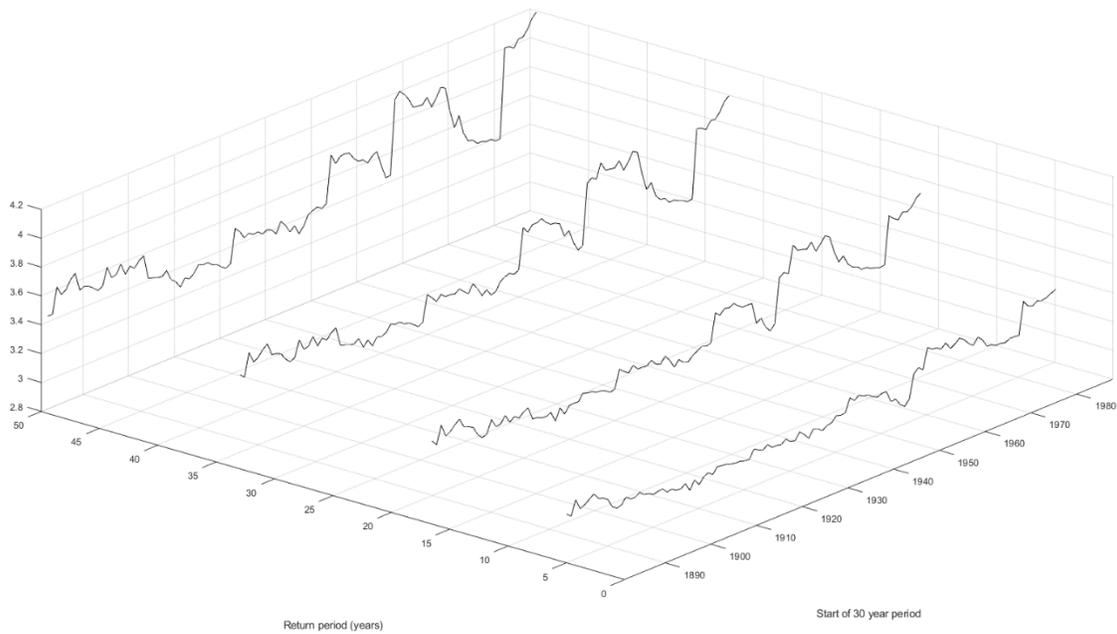
Γράφημα 11: Επάνω ουρά της μέσης θερμοκρασίας (σταθμός: Αγίας Πετρούπολη, Ρωσία)
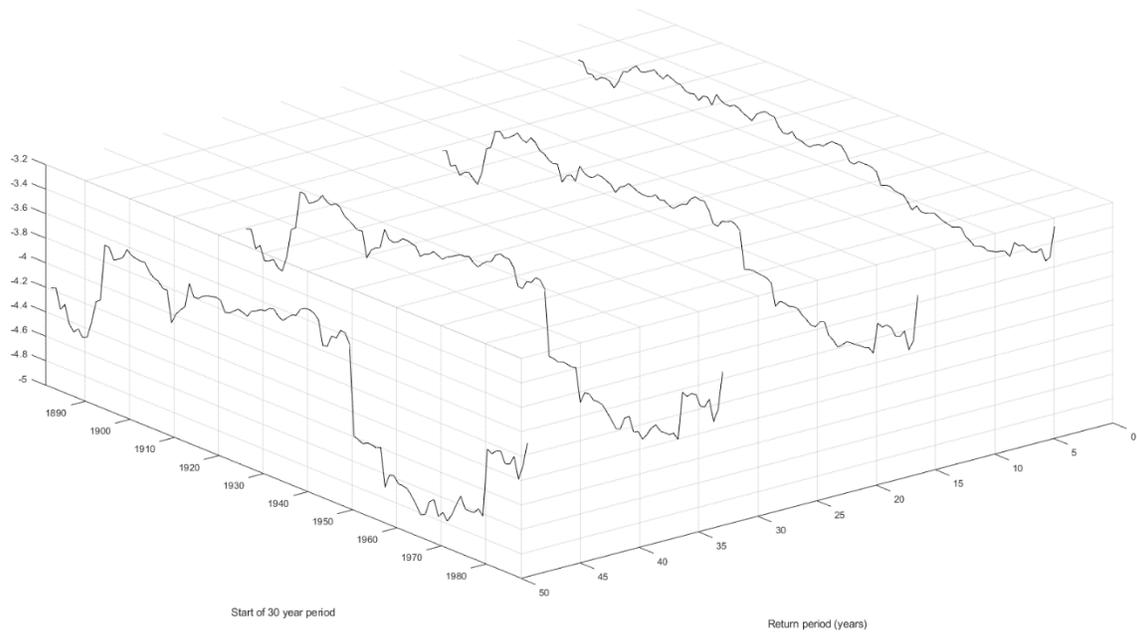
Γράφημα 12: Κάτω ουρά της μέσης θερμοκρασίας (σταθμός: Αγίας Πετρούπολη, Ρωσία)
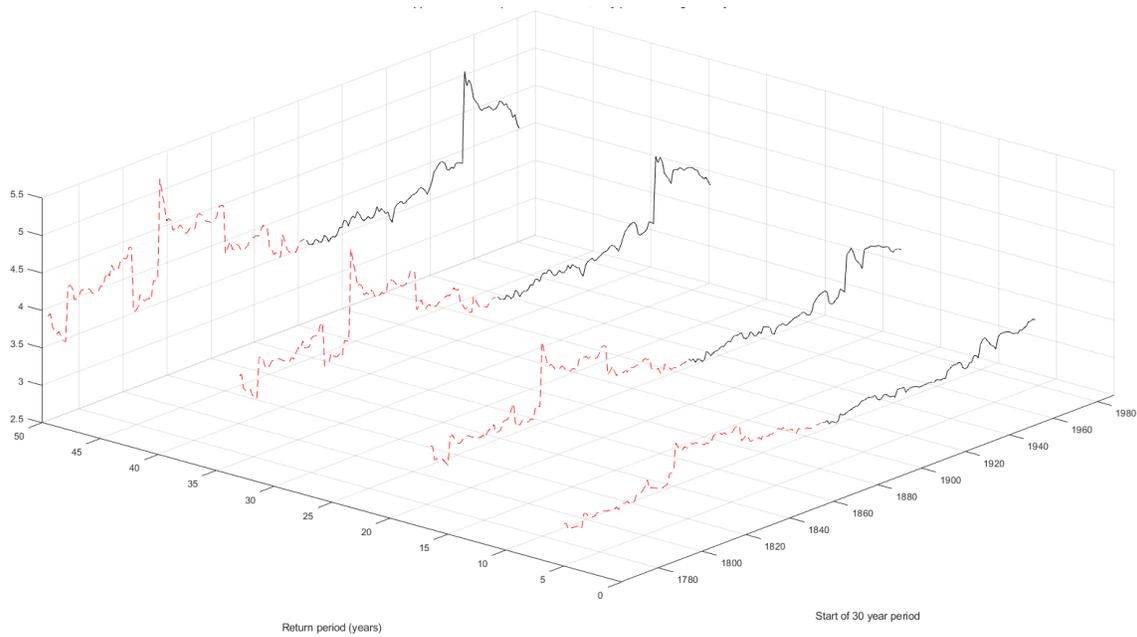
Γράφημα 13: Επάνω ουρά της μέγιστης θερμοκρασίας (σταθμός: Μιλάνο, Ιταλία)
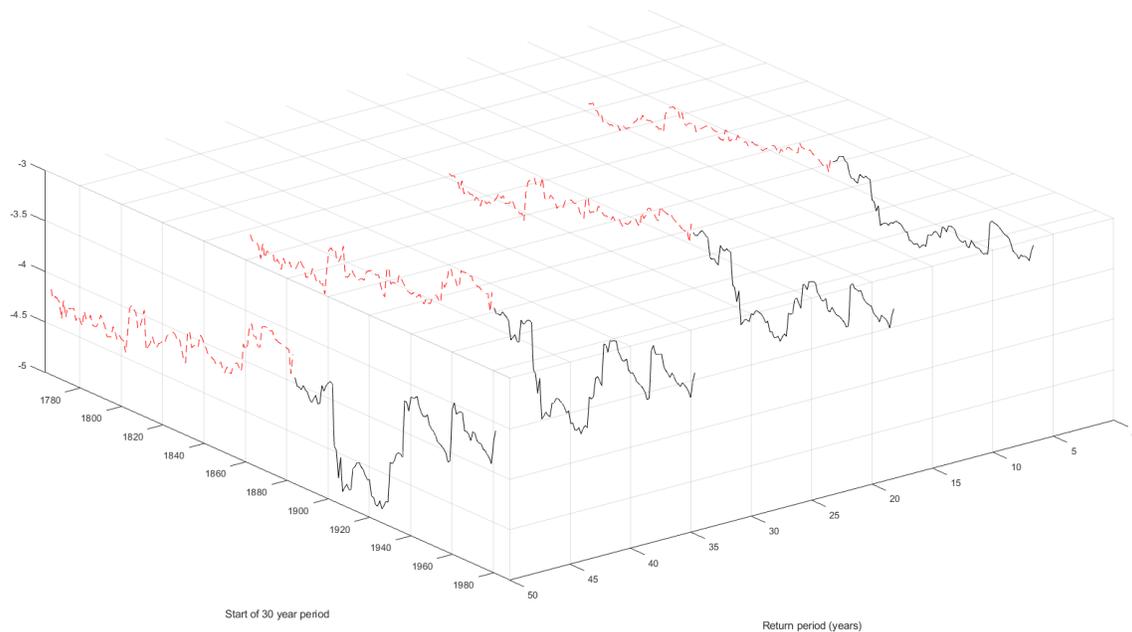
Γράφημα 14: Κάτω ουρά της ελάχιστης θερμοκρασίας (σταθμός: Μιλάνο, Ιταλία)

Συμπεράσματα

Με βάση τα αποτελέσματα που προκύπτουν από τη μελέτη της παρατηρημένης μέσης θερμοκρασίας προκύπτει ότι η επάνω ουρά τείνει να αυξηθεί σε πάχος, ενώ η κάτω ουρά τείνει να λεπτύνει. Επειδή, όμως, οι μεταβολές αυτές φαίνεται να είναι ίσες σε όλα τα επίπεδα των περιόδων επαναφοράς, η μεταβολή μάλλον οφείλεται σε μετατόπιση της μέσης τιμής της κατανομής (προς τα πάνω) και όχι σε μεταβολή της διασποράς. Η παρατηρημένη μέγιστη θερμοκρασία εμφανίζει ουρά, η οποία φαίνεται να παραμένει σχετικά αμετάβλητη στο χρόνο, και μάλιστα τα τελευταία χρόνια ίσως και να λεπταίνει ελαφρά. Η κάτω ουρά της ελάχιστης παρατηρημένης θερμοκρασίας εμφανίζεται να παραμένει σταθερή, μέχρι περίπου τη δεκαετία του 1990 (δηλαδή τριακονταετίας, που ξεκινούν τη δεκαετία του 1960), αλλά μετά εμφανίζεται να λεπταίνει σημαντικά σε όλα τα επίπεδα περιόδων επαναφοράς. Η μετατόπιση αυτή, όπως και στην περίπτωση της

xxiv

παρατηρημένης μέσης θερμοκρασίας μάλλον οφείλεται σε μεταβολή της μέσης τιμής και όχι της διασποράς της κατανομής.

Από τα γραφήματα των ουρών των συνθετικών χρονοσειρών καταλαβαίνουμε ότι, στις περισσότερες περιπτώσεις, η συμπεριφορά των ουρών είναι μέσα στα πλαίσια των αναμενόμενων μεταβολών. Όπως φαίνεται από τα γραφήματα των συνθετικών χρονοσειρών, τόσο η εξέλιξη της μέσης τιμής, όσο και το εύρος των δύο ακραίων εκατοστημορίων φαίνεται να ταυτίζονται με τα παρατηρημένα δεδομένα. Μοναδική εξαίρεση αποτελεί η κάτω ουρά της μέσης θερμοκρασίας, η οποία στα παρατηρημένα δεδομένα φαίνεται να είναι πιο χοντρή απ' ότι στα συνθετικά δεδομένα. Αυτό σημαίνει ότι ακόμα και το μοντέλο που διαλέξαμε για την εκτίμηση του συντελεστή Hurst και το μοντέλο SMA για την αναπαραγωγή της στοχαστικής συμπεριφοράς, δεν ήταν αρκετά, για να απεικονίσουν ρεαλιστικά τη συγκεκριμένη συμπεριφορά.

Οι μεμονωμένες χρονοσειρές των μακροβιότερων σταθμών εμφανίζουν μία τάση θέρμανσης, όπως αυτή μεταφράζεται από την αύξηση του πάχους της πάνω ουράς και τη μείωση της κάτω ουράς. Αυτό πιθανόν οφείλεται σε γεωγραφική μεροληψία, μιας και οι δύο σταθμοί βρίσκονται στην Ευρώπη, ή την αστικοποίηση των δύο αυτών πόλεων, ο πληθυσμός των οποίων (και κατ' επέκταση η αστική χρήση γης) έχει πολλαπλασιαστεί στη διάρκεια της περιόδου καταγραφής των θερμοκρασιών.

Ευρετήριο Σχημάτων

Table of Contents

List of Figures

List of Tables

1. Introduction

1.1 Research scope

The aim of the present diploma thesis is to identify the temporal evolution of the extreme land surface air temperature events, at specific return period levels, and to evaluate if such variations are within the expected inherent fluctuations of a stochastic process representing a natural process like temperature. In this respect, we investigate possible past and current trends of land surface air temperature, and how these are related within the context of global climate variations.

Over the last decades, climate change and its effects on both humans and the natural world have emerged to be at the forefront of political, financial and scientific agendas. Due to the vulnerability of human infrastructure, as well as the entire system of food and energy harvesting and logistics chain, slight disturbances in very delicate climatic conditions can cause severe disruptions. That is why it is imperative to understand, not only the trend of the average land surface air temperature, but also the evolution of the maximum and minimum land surface air temperature. In the scientific level, we need to be able to understand the problem, before attempting to mitigate, let alone solve it.

The understanding of the evolution of air temperature, in terms of distribution, is also beneficial in helping us identify the major factors of climate change, and if, and how, we will be able to moderate its effect, in order for us to better adapt. There are numerous causes of climate change, both internal and external. The internal variability of the climate includes factors like ocean-atmosphere variability (Brown et al., 2015; Hasselmann, 1976) as well the effects of the biosphere through the carbon and water cycles. In the external forcing mechanisms, we take into account greenhouse gases (Cronin, 2010), orbital variations, solar output and volcanic activity among others. Identifying the exact changes of the air temperature, together with an interdisciplinary approach, will facilitate the deciphering of how the Earth's climate works.

1.2 State-of-the-art

The vast majority of scientific studies of the land surface air temperature has focused on the evolution of the average (arithmetic mean) temperature, while the maximum and minimum temperature have remained largely out of the spotlight. As shown by Peterson et al. (1999) and Peterson and Vose (1997), there is slightly diverging behavior of the average air temperature among the rural and urban meteorological records. While there is little difference in the long-term (1880 to 1998) rural (0.70 °C/century) and full set of station temperature trends (actually less at 0.65 °C/century), more recent data (1951 to 1989) do suggest a slight disparity in the rural (0.80 °C/century) and full set of station trends (0.92 °C/century). More recent independently produced instrumental datasets confirm that the 2009−2018 decade was 0.93 ± 0.07 °C warmer compared to the pre-industrial baseline (1850−1900) (IPCC, 2018). Overall, the trend seems to be increasing in both cases.

In addition, multiple studies (Lawrimore et al., 2011; Hansen et al., 2010; Jones et al., 2012; Rohde et al., 2013a), which have accounted for urban impact, have used additional station series and newly homogenized versions of many individual record stations, attest to the increase of the land surface air temperature, particularly after 1900. Global average land surface air temperature has increased substantially, as shown in the figure 1.1.
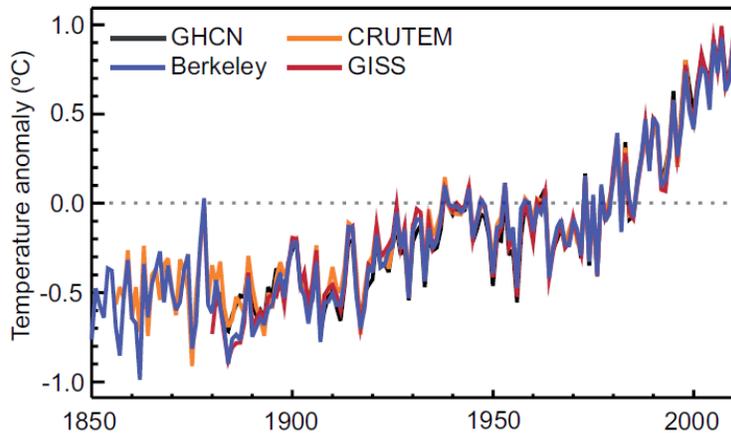
Figure 1.1 Global annual average land-surface air temperature (LSAT) anomalies relative to a 1961−1990 climatology from the latest versions of four different data sets (Berkeley, CRUTEM, GHCN and GISS) | Source: Stocker et al. (2013)

Since the Fourth Assessment Report (AR4) of the Intergovernmental Panel on Climate Change (Trenberth et al., 2007) many theoretical challenges of the veracity of global land surface air temperature records have arisen (Pielke et al., 2007). Globally, different methods have been used to evaluate such claims, such as sub-sampling (Parker et al., 2009; Jones et al., 2012) and the creation of an entirely new and structurally complete products (Rohde et al., 2013b). None of these have yielded significant variations of the global land surface air temperature records. Further controversy has arisen over the siting quality of weather stations, especially in the United States, which does not correspond to the WMO suggestions and may be expected to suffer potentially large siting-induced absolute biases (Fall et al., 2011). However, it has been pointed out by numerous studies (Menne et al., 2010; Williams et al., 2012) that any such bias has been probably caused by replacement of Stevenson's screens with maximum minimum temperature recorders rather than siting.

As for the maximum and minimum land surface air temperature, as reported in the Second Assessment Report (SAR) of the Intergovernmental Panel on Climate Change (1995) and later updated by Easterling et al. (1997), the daily minimum temperature has increased faster than the daily maximum temperature. This has caused a decrease in the diurnal

temperature range (DTR) in many parts of the world. In the relatively narrow time window between 1950 and 1993, the overall global trend for the maximum temperature appears to be approximately 0.1 °C/decade, while the minimum temperature increases at a rate of 0.2 °C/decade Thus the DTR is decreasing by about 0.1 °C/decade (Easterling et al., 1997). Further studies include different trend estimates (−0.04 ± 0.01 °C per decade over 1950−2011 (Rohde et al., 2013b) and −0.066 °C per decade over 1950−2004 (Vose et al., 2005)), which are much smaller than the smallest estimated global mean average land surface air temperature trend over 1951−2012, which is 0.175 ± 0.029 °C (Rohde et al., 2013b).
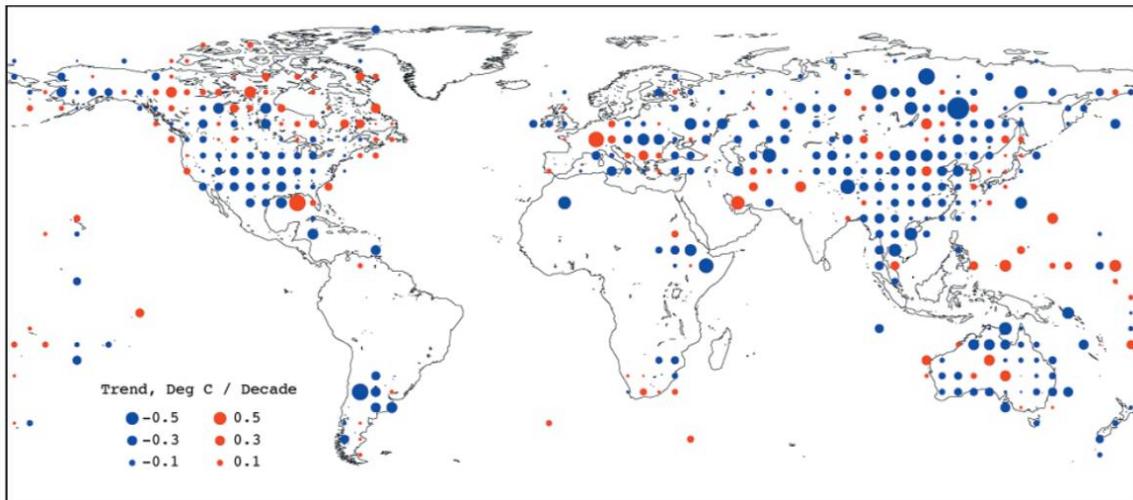
Figure 1.2 Trends in annual diurnal temperature range (DTR, °C/decade), from 1950 to 1993, for non-urban stations only, updated from Easterling et al. (1997). Decreases are in blue and increases in red. | Source: Folland et al. (2001)

What the aforementioned studies have omitted to take into account, however, is the inherent seasonal variability of the land surface air temperature, which can only be taken into account be standardizing the record values with respect to their specific season. As presented by Lindzen (2010) winter daily temperature in the arctic has a much greater variability (often as large as 20 °C) than the summer daily, thus the increase most

researchers find in the minimum temperature in these areas may be within the boundaries of natural variability. By not regarding the inter-seasonal variability into account and focusing, instead, solely on the average air temperature is inconsistent with the scientific intuition and may be misleading.

In the present study we consider the inter-seasonal variability of the air temperature to be an integral part of the expected trend, thus releasing ourselves from any bias imposed by persistent slightly increased, yet normal, temperature recordings.

Furthermore, in the present study we introduce the concept and make use of K-moments, which have several advantages, compared to both classical and L-moments, and are particularly strong for an extreme-oriented modelling (Koutsoyiannis, 2020). The following three properties are highlighted:

1. They are knowable with unbiased estimators for high orders, up to the sample size n, while the estimation uncertainty is by orders of magnitude lower than in the classical moments.
2. The estimators can explicitly (albeit approximately) take into account any existing dependence structure.
3. The K-moment values, can be directly assigned return periods, through Λ coefficients, similar to happens with order statistics, but with some advantages over the latter.

1.3 Work structure

The thesis is structured into eight distinct chapters, all of whom are sorted in a way similar to the line of reasoning required for the understanding of the objective.

In this **first chapter** we introduce a preamble to the subject, as well as the research objectives and the points that differentiate it from similar state-of-the-art research.

In the **second chapter** we provide some insight of the importance of land surface air temperature, as well as lay out the prime factors of climate variations, on which increased scientific importance has been given. We also present a brief historical overview of the instruments used for recording air temperature.

In the **third chapter** we make an extensive presentation of the basic theoretical tools used, as well as the rudimentary mathematical and statistics theory behind it. As part of it we also explain all the information required for the understanding of the methodology and procedures followed, including the very nature of stochastic processes and its quantification introduced by Hurst.

In the **fourth chapter** we introduce a concise presentation of the computational tools used for the purpose of this study, namely MathWorks Matlab and Microsoft Office Excel spreadsheet. To this purpose, we scrutinize all the ready-to-use functions utilized, their fundamental properties, as well the operation of the software used.

In the **fifth chapter** we present the database, from which the data studied were downloaded and the quality checks performed to isolate flagged problematic data entries. In addition, we explain the qualitative and quantitative criteria with which data were selected for processing, as well the preliminary data processing of them.

In the **sixth chapter** we present an extensive overview of the methodology followed. We explain all the steps of the procedures, both in depth and in relation to the previous and following steps. Furthermore, we present all the intermediate calculation steps, as well as the intermediate findings used for the identification of air temperature trends.

In the **seventh chapter** we present the results of the study of both the observed temperature records and the synthetic ones produced by the calculation of the Hurst coefficient and basic moments of the former. Moreover, we present the temporal evolution of the longest-lived individual instrumental records, with the objective of comparing them with general trend.

In the **eighth chapter** we make an allusion to the methodology followed and present the major conclusions deduced from the findings, regarding them both individually and together. In addition, we take a closer look at what these findings mean for the tail of the surface air temperature and provide suggestions for future research.

2. Air temperature

2.1 Importance of air temperature

Temperature is a physical quantity measuring the kinetic energy of matter. Temperature is a widely studied quantity within meteorology, and thermometers exposed to air, but sheltered from direct solar radiation, are used to record it (Huschke, 1959; Glickman, 2000).

Near-land-surface air temperature, which is measured at meteorological stations at a typical height of 1.5 or 2m, is one of the most important physical variables used to evaluate climatic trends in multiple scales, as well as the exchange of thermal energy between the Earth's surface and the atmosphere (Prihodko and Goward, 1997). Because of its paramount importance for a variety of physical processes, such as photosynthesis, evapotranspiration, and energy flows, land surface air temperature is essential in all land surface process models, including, but not limited to, climatology and hydrology (Huld et al., 2006).

Climate change, whether driven by natural or human forcings, can lead to changes in the likelihood of the occurrence or strength of extreme weather (Seneviratne et al., 2012). The probability of occurrence of values of a climate or weather variable can be described by a probability density function (PDF) that for some variables (e.g., temperature) is shaped similar to a Gaussian curve (Stocker et al., 2013). Since the definition of extreme events varies, it is important to identify the evolution of the whole distribution of land surface air temperature, because changes in the mean or variance have a profound impact on extreme weather. The figure 2.1 depicts the changes likely to happen form some probable changes in the mean and variance of air temperature.

In agricultural areas, where there is a strong, yet volatile, mixing of hot and cold air masses, such as in the Mediterranean, slight changes in the extreme occurrence may have impact of paramount importance to the food supply of many countries, including those which

receive exports of the region. In addition, a change of the extremes' magnitude will inadvertently alter the definition of norm as well. Heatwaves and winter storms may have a different meaning for the people of the future, since their very definition relies upon the probability of happening.
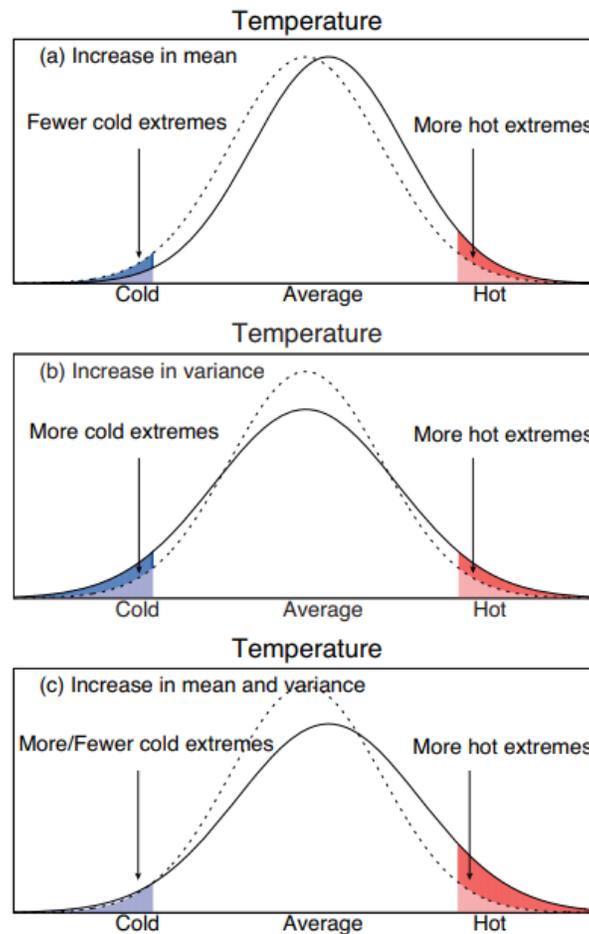
Figure 2.1 Schematic representations of the probability density function of daily temperature, which tends to be approximately Gaussian. Dashed lines represent a previous distribution and solid lines a changed distribution. The probability of occurrence, or frequencies of extremes are affected by changes (a) in the mean, (b) in the variance or shape, and (c) in both the mean and the variance | Source: Stocker et al. (2013)

2.2 Physical drivers for air temperature changes

Factors affecting the air temperature of an area, as well as the whole planet, include:

<u>Solar irradiation</u>

The climate of Earth has undergone serious changes during our planet's lifetime. Alternating ice ages have shaped, not only the surface of the ground, but have, also, changed the evolutionary path of many organisms. A major factor of such great changes is no other than the variations of incoming solar radiation, caused by either change of the activity of Sun's magnetic field, or by astronomical factors. Solar radiation, and heated plasma particles, i.e. solar wind, emitted by the surface of the Sun are the fundamental drives of our climatic system. Even small variations in solar irradiance can have a profound impact on Earth's climate with both regional and global-scale responses (Lean and Rind, 2009).

Despite the correlation between the Sun's activity and climate change is considered to be evident, lack of longtime records of solar activity inhibits statistically important research. For many years, the Earth Climate-Solar Activity relationship belonged to the sphere of ambiguity. Yet recent space probes' recordings show that total solar irradiance changes at multiple time scales, ranging from minutes up to the solar circle.

Due to the ongoing debate of the human interaction with the climate of Earth, more research has been done in the field of total solar irradiance. In order for the quantification of the climate change, attributed to human activities, to be precise, first the portion of the naturally-caused climate change needs to be assessed. One of the most important natural factors is solar activity.

Climatic models show that the total amount of solar radiation change may be responsible, to a great degree, for the pre-industrial change of Earth's air temperature. During the 20th century. however, the relative influence of solar activity changes to climate change has been reduced, thus making probable that other, non-natural, factors may alter the climate.

Solar irradiance (SI) is the power per unit area (watt per square meter, W/m^2), in the form of electromagnetic radiation, that is emitted by the Sun, and is recorded by instruments, according to each instrument wavelength range. Solar irradiance can be measured in space

or in the Earth's surface, after atmospheric absorption and scattering, and after compensating for the inclination of the solar rays in relation to the surface, as well as atmospheric conditions, like cloud coverage.
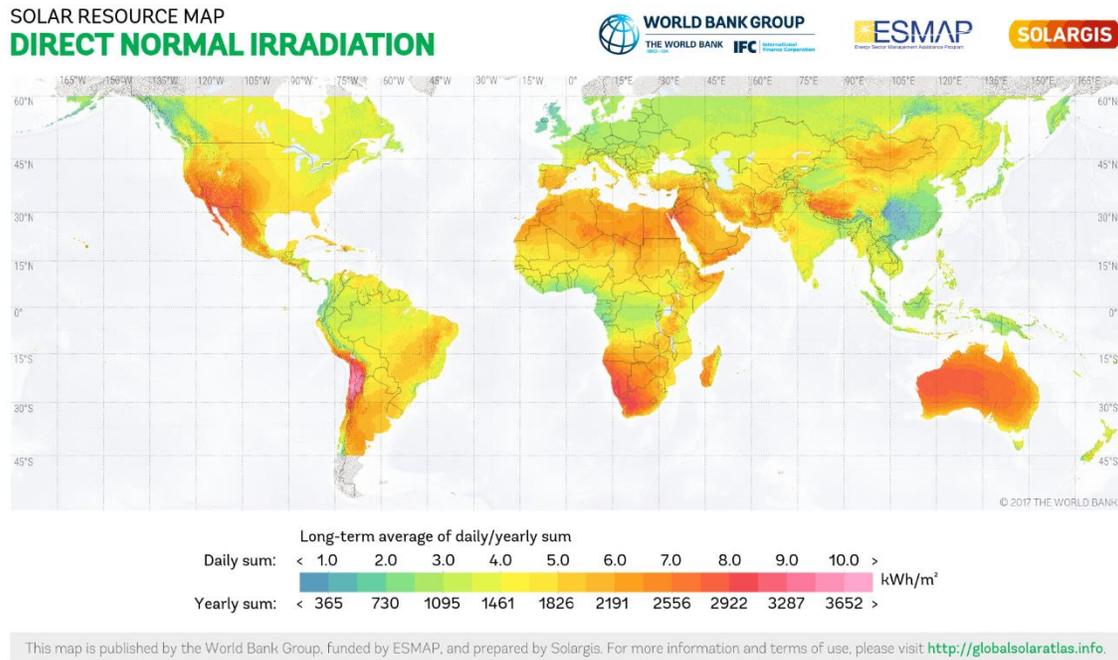
Figure 2.2 Global map of direct normal irradiation | Source: World Bank Group

El Niño Southern Oscillation

The El Niño Southern Oscillation (ENSO) is the strongest climate fluctuation on interannual time scales and has global impacts, despite originating only from the tropical Pacific Ocean. Many methods have been used to quantify the severity of El Niño Southern Oscillation events, but the Multivariate ENSO Index (MEI) is considered as the most comprehensive, since it links six different meteorological parameters measured over the tropical Pacific. (Mazzarella et al., 2013)

Historically El Niño events occur about every 3 to 7 years and alternate with the opposite phase of below-average temperature in the eastern tropical Pacific, called La Niña.

Variations in the trade winds, atmospheric circulation patterns, precipitation and associated atmospheric heating cause responses outside of the tropics. Ripple-like extratropical teleconnections are accompanied by changes in the jet streams and storm tracks in mid-latitudes (Chang and Fu, 2002). The El Niño-Southern Oscillation has global impacts, apparent most vividly in the northern winter months (November–March). Anomalies in Mean Sea Level Pressure are much greater in the temperate and arctic zones, while the tropics feature large precipitation variations. Associated patterns of surface temperature and precipitation anomalies around the globe are given in the following figure (Trenberth and Caron, 2000), and the evolution of these patterns and links to global mean temperature disturbances are given by Trenberth et al. (2002).
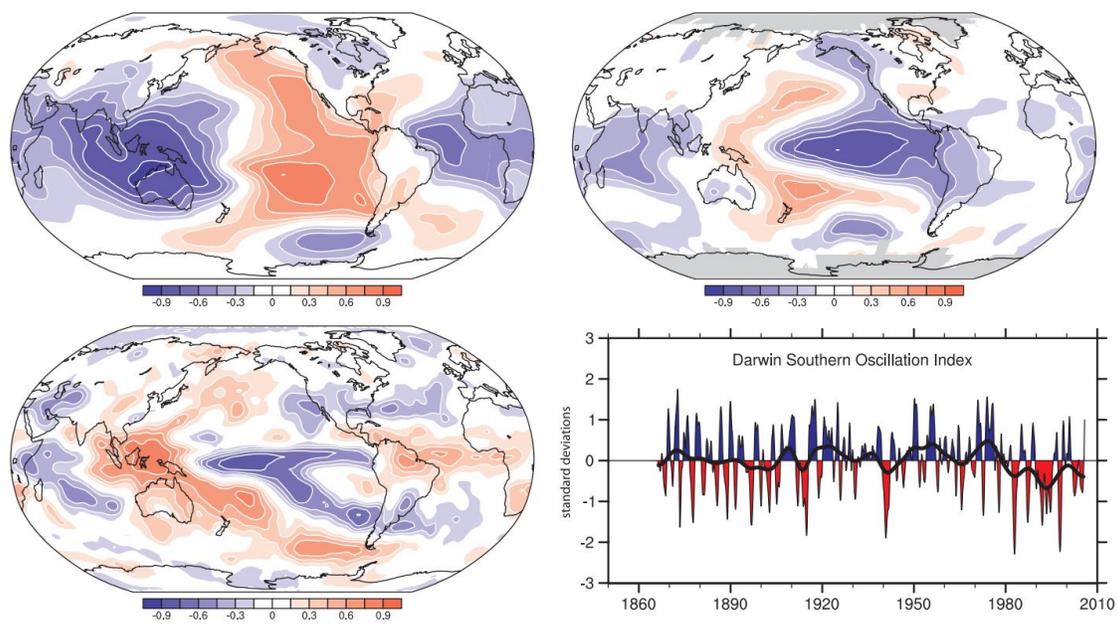
Figure 2.3 Correlations with the SOI, based on normalized Tahiti minus Darwin sea level pressures, for annual (May to April) means for sea level pressure (top left) and surface temperature (top right) for 1958 to 2004, and GPCP precipitation for 1979 to 2003 (bottom left), updated from Trenberth and Caron (2000). The Darwin-based SOI, in normalized units of standard deviation, from 1866 to 2005 (Können et al., 1998; lower right) features monthly values with an 11-point low-pass filter, which effectively removes fluctuations with periods of less than eight months (Trenberth, 1984). The smooth black curve shows decadal variations. Red values indicate positive sea level pressure anomalies at Darwin and thus El Niño conditions. | Source: Trenberth et al. (2007)

<u>Suspended particles</u>

Although suspended particles constitute only a small fraction of our atmosphere, they have a great influence on it. They scatter and absorb solar radiation, while also alter the dynamics of the clouds. Because of their great spatiotemporal variations, the study of suspended particles is rendered extremely important for the understanding of the mechanisms behind the physics of the atmosphere.

Suspended particles are solid or liquid particles of the atmosphere, without be constrained to a specific of chemical composition. Their size varies between 10 nm and 100 μm. They originate from either natural processes (like desert sand, sea salt or volcanic ash), or human activities (such as fossil fuel burning). In urban areas, where there are multiple human activities emitting particles, it is easy to discern their increased concentration.

Presence of suspended particles is mostly limited to the lower layers of the atmosphere, due to the fact that most of their sources are on the surface of the planet. Almost 80% of their total mass is found within 1 km from the surface. However, natural processes like volcanic eruptions may cause suspended particles to transcend the lower layers and infiltrate the upper layers. Atmospheric suspended particles affect the Earth's climate by changing the amount of incoming solar radiation and outgoing infrared radiation retained. This occurs through a wide variety of mechanisms, which have been categorized into direct and indirect (Haywood and Boucher, 2000; Twomey, 1977)

The direct aerosol effect includes any direct interaction between radiation and suspended particles, such as absorption and scattering. It affects both short (UV) and longwave (infrared) radiation to produce a net negative equilibrium, meaning more energy gets trapped on Earth than escapes it (Charlson et al., 1992)

Indirect effects of suspended particles include their influence on the radiation balance and hydrology through their effect on cloud microphysical processes (first indirect effect) and amount (second indirect effect). There is a semi-direct effect as well, in which the heating by aerosol particles, because of the absorption of solar radiation, results in a decrease of

cloud amount. The indirect effect is a significant source of uncertainty for climatologists, due to the complexity and number of the atmospheric interactions involved, as well as the wide range of scales in which these interactions occur (Fan et al., 2009)
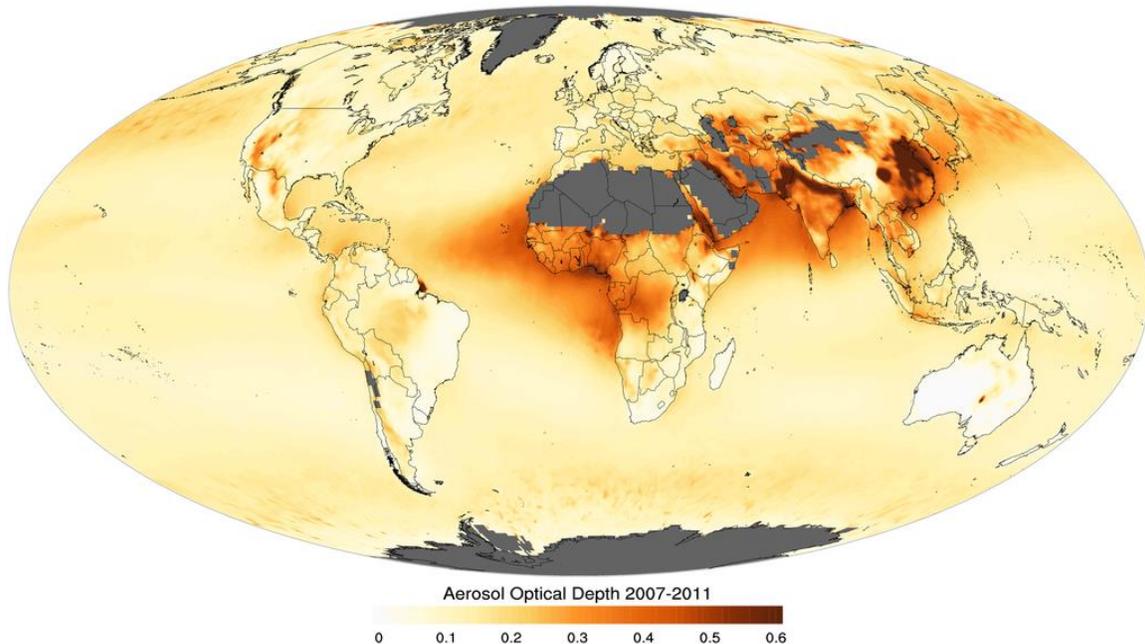
Figure 2.4 NASA Moderate Resolution Imaging Spectroradiometer (MODIS) Terra aerosol optical depth at 550nm. Average (arithmetic mean) data of period 2007-01 to 2011-12. | Source: Acker and Leptoukh (2007)

Greenhouse gases

The greenhouse effect is the natural process by which outgoing radiation from a planet's surface gets trapped by the planet's atmosphere, and, through re-emitting as heat, warms the planet's surface to a temperature above what it would be without the atmosphere (Claussen et al., 2001).

Relatively active gases (i.e. greenhouse gases or GHG) absorb and emit radiate energy within the thermal infrared range. Part of this emitted radiation heads toward the surface, leading to its warming (Vaclav, 2003). The intensity of this downward radiation depends

on both the atmosphere's temperature, as well as the concentration of greenhouse gases that it contains. To understand the scale of their effect, it is worth noting that if the greenhouse gases had not been present in the Earth's atmosphere, the average temperature of the planet would be about -18 °C, rather than the present 15 °C (Le Treut et al., 2007).

The contribution of each gas to the greenhouse effect relies upon its abundance, its characteristics and any possible indirect effect it may have. For instance, in a period of 20 years, a mass of methane is about 84 times more potent than carbon dioxide in trapping outgoing infrared radiation.

In order, the most abundant greenhouse gases in Earth's atmosphere are:

- Water vapor (H_2O)
- Carbon dioxide (CO_2)
- Methane (CH_4)
- Ozone (O_3)
- Chlorofluorocarbons (CFCs)
- Hydrofluorocarbons (HFCs)

The most effective greenhouse gases in the atmosphere, are (Kiehl and Trenberth, 1997):

Table 2.1 Effectiveness of greenhouse gases

Compound	Chemical formula	Contribution
Water vapor	H_2O	36-72%
Carbon dioxide	CO_2	9-26%
Methane	CH_4	4-9%
Ozone	O_3	3-7%

The precipitable water over the globe, which basically is the water vapor, has been fluctuating with lowest values during the 1980s and highest values during the 1950s and 2010s (Koutsoyiannis, 2018). Thus, the estimation of its exact contribution to the greenhouse effect at each specific time is extremely precarious.

Radiative forcing (or climate forcing) is the difference between insolation (sunlight) absorbed by the Earth's atmosphere and energy radiated back to space (Shindell, 2013). The factors that cause alterations to the Earth's complex climate system changing Earth's radiative balance, forcing temperatures to rise or fall, are called climate forcings. For the past 100-150 years concentration of greenhouse gases, and consequently global radiative forcing, have been steadily increasing, causing much concern to the scientific community.

As presented in the following graph (figure 2.5), from 1979 to 2018, the global radiative forcing has increased from about 0.67 W/m² to about 1.07 W/m². Data for the creation of the graph were derived from the NOAA Annual Greenhouse Gas Index (AGGI).
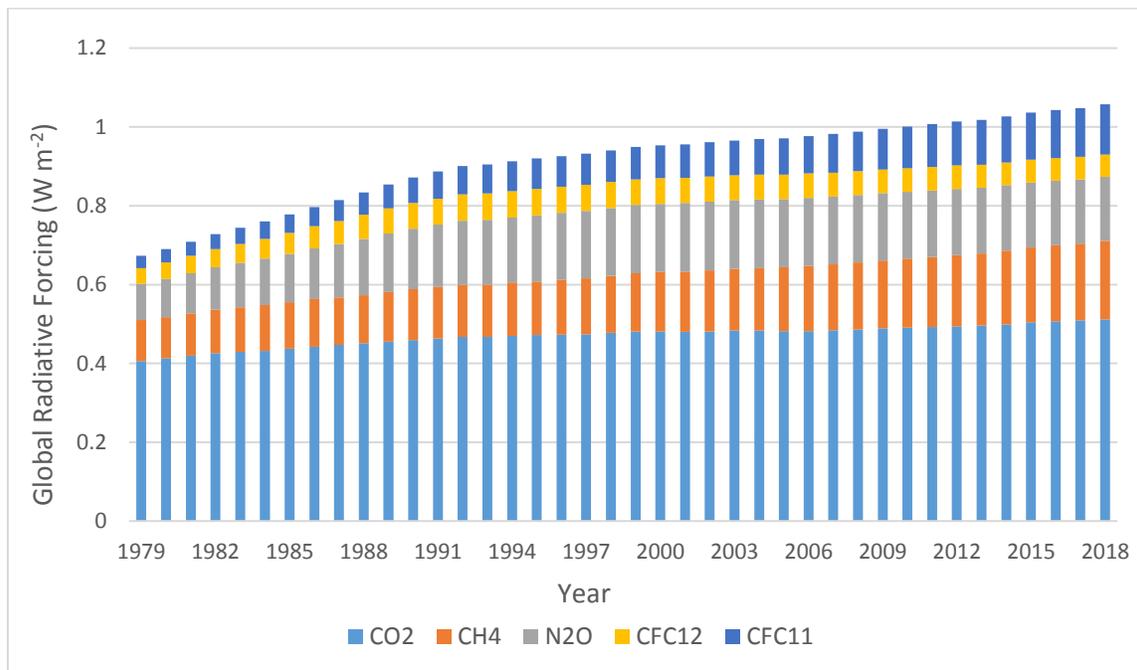
Figure 2.5 Global Radiative Forcing for the period 1979-2018 | Source: Butler and Montzka (2011)

Despite the greater emphasis given to greenhouse gases emitted by nature, as well as humans (such as carbon dioxide), water vapors account for the largest portion of the greenhouse effect. Water vapor concentration fluctuates regionally, but human activities are extremely difficult to directly affect them, except for large-scale operations, such as extended-area irrigated fields. Indirectly, however, if human activities do cause an increase of global temperatures, then water vapor concentrations are likely to increase, in a process known as "water vapor feedback" (Held and Soden, 2000).

2.3 Instrumental air temperature recording

The land surface air temperature is measured at meteorological observatories and weather stations, either manned or automatic, with the latter being the most common. Usually thermometers used to record the temperature are enclosed in a shelter to prevent either precipitation or direct heat radiation to tamper the real air temperature recording. According to the setup suggested by the World Meteorological Organization (WMO), the thermometers ought to be positioned 1.2 to 2 m above the surface.

A popular, yet increasingly obsolete, instrument of measuring air temperature is Stevenson screen, a standardized well-ventilated instrument shelter. The screen consists of a white-painted box, with louvres in all its vertical sides to enable ventilation, a ventilated floor and upper part and an air space between an inner and an outer roof. The innovative protecting layout of Stevenson screen enables the unobstructed flow of air through the louvres, without adulterating the results with influences such as direct solar radiation, as well as radiation emitted from surrounding objects (Allaby, 2019). Scottish civil engineer Thomas Stevenson (1818-1887) invented the homonym screen, which can be seen in the figure 2.6.
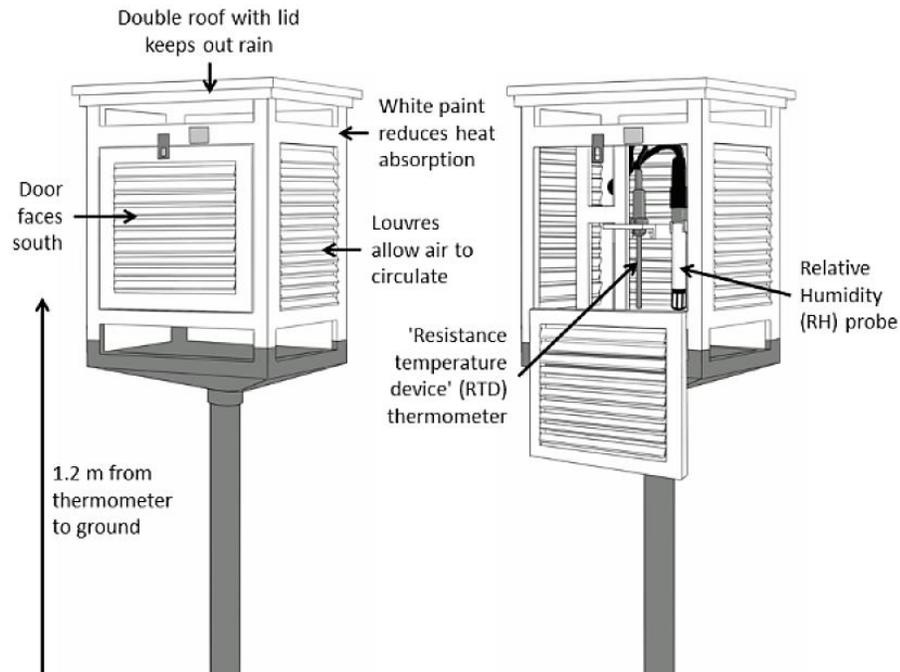
Figure 2.6 Stevenson screen | Source: Allaby (2019)

Since the advent of technology slowly takes over the temperature instrument area, Stevenson screen is replaced by more standardized and automated instruments, such as automatic weather stations. An automatic weather station (AWS) is defined as a "meteorological station at which observations are made and transmitted automatically" (WMO, 1992). The automatic weather station (AWS) is similar in function with the traditional weather station, with the difference that no human work is required for its operation. Major reasons for adopting AWS are human labor saving and the potential of measuring in remote or inhospitable areas.

In an automatic weather station, the instrument (including temperature) measurements are read out or received by a central data-acquisition unit. The data collected by the autonomous measuring devices can be processed either locally at the AWS or elsewhere, for example, at the central processor of the network (WMO, 2010a). Automatic weather stations may be designed as an integrated concept of various measuring devices in combination with the data-acquisition and processing units. Such a combined system of

instruments, interfaces and processing and transmission units is usually called an automated weather observing system (AWOS) or automated surface observing system (ASOS). It has become common practice to refer to such a system as an AWS, although it is not a "station" fully in line with the stated definition.

Automatic weather stations are used in order to expand the pool of instrumental measurements available to scientists, while also increasing the reliability of surface measurements. They achieve this for the following reasons (WMO, 2008):

- Densification of an existing network increases available data, by including data from new sites and from sites that are difficult to access;
- AWS are able to supply, for manned stations, data outside the normal working hours;
- Use of sophisticated technology and modern, digital measurement techniques increase the reliability of measurements;
- Preservation of the homogeneity of networks by standardizing the measuring techniques;
- Satisfying new observational needs and requirements;
- Reduction of human errors, since all procedures are automated;
- Reduction of the number of observers, thus lowering the cost of operation;
- Measuring and reporting with high frequency or even continuously.

Automatic weather stations fulfill many different needs, ranging from a simple aid-to-the observer, at already manned stations, to complete replacement of observers at fully automatic stations. According to the respective functions, it is possible to classify automatic weather stations into not very easily distinguishable groups. A general criterion for the classification is the ability to provide recorded data in real time or post hoc. The need for real-time transmission of data depends on the necessity of data analysis (WMO, 2008).

The two most fundamentally different categories of AWS are (WMO, 2008):

- Real-time AWS: Stations providing data to users of meteorological observations in real time, typically at programmed times, but also in emergency conditions or upon external request. Typical real-time use of an AWS is the provision of synoptic data and the monitoring of critical warning states such as storms and river or tide levels.

- Off-line AWS: Stations recording data on site on internal or external data storage devices possibly combined with a display of actual data. The intervention of an observer is required to send stored data to the remote data user. Typical stations are climatological and simple aid-to-the-observer stations.

Since the cost of AWSs can be substantial, the stations' facilities can also be used to satisfy the common and specific needs and requirements of several applications, like synoptic, aeronautical and agricultural meteorology, hydrology and climatology. They may also be used for special purposes, such as nuclear power safety, air and water quality, and road meteorology. Some automatic weather stations, therefore, transcend the boundaries of these categories and are actually multipurpose automatic weather stations.

It is very often that an AWS forms part of a network of meteorological stations, each transmitting its recorded and processed data to a central network processing unit by various data transmission means (WMO, 2008). As the tasks to be executed by this central system are strongly related, and often complementary, to the tasks of the AWSs, the functional and technical requirements of both the central system and the AWSs should be very well coordinated, in order to avoid faulty or incomprehensible from the main system measurements.

The time period for which reliable temperature instrumental records exist is generally considered to begin around 1830-1850. Earlier records do exist, but their limited availability, sparse coverage and less standardized instrument calibration renders them problematic for most scientific applications.

Satellite temperature measurements are also used to assess the temperature changes both in local and in global scale. However, weather satellites do not measure temperature

directly, but rather radiances in various wavelength bands. When measuring the land surface air temperature, the influence of stratospheric contamination on the radiance emitted by the surface may alter the recorded data. Because of this, land-based instrumental records are used to calibrate satellite records, in order to use the latter for large scale temperature variations assessment.

3. Theoretical tools

3.1 Basic statistics

The primary goal of statistics is the evaluation of real-life observations, in order to deduce generalized conclusions about the physical processes around us. The basic "unit", on which it relies is the observation, while the results come from processing the set of observations. This set is named sample and is basically part of the ensemble of possible observations, i.e. the population.

In classical statistics, sample size n of a random variable X, with probability density function $f(X)$ is a sequence of n independent random variables $X_1, X_2, \ldots, X_n$ with joint probability density function $f(x)$, which is defined in the domain $\Omega^n = \Omega \times \Omega \times \ldots \Omega$ (Papoulis, 1990). Each one of the variables X_i corresponds to the possible outcomes of a measurement. Since we are to have one measurement for each variable, we are to have the sequence $x_1, x_2, \ldots, x_n$, which we call observed sample or observations (Koutsoyiannis, 1997). There must be given great attention in taking a representative sample of the population, in order to avoid any bias, and consequently a misleading outcome.

Suppose a fixed parameter θ needs to be estimated. Then *estimator* is the function that maps the sample space to a set of sample estimates. The estimator of θ is denoted by the symbol $\hat{\theta}$. If X is the random variable, the estimator (itself a random variable) is symbolized as a function of X; $\hat{\theta}(X)$. The estimate for a particular observation x is $\hat{\theta}(x)$.

Another important term of statistics, extremely useful in stochastic investigation, is that of expectation. The *expectation* of X is defined as:

$$E[X] = \sum_{i=1}^{k} x_i p_i = x_1 p_1 + x_2 p_2 + \cdots + x_k p_k \tag{3.1}$$

Since all probabilities p_i add up to 1 ($p_1 + p_2 + \cdots + p_k = 1$), the expected value of the weighted average, with p_i's being the weights. In the case that all outcomes are

equiprobable, (i.e. $p_1 = p_2 = \cdots = p_k$, then the weighted average turns into simple average.

A *stochastic process* is defined as a collection of random variables defined on a common probability space (Ω, F, P), where Ω is a sample space, F is a σ-algebra, and P is a probability measure. The random variables, indexed by some set T, take values in the same mathematical space S, which has to be measurable with respect to some σ-algebra Σ (Lamperti, 1977). In other words, for a given probability space (Ω, F, P) and a measurable space (S, Σ), a stochastic process is a set of S-valued random variables (Florescu, 2014), i.e. $\{X(t) : t \in T\}$

In the context of this study, the land surface air temperature evolution is the stochastic process, and the observations, with which we work, are part of the random variable, whose estimation is the ultimate goal.

3.2 Hurst phenomenon

Climatic and hydrological processes, such as temperature, rainfall, evaporation, are often modelled as stationary discrete-time stochastic processes. Let X_i be such a process with $i = 1,2,3, \dots$ denoting discrete time (e.g. days). In addition, let its mean be $\mu = \mathrm{E}[X_i]$, its autocovariance $\gamma_j = \mathrm{cov}[X_i X_{i+j}]$ and its autocorrelation $\rho_j = \mathrm{corr}[X_i X_{i+j}] = \gamma_j/\gamma_0$, where $j = 0, \pm 1, \pm 2, \pm 3, \dots$.

If we assume δ to be the time scale of interest, then i represents the continuous time interval $[(i-1)\delta, i\delta]$. Let $k\delta$ be a time scale larger than δ where k is a positive integer. The aggregated stochastic process on that time scale is denoted as $Z_i^{(k)}$ and is equal to:

$$Z_i^{(k)} := \sum_{l=(i-1)k+1}^{ik} X_l \tag{3.2}$$

From this definition, it is easy to deduce that for $k = 1$, $Z_i^{(1)} = X_i$, for $k = 2$, $Z_1^{(2)} = X_1 + X_2$, $Z_2^{(2)} = X_3 + X_4$, etc. The statistical properties of $Z_i^{(k)}$ can be derived from those of the process X_i. For instance, the mean of is found by:

$$\mathrm{E}\left[Z_i^{(k)}\right] = k\mu \tag{3.3}$$

whilst the variance and autocorrelation can be found by:

$$\gamma_j^{(k)} = \mathrm{cov}\left[Z_i^{(k)}, Z_{i+j}^{(k)}\right] = \sum_{l=1}^{k} \sum_{m=j \cdot k+!}^{(j+1)k} \gamma_{m-l}, \quad j = 0, \pm 1, \pm 2, \pm 3, \dots \tag{3.4}$$

Hurst was the first to discover long-term persistence in natural processes (1951), yet Kolmogorov (1940) was the first to mathematically describe it, when working on self-similar processes of turbulent fields (Koutsoyiannis, 2011). This behavior (i.e. the tendency of low or high values to aggregate in larger time scales) is known as the Hurst phenomenon, Hurst-Kolmogorov (HK) behavior, or Hurst-Kolmogorov (HK) dynamics (Mandelbrot, 1983; Koutsoyiannis, 2011). A stochastic process with HK behavior is also known as Hurst-Kolmogorov process (HKp) or Fractional Gaussian noise (fGn); although fGn assumes that the noise is Gaussian, which is not always the case. Fractional Gaussian noise can be defined in discrete time (which is the scope here) in a manner similar to that used in continuous time. Specifically, FGN can be defined as a process satisfying the condition:

$$\left(Z_i^{(k)} - k\mu\right) = \left(\frac{k}{l}\right)^H \left(Z_j^{(l)} - l\mu\right) \tag{3.5}$$

which is applicable only in (finite-dimensional joint) distribution. H is a positive constant ($0 < H < 1$) known as Hurst exponent (or coefficient). This equation is valid for any integer i and j (with the process being stationary as a prerequisite) and any time scale k and l (Koutsoyiannis, 2002). As a result, for $i = j = l = 1$ one obtains:

$$\gamma_0^{(k)} = k^{2H}\gamma_0 \tag{3.6}$$

Hence, the standard deviation of the aggregate stochastic process is power law of k with exponent H, which corroborates the observations on real-world cases as described by

Koutsoyiannis (2002). This extremely simple equation serves as the basis for estimating H (Montanari et al., 1997).

3.3 Climacogram

The Climacogram (Cg) is an amalgam of the Greek words climax (meaning scale) and gram (from the word γράμμα meaning letter) and is a two dimensional plot of the standard deviation SD(k) of the mean-aggregated series of the random variable Z on the vertical axis, and the aggregated scale k on the horizontal axis (Koutsoyiannis, 2010):

$$Z_u^{(k)} = \frac{1}{k} \sum_{i=(u-1)k}^{uk} Z_i \qquad (3.7)$$

where Z and Z_u represent the random field of interest and the mean aggregated field respectively, while u is the vector index of the field showing the lag; i.e. the location in the field.

There are multiple definitions of Climacogram (Dimitriadis and Koutsoyiannis, 2015), depending on the nature of the stochastic process; there is fundamental difference between continuous and discrete time processes:

Table 3.1 Climacogram definition and expressions for processes in continuous as well as discrete time, as well as the properties of the estimator

Type	Climacogram
Continuous	$$\gamma(m) := \frac{Var\left[\int_t^{t+m} \underline{x}(\xi)d\xi\right]}{m^2} = Var\left[\int_0^m \underline{x}(\xi)d\xi\right] \Big/ m^2$$ where $m \in \mathbb{R}^+$ and $\gamma(0) := Var[\underline{x}(t)]$
Discrete	$$\gamma_d^{(\Delta)}(k) := \frac{Var\left[\sum_{l=k(i-1)+1}^{ki} \underline{x}_l^{(\Delta)}\right]}{k^2} = \frac{Var\left[\sum_{l=1}^{k} \underline{x}_l^{(\Delta)}\right]}{k^2} = \gamma(k\Delta)$$ where $k \in \mathbb{N}$ is the dimensionless scale for a discrete time process
Classical estimator	$$\hat{\underline{\gamma}}_d^{(\Delta)}(k) = \frac{1}{n-1}\sum_{i=1}^{n}\left(\frac{1}{k}\left(\sum_{l=k(i-1)+1}^{ki} \underline{x}_l^{(\Delta)}\right) - \frac{\sum_{l=1}^{n} \underline{x}_l^{(\Delta)}}{n}\right)^2$$
Expectation of classical estimator	$$E\left[\hat{\underline{\gamma}}_d^{(\Delta)}(k)\right] = \frac{1 - \gamma_d^{(\Delta)}(n)\Big/\gamma_d^{(\Delta)}(k)}{1 - k/n}\gamma_d^{(\Delta)}(k)$$

The Climacogram is used for the detection of long-term change of a process and the persistence (or else dependence, clustering) it may present. This persistence can be effectively quantified through the Hurst coefficient (H). H can usually be derived from the slope of the Cg in a log-log plot (H=1-slope). For 0<H<0.5 the process is anticorrelated, for 0.5<H<1 the process is correlated (most common behavior of geophysical processes) and for H=0.5 the process is purely random (with zero autocorrelation, hence white noise behavior).

However, in some cases, such as in this study, fitting of straight line in the climacogram derived from the observed data results in considerable divergence in the area of large scales. That is why an equally weighted sum of Hybrid Hurst-Kolmogorov and Markov processes was used to maximize entropy production both at small- and large-time scales (Koutsoyiannis et al, 2018).

The equation of the model is:

$$\gamma(k) = \frac{\lambda}{2}\left(1 + (k/a)^{2M}\right)^{\frac{H-1}{M}} + \frac{\lambda}{k/a}\left(1 - \frac{1 - e^{-k/a}}{k/a}\right) \tag{3.8}$$

where H, M and a are the three independent parameters and λ is a dependent parameter, resulting from the value of the climacogram for scale $k = 1$. The parameters H and M are bounded between zero and one inclusive, while parameter a is positive.

3.4 K-moments

Classical moments, raw or central, express important theoretical properties of probability distributions, but cannot be estimated from typical samples for order beyond 2 – cf. Lombardo et al. (2014): "*Just two moments!*".

L-moments are better-than classical moments-estimated, but they are all of first order in terms of the random variable of interest. They enable the characterization of independent series or inference of the marginal distribution of stochastic processes, but not even the second order dependence of processes.

For the aforementioned reasons, K-moments were introduced, which combine advantages of both classical and L-moments. K-moments enable reliable estimation from samples, and in some cases even more reliable than L-moments. They also describe effectively high order statistics, which is useful for marginal and joint distributions of stochastic processes.

Let $\underline{x}$ be a stochastic variable and $\underline{x}_1, \underline{x}_2, \dots, \underline{x}_p$ be copies of it, independent and identically distributed, forming a sample. The maximum of all, which is identical to the pth order stochastic, is by definition:

$$\underline{x}_{(p)} := \max\left(\underline{x}_1, \underline{x}_2, \dots, \underline{x}_p\right) \tag{3.9}$$

It is readily obtained that if $F(x)$ is the distribution function of $\underline{x}$ and $f(x)$ its probability density function, then those of $\underline{x}_{(p)}$ are:

$$F^{(p)}(x) = (F(x))^p, \quad f^{(p)}(x) = pf(x)(F(\underline{x}))^{p-1} \tag{3.10}$$

where the former is the product of p instances of $F(x)$ (justified by the independent and identically distributed assumption), while the latter is the derivative of $F^{(p)}(x)$ with respect to x. The *expected maximum order of p* of $\underline{x}$, i.e. the expected value of $\underline{x}_{(p)}$, is therefore:

$$E[\underline{x}_{(p)}] = E[max(\underline{x}_1, \underline{x}_2, \ldots, \underline{x}_p)] = pE\left[(F(\underline{x}))^{p-1}\underline{x}\right] \tag{3.11}$$

It is worth to stress that the variables $\underline{x}_1, \underline{x}_2, \ldots, \underline{x}_p$ considered here, are not meant in temporal succession and, in this respect, do not form a stochastic process, but are rather regarded to be an ensemble of copies of $\underline{x}$. In other words, the possible dependence in time of a stochastic process is not considered to be prerequisite for the application.

To derive *knowable* moments for high orders p, in the expectation defining the pth moment, we raise $(\underline{x} - \mu)$ to a low power $q < p$ and for the remaining $(p - q)$ multiplicative terms, we replace $(\underline{x} - \mu)$ with $(2F(\underline{x}) - 1)$, where $F(x)$ is the distribution function. This leads to the following definition of central *K-moment* of order (p, q) (Koutsoyiannis, 2019):

$$K_{pq} := (p - q + 1)E[(2F(\underline{x}) - 1)^{p-q}(\underline{x} - \mu)^q], \quad p \geq q \tag{3.12}$$

Likewise, the non-central K-moment of order (p, q) is defined (Koutsoyiannis, 2019):

$$K'_{pq} := (p - q + 1)E\left[(F(\underline{x}))^{p-q}\underline{x}^q\right], \quad p \geq q \tag{3.13}$$

The quantities $(F(\underline{x}))^{p-q}$ and $(2F(\underline{x}) - 1)^{p-q}$ are estimated from a sample, without the use of powers of $\underline{x}$, thus making the estimation more reliable. Specifically, for the ith element of a sample $x_{(i)}$ of size n, sorted in ascending order, $F(x_{(i)})$ and $(2F(x_{(i)}) - 1)$ are estimated as:

$$\widehat{F}(x_{(i)}) = \frac{i-1}{n-1}, \quad 2\widehat{F}(x_{(i)}) - 1 = \frac{2i-n-1}{n-1} \tag{3.14}$$

taking values in [0,1] and [-1,1], respectively, irrespective of the values $x_{(i)}$. Hence, the estimators of K-moments are:

$$\widehat{K}'_{pq} = \frac{p - q + 1}{n} \sum_{i=1}^{n} \left(\frac{i - 1}{n - 1}\right)^{p-q} \underline{x}_{(i)}^{q} \tag{3.15}$$

$$\widehat{K}_{pq} = \frac{p - q + 1}{n} \sum_{i=1}^{n} \left(\frac{2i - n - 1}{n - 1}\right)^{p-q} (\underline{x}_{(i)} - \hat{\mu})^{q} \tag{3.16}$$

The rationale of the definition is very relatively easy to grasp. Assuming that the distribution mean is close to the median, so that $F(\mu) \approx 1/2$ (this is precisely true for a symmetric distribution), the quantity whose expectation is taken from the definition of the central K-moment of order (p, q) is: $A(\underline{x}) := (2F(\underline{x}) - 1)^{p-q}(\underline{x} - \mu)^{q}$ and its Taylor expansion is:

$$A(\underline{x}) = (2f(\mu))^{p-q}(\underline{x} - \mu)^{p} + (p - q)(2f(\mu))^{p-q-1}f'(\mu)(\underline{x} - \mu)^{p+1}$$
$$+ O((\underline{x} - \mu)^{p+2}) \tag{3.17}$$

where $f(x)$ is the probability density function of $\underline{x}$. Clearly then, K_{pq} depends on μ_p as well as on classical moments of $\underline{x}$ of order higher than p. The independence of K_{pq} from classical moments of order smaller than p is the reason why it is a competent surrogate of the unknowable μ_p.

In addition, as p becomes large, by virtue of the multiplicative term $(p - q + 1)$ in the definition of K-moments, K_{pq} shares similar asymptotic properties with $\hat{\mu}_p^{q/p}$ (the estimate, not the true $\mu_p^{q/p}$). To illustrate this for $q = 1$ and for independent variables $\underline{x}_i$, we consider the variable $\underline{z}_p := max_{1 \leq i \leq p}\underline{x}_i$ and denote $f()$ and $h()$ the probability densities of $\underline{x}_i$ and $\underline{z}_i$ respectively. Then (Papoulis, 1990):

$$h(z) = pf(z)(F(z))^{p-1} \tag{3.18}$$

and thus, by virtue of the definition of non-central *K-moment* of order (p, q):

$$E[\underline{z}_p] = pE[(F(\underline{x}))^{p-1}\underline{x}] = K'_{p1} \tag{3.19}$$

On the other hand, for positive $\underline{x}$ and large $p \to n$,

$$\left(E\left[\widehat{\underline{\mu'}_P}\right]\right)^{1/p} = \left(E\left[\left(\frac{1}{n}\sum_{i=1}^n \underline{x_i}^p\right)\right]\right)^{1/p}$$

$$\approx \left(E\left[\left(\frac{1}{n}max_{1\leq i\leq n}(x_i^p)\right)\right]\right)^{1/p} \qquad (3.20)$$

$$\approx n^{-1/p}E\left[max_{1\leq i\leq n}(\underline{x_i})\right] \approx E\left[\underline{z}_n\right]$$

It is also worth noting that the multiplicative term $(p - q + 1)$ in the definitions of central and non-central K_{pq} and K'_{pq} makes K-moments generally increasing functions of p.

Furthermore, a pivotal point of K-moments theory is their asymptotic properties of their estimates. The following rules apply:

- In general, as p becomes large approaching n^*, estimates of both classical and K moments, central or non-central, become estimates of expressions involving extremes such as $\left(max_{1\leq i\leq p}x_i\right)^q$ or $max_{1\leq i\leq p}(x_i - \mu)^q$. For negatively skewed distributions these quantities can also involve minimum, instead of maximum quantities.

- For the K-moments, this is consistent with their theoretical definition. For the classical moments this is an inconsistency.

- A common property of both classical and K moments is that symmetrical distributions have all their odd moments equal to zero.

- For unbounded variables, both classical and K moments are non-decreasing functions of p, separately for odd and even p.

- In geophysical processes it is justifiable to assume that the variance $\mu_2 \equiv \gamma_1 \equiv \sigma^2 \equiv K_{22}$ is finite (since an infinite variance would presuppose infinite energy to materialize, which is absurd). Thus, high order K-moments K_{p2} will be finite as well, even if classical moments μ_p diverge to infinity beyond a certain p (i.e., in heavy tailed distributions).

K-moments have not been constructed in such a way as to be isolated from other moments, but have an integral relationship with them, which stems from their definition.

- The classical moments can be recovered as a special case of K-moments: $M_p \equiv K_{pp}$. In particular, in uniform distribution, classical and K-moments are proportional to each other:

$$K'_{pq} := (p - q + 1)\mu'_p, \; K_{pq} := (p - q + 1)\mu_p$$

- The probability weighted moments (PWM) can also be recovered from the K-moments. The typical PWM form $\beta_p := E\left[\underline{x}(F(\underline{x}))^p\right]$ is a special case of K-moments corresponding to $q = 1$:

$$K'_{p1} = p\beta_{p-1}$$

- The L-moments are defined as $\lambda_p := \frac{1}{p}\sum_{k=0}^{p-1}(-1)^k\binom{p-1}{k}E[\underline{x}_{(p-k):p}]$, where $\underline{x}_{k:p}$ is the kth order statistic in a sample of size p. L-moments are also related to PWM and through them to K-moments. The relationships for the different types of moments for the first four orders are:

$K'_{11} = \mu = \beta_0, \quad K_{11} = 0$

$K'_{21} = 2\beta_1, \qquad K_{21} = 2(K'_{21} - \mu) = 4\beta_1 - 2\beta_0 = 2\lambda_2$

$K'_{31} = 3\beta_2, \qquad K_{31} = 4(K'_{31} - \mu) - 6(K'_{21} - \mu) = 12\beta_2 - 12\beta_1 + 2\beta_0 = 2\lambda_3$

$K'_{41} = 4\beta_3, \qquad K_{41} = 8(K'_{41} - \mu) - 16(K'_{31} - \mu) + 12(K'_{21} - \mu) = 32\beta_3 - 48\beta_2 + 24\beta_1 - 4\beta_0 = \frac{8}{5}\lambda_4 + \frac{12}{5}\lambda_2$

- Both PWM and L-moments are better estimated from samples than classical moments but they are all of first order in terms of the random variable of interest. PWM and L-moments are good to characterize independent series or to infer the marginal distribution of stochastic processes, but they cannot characterize even second order dependence of processes; K-moments can.

Within the framework of K-moments, while respecting the rule of thumb "Just two moments" in terms of the power of $\underline{x}$, i.e. $q = 1$ or 2, it is easy to obtain knowable statistical characteristics from much (even enormously) higher orders p.

In this manner, for $p > 1$ there are two alternative options to define statistical characteristics related to moments of the distribution, as in the following table. Whichever of the two option is to be used for the estimation of the statistical characteristics depends

on the statistical behavior, and in particular, the mean, mode and variance of the estimator (Koutsoyiannis, 2019).

Table 3.2 Characteristics of marginal distribution using K-moments

Characteristic	Order p	Option 1	Option 2
Location	1	$K'_{11} = \mu$ (*the classical mean*)	
Variability	2	$K_{21} = 2(K'_{21} - \mu)$ $= 2\lambda_2$	$K_{22} = \mu_2 = \sigma^2$ (*the classical variance*)
Skewness	3	$\dfrac{K_{31}}{K_{21}} = \dfrac{\lambda_3}{\lambda_2}$	$\dfrac{K_{32}}{K_{22}}$
Kurtosis	4	$\dfrac{K_{41}}{K_{21}} = \dfrac{4}{5}\dfrac{\lambda_4}{\lambda_2} + \dfrac{6}{5}$	$\dfrac{K_{42}}{K_{22}}$

3.5 Return periods

Let $Z(\tau)$ be a stochastic process that characterizes a natural process evolving in continuous time τ. As human instruments cannot make observations at truly continuous time, these observations are made in discrete time defined by constant time intervals $\Delta\tau$. This interval is therefore considered to be the unit of time. By sampling $Z(\tau)$, we consider the corresponding discrete-time process at spacing $\Delta\tau$ (Volpi et al., 2015):

$$Z_j = Z(j\Delta\tau) \tag{3.21}$$

where $j(=1,2,3,...)$ denotes discrete time. For ease of understanding, let $t = j - j_0$ be the expression of discrete time, where j_0 is the current time step. By extending this notion, the discrete-time process is indicated as Z_t and $t = 0$ denotes the present time. In order for the process to be fully describable up to the second order properties by its marginal probability function and its autocorrelation structure, we need to assume that Z_t is a stationary process (Papoulis, 1991).

We are interested in possible exceedances of the values of process Z_t above or below a specific level (threshold) z, which may determine the extremity or not of a specific observation. In particular, let $A = \{Z > z\}$ be a dangerous event, which is an extreme. A could very well be either maximum or minimum. We denote by p the probability of the event $B = \{Z \leq z\}$, which is the complement set of A; the probability of occurrence of event A is given by $1 - p = \Pr\{Z > z\} = PrA$.

In civil engineering applications, it is usually assumed that the event A will occur on average every return period T, where T is a time interval (Volpi et al., 2015). For example, a great-magnitude earthquake or a flash-flood event occur on average every T time. In other words, the average time until the threshold z is met, or exceeded, equals T years (Stedinger et al., 1993), such as:

$$\frac{T}{\Delta\tau} = \mathrm{E}[X] = \sum_{t=1}^{\infty} t f_X(t) \tag{3.22}$$

where X is the number of discrete time steps required for an event A to occur, $f_X(t) = \Pr\{X = t\}$ is the probability mass function and $\mathrm{E}[\ ]$ denotes expectation. The above definition of return period of an event logically reasonably to the formulation of the *probability of failure* $R(l)$, which measures the probability that the event A occurs at least once over a specific time span: the design life or study period l of a system, where $l/\Delta\tau$ is a positive integer. The mathematic relationship engulfing the aforementioned definitions is as follows:

$$R(l) = \Pr\left\{X \leq \frac{l}{\Delta\tau}\right\} = \sum_{t=1}^{1/\Delta\tau} f_X(t) \tag{3.23}$$

At this point, it is easy to deduce that the probability of failure $R(l)$ is nothing else than the distribution function computed at $t = l/\Delta\tau$.

As it can be easily understood, order statistics have a substantial advantage over other statistics in the context of return periods, as we can assign a distinct value of the distribution function to each one of them, hence pair them with the equivalent return

period. This turns out to be the case with K-moments as well, as they are closely related to order statistics. Intuitively, we anticipate that the return period corresponding to the non-central K-moment of orders $(p, 1)$, the value $x = K'_{p1}$ will correspond to a return period of about $2p$. This is accurate for a symmetric distribution and for $p = 1$, as K'_{11} is the mean value, which has return period 2, and as explained by Koutsoyiannis (2019), it cannot be much lower than $2p$ for any p and for any distribution.

Generally, the return period can be expressed by the relationship:

$$\frac{T(K'_{p1})}{D} = \Lambda_p p \tag{3.24}$$

where D is a time reference for the specification of return period and Λ_p is a coefficient generally depending on the distribution function and the order p.

The precise definition of Λ_p is (Koutsoyiannis, 2019):

$$\Lambda_p := \frac{1}{p\big(1 - F(K'_{p1})\big)} \tag{3.25}$$

For given p and distribution function $F(x)$, K'_{p1} is analytically or numerically determined from its definition. Then $T(K'_{p1})$ and Λ_p are determined from their definitions.

In absence of an analytical solution, an exact relationship between p and T has been established by doing numerical calculations for several p. The slight variation of Λ_p with p can be very well approximated if first the specific values Λ_1 and Λ_∞ are accurately determined. The value of Λ_1 is easily determined, as practically is equal to the return period of the mean:

$$\Lambda_1 = \frac{1}{1 - F(\mu)} = \frac{T(\mu)}{D} \tag{3.26}$$

In addition, in a number of customary distributions, specifically those belonging to the domain of the Extreme Value Type 1 distribution, Λ_∞ has a constant value, independent of the distribution. As shown by Koutsoyiannis (2019), this value is:

$$\Lambda_\infty = e^\gamma = 1.781 \tag{3.27}$$

where γ is the Euler–Mascheroni constant.

For the approximation of Λ_p, the following simple relationship is used, which is satisfactory for several distributions:

$$\Lambda_p \approx \Lambda_\infty + (\Lambda_1 - \Lambda_\infty)\frac{1}{p} \tag{3.28}$$

This yields a linear relationship between the return period T and p:

$$\frac{T(K'_{p1})}{D} = p\Lambda_p \approx \Lambda_\infty p + (\Lambda_1 - \Lambda_\infty) \tag{3.29}$$

For the Normal distribution, which most closely resembles the real distribution of the surface temperature, the approximated values of Λ_1 and Λ_∞ are: $\Lambda_1 = 2$ and $\Lambda_\infty = e^{1/2} = 1.649$.

However, in some distributions, like the lognormal and Weibull, the decays of Λ_p with increasing p is very slow. Furthermore, in some cases Λ_p is not always a decreasing function of p, as implied by its relationship with Λ_∞. To account for such cases, the definition of Λ_p is generalized to the form:

$$\Lambda_p = \Lambda_\infty + (a_p\Lambda_1 - \Lambda_\infty)\beta_p \tag{3.30}$$

where a_p and β_p are non-increasing functions of p, such that $a_1 = \beta_1 = 1$ and $lim_{p\to\infty}\beta_p = 0$. Generally, if $a_p = 1$ then the above equation is again a monotonic (decreasing) function of p for all values of p. A criterion to decide whether this is the case for a particular distribution requires at least one more Λ value, most conveniently Λ_2. The following criterion (related to the convexity of the curve of Λ_p as a function of $1/p$) has been tested and found suitable

$$C_T = \frac{\frac{\Lambda_1 + \Lambda_\infty}{2} - \Lambda_2}{\Lambda_1 - \Lambda_2} \tag{3.31}$$

The monotonic property holds when $C_T < 0$. In this case the following approximations were tested on both the lognormal and Weibull distribution and found satisfactory

$$a_p = 1, \qquad \beta_p \approx \left(\frac{\ln(1+c_1)}{\ln(p+c_1)}\right)^{c_2}, \qquad c_1 = 1.4, \qquad c_2 = 1.9 - 1.1\sqrt{|C_T|}$$

69

When $C_T < 0$, Λ_p initially decreases with p, but for larger values of p becomes and increasing function. In this case, the approximation takes the form:

$$a_p = \frac{1}{p^{0.16}}, \qquad \beta_p \approx \left(\frac{\ln(1+c_1)}{\ln(p+c_1)}\right)^{c_2}, \qquad c_1 = 3.5, \qquad c_2 = 2.4 - 1.1\sqrt{|C_T|}$$

Summarizing the above, Λ-coefficients have the following important properties:

- They vary in a narrow range (close to 2) and this facilitates the determination of the complete series by only a few of them (namely, Λ_1 and Λ_∞, and occasionally Λ_2).
- They are well approximated by generic functions, irrespective of the particular distribution function.
- Their definition in terms of return period renders them suitable for studying extreme values, as is the case of the present study of land surface air temperature.
- Moreover, their definition, in connection to their generic approximators, supports the indirect but quick determination of theoretical (true) values of K-moments of any order in absence of analytical relationships.

The last property indicates that a similar approach can be followed for the calculation of K-moments for higher values of q. Specifically, an alteration of the precise definition of Λ_p for precisely calculating the Λ-coefficients of orders (p, q) is:

$$\Lambda'_{pq} := \frac{1}{(p - q + 1)\left(1 - F\left(K'^{1/q}_{pq}\right)\right)} \tag{3.32}$$

for non-central moments, while for central ones is:

$$\Lambda_{pq} := \frac{1}{(p - q + 1)\left(1 - F\left(K^{1/q}_{pq} + \mu\right)\right)} \tag{3.33}$$

It is easily observable that for $q = 1$:

$$\Lambda'_{p1} = \Lambda_{p1} = \Lambda_p \tag{3.34}$$

as is $K'_{p1} = K_{pq} + \mu$. However, for $q > 1$, $\Lambda'_{p1} \neq \Lambda_{p1}$, except in the limit as $q \to \infty$. Like the Λ-coefficients of $q = 1$, Λ_{pq} will also vary in a narrow range. In particular, as the tail index of the distribution of $\underline{x}^q$ will be qk, the limit $\Lambda'_{\infty q} = \Lambda_{\infty q}$ can be readily determined.

3.6 Optimization

A significant part of theory of optimization is the definitions of a real function of a vector variable and maxima conditions of a function.

Real function of a vector variable

Let us assume f to be a real function of a vector variable, such that $f : \mathbb{R}^n \to \mathbb{R}$

The derivative of function f with respect to the vector variable $\mathbf{x}$ is given by the vector:

$$\frac{df}{d\mathbf{x}} := \left[\frac{df}{dx_1}, \frac{df}{dx_2}, \dots, \frac{df}{dx_n} \right] \tag{3.35}$$

The gradient of function $f(\mathbf{x})$ of vector variable $\mathbf{x}$ is given by vector (Marlow, 1993):

$$grad(f) := \nabla f = \left[\frac{df}{dx_1}, \frac{df}{dx_2}, \dots, \frac{df}{dx_n} \right]^T = \left(\frac{df}{d\mathbf{x}} \right)^T \tag{3.36}$$

The second derivative of $f(\mathbf{x})$ of vector variable $\mathbf{x}$ is given by the Hessian matrix (Gunning and Rossi, 1965):

$$\frac{d^2 f}{d\mathbf{x}^2} = \begin{bmatrix} \dfrac{\partial^2 f}{\partial x_1^2} & \dfrac{\partial^2 f}{\partial x_1 \partial x_2} & \cdots & \dfrac{\partial^2 f}{\partial x_1 \partial x_n} \\ \dfrac{\partial^2 f}{\partial x_2 \partial x_1} & \dfrac{\partial^2 f}{\partial x_2^2} & \cdots & \dfrac{\partial^2 f}{\partial x_2 \partial x_n} \\ \vdots & \vdots & \ddots & \vdots \\ \dfrac{\partial^2 f}{\partial x_n \partial x_1} & \dfrac{\partial^2 f}{\partial x_n \partial x_2} & \cdots & \dfrac{\partial^2 f}{\partial x_n^2} \end{bmatrix} \tag{3.37}$$

Extrema of a function

In mathematics, the maxima and minima of a function f, known collectively as extrema, are the largest and smallest value of the function, either within a given (i.e. bounded) range, or on the entire domain of the function (Stewart, 2008; Larson and Edwards, 2009).

Let us assume $f(\mathbf{x})$ to be a real function of a vector variable, which is continuous $\forall\, \mathbf{x} \in \mathbb{R}^n$. In these conditions, the problem of finding the minimum value of function f evolves into finding the vector $\mathbf{x}$, such that:

$$f(\mathbf{x}_*) = min[f(\mathbf{x})] \tag{3.38}$$

In order for $\mathbf{x}_*$ to be the global minimum of function f, the following necessary conditions have to be met:

- $\mathbf{x}_*$ has to be stationary point of function f, meaning:

$$\left(\frac{df(\mathbf{x}_*)}{d\mathbf{x}}\right) = \mathbf{0}^T \tag{3.39}$$

- The Hessian matrix of function f has to be positive definite matrix in point $\mathbf{x}_*$:

$$\mathbf{y}^T \left(\frac{d^2 f(\mathbf{x}_*)}{d\mathbf{x}^2}\right)\mathbf{y} > 0 \quad \forall\, \mathbf{y} \in \mathbb{R}^n - \{0\} \tag{3.40}$$

The aforementioned necessary conditions are sufficient, in the case that function f is convex, namely in the case that its Hessian matrix is positive definite for every $\mathbf{x}$,

$$\mathbf{y}^T \left(\frac{d^2 f(\mathbf{x}_*)}{d\mathbf{x}^2}\right)\mathbf{y} > 0 \quad \forall\, \mathbf{x} \in \mathbb{R}^n, \forall\, \mathbf{y} \in \mathbb{R}^n - \{0\} \tag{3.41}$$

If this is not the case, $f(\mathbf{x})$ may have more than one stationary points, which, as shown in the following figure, could be local minima (a), local maxima (b) or neither of the above; the latter-case points are named saddle points (c).
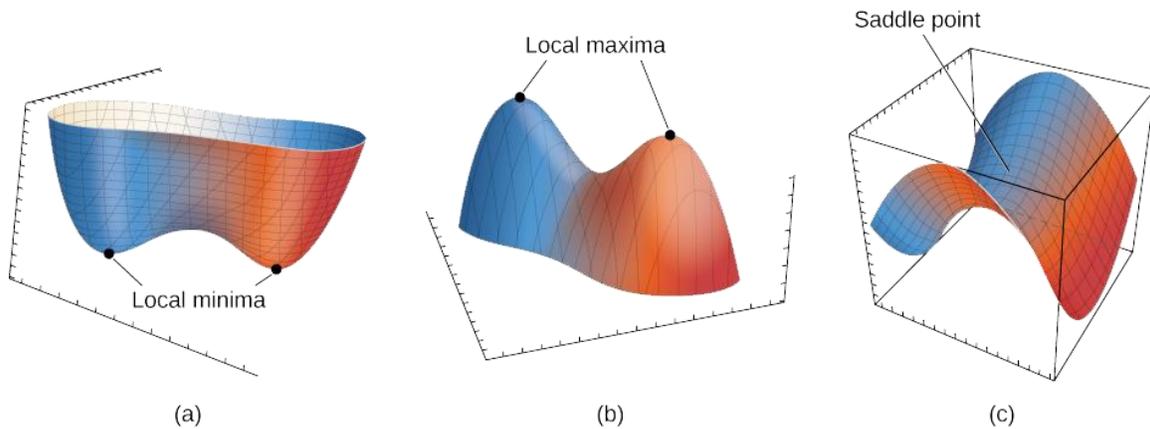
Figure 3.1 Cases of more than one-stationary points of a function. (a) Local minima, (b) Local maxima, (c) Saddle point | Source: LibreTexts library

There are numerous algorithms used worldwide to find an optimum solution to a problem, whose numerical solution is too hard, or time and resource consuming to calculate. One such method is gradient-based – a technique of optimization, which uses the differentials of the objective function. Sometimes optimization problems do have constraints, but this is not always the case. Problems without constraints, ordinary differential calculus method is considered to be the best approach in achieving an optimum solution. Problems that do have constraints can be solved using differential calculus methods (such as Lagrangean and Kuhn-Tucker) and search methods (such as Linear Programming).

Generalized Reduced Gradient algorithm (GRG2)

The Generalized Reduced Gradient method belongs to a family of optimization techniques called reduced-gradient methods, which are based on extending methods for linear constraints to apply to non-linear constraints (Gill et al., 1981). The reduced-gradient methods adjust the variables, in order for the active constraints to continue to be satisfied, as the optimization process moves from one point to another.

The GRG2 scheme is based on the concept of eliminating variables using the equality constraints imposed. The idea of generalized reduced gradient method is to convert the

constrained problem into an unconstrained one through the use of direct substitution (Arum, 2014).

Many commercial spreadsheet programs use the Generalized Reduced Gradient (GRG2) algorithm for optimizing problems. They do so, by combining the functions of a graphical user inter-phase (GUI) and algebraic modelling language for linear, nonlinear and integer programs.

Evolutionary algorithm

One of the most widely used optimization algorithms is the evolutionary algorithm. Evolutionary algorithm is a subset of evolutionary computation method, which uses mechanisms inspired by biological processes, such as reproduction, mutation, recombination and natural selection, in order to find the optimal solution to the problem.

The inspired-by-nature procedures being used by an Evolutionary Algorithm are:

- Population: Contrary to most classical optimization methods, which maintain a single best solution at each stage of the optimization, an evolutionary algorithm maintains a population of candidate solutions. Only one of these individual solutions is the "best", but the other members of the population act as "sample points" in other regions of the search space, from which a better solution may later derive from.
- Randomness: An evolutionary algorithm relies on random sampling, so as to minimize, or nearly eliminate, the bias in choosing which individual solutions to "reproduce" for the next repetition of the optimization method. In addition, random choice traverses all the mechanisms of the algorithm, from the possibility of mutation to reproduction.
- Mutation: Inspired by the mechanisms of mutating specific parts of the genetic code in natural evolution, the evolutionary algorithm periodically, yet randomly, makes specific changes to parts of the "genome" of each solution. This mutation

usually yields genetically inferior; i.e. worst, solutions, but it is extremely useful of disengaging the algorithm from trapping in local minima of the search space.

- Crossover: Like in the natural world, where sexual reproduction promotes useful genes to the next generation by combining genes from two different parents, an evolutionary algorithm attempts to combine elements of existing solutions, in order to produce superior solutions. The elements (e.g. decision-making values) of existing solutions of the population are combined in a "crossover" operation, resulting in a solution with mixed attributes from both "parent" solutions.

- Selection: Much like in natural selection of organisms, an evolutionary algorithm performs a selection process, in which the most "competent" members of the population survive, and the least "competent" members are eliminated. In a constrained optimization process, the notion of "competence" depends partly on the feasibility of the solution and partly on its objective function value. The selection process is the step that leads the evolutionary algorithm towards ever-improving solutions.

Since evolutionary algorithms are a time-consuming process, the operation of the algorithm stops, when an adequately "good" accurate solution of the target function has been achieved.

The following figure presents a schematic representation of the basic processes an evolutionary algorithm uses to find the optimum solution.
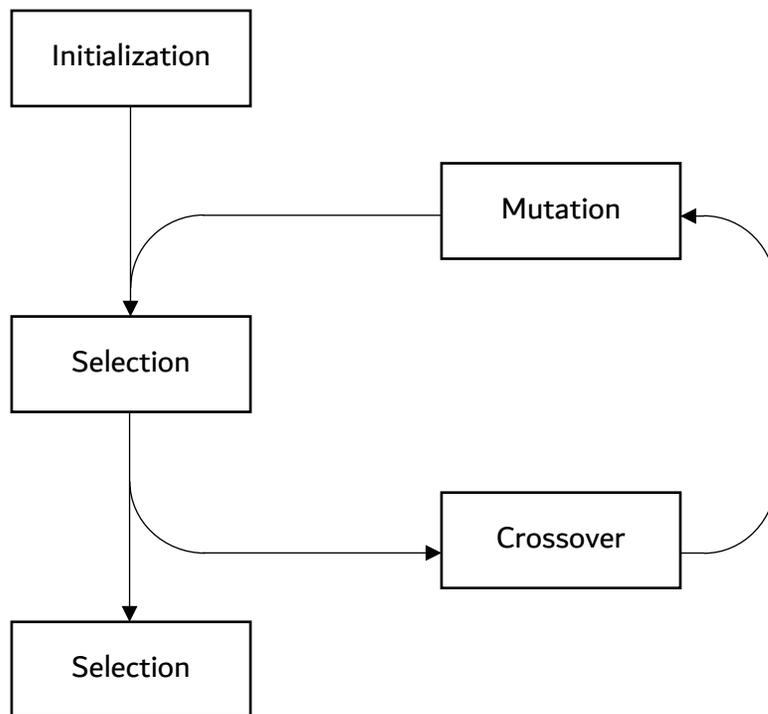
Figure 3.2 General scheme of an evolutionary algorithm

3.7 Stochastic simulation

Stochastic simulation (also known as Monte-Carlo simulation) is an important computerized mathematical technique for resolving problems that have no analytical solution, or whose analytical solution is an extremely time and resource-consuming process. A pivotal point of the simulation is the production of synthetic timeseries. In the case of a stationary stochastic process with long-term persistence, like temperature timeseries, the production of synthetic timeseries requires the preservation of such behavior. An elaborate method of doing so, is the symmetric moving average scheme.

The symmetric moving average (SMA) method (Koutsoyiannis, 2000; Koutsoyiannis, 2016) can exactly simulate a Gaussian process, with no limitations to its arbitrary autocovariance function (provided that it is mathematically feasible). In addition, it can

approximate, with controlled accuracy, any non-Gaussian stochastic process with an arbitrary autocovariance function and any marginal distribution function.

Like the conventional (backward) moving average (MA) process, the SMA scheme transforms a white noise sequence V_i into a process with autocorrelation by taking the weighted average of a number of V_i. In the SMA process, the weights a_j are symmetrical about a center (a_0), that corresponds to the variable V_i, i.e.:

$$X_i = \sum_{j=-q}^{q} a_{|j|} V_{i+j} = a_q V_{i-q} + \ldots + a_1 V_{i-1} + a_0 V_i + a_1 V_{i+1} + \ldots + a_q V_{i+q} \qquad (3.42)$$

where q theoretically is infinity, but, in practice, is restricted to a finite number, as the sequence of weights a_j tends to zero for increasing j. Furthermore, as shown by Koutsoyiannis (2000), the discrete Fourier transform $s_a(\omega)$ of the a_j sequence is related to the power spectrum of the process $s_\gamma(\omega)$ by:

$$s_a(\omega) = \sqrt{2s_\gamma(\omega)} \qquad (3.43)$$

which enables the direct calculation of $s_a(\omega)$, which in the case of FGN will be:

$$s_a(\omega) \approx 2\sqrt{(2-2H)\gamma_0 (2\omega)^{0.5-H}} \qquad (3.44)$$

Knowing that the power spectrum of a process can by derived as:

$$s_\gamma^{(k)}(\omega) = 2\sum_{j=-\infty}^{\infty} \gamma_j^{(k)} \cos(2\pi j\omega) \approx 4\int_0^\infty a\tau^{2H-2} \cos(2\pi\tau\omega)\, d\tau \qquad (3.45)$$

which, in order to preserve exactly the process variance γ_0, can be rewritten as:

$$s_\gamma^{(k)}(\omega) = 4(1-H)\gamma_0^{(k)}(2\omega)^{1-2H} \qquad (3.46)$$

it is observable that $s_a(\omega)$ is approximately equal to the power spectrum of another FGN process with Hurst exponent $H' = (H + 0.5)/2$ and variance a_0. As shown by Koutsoyiannis (2000), the approximation of the inverse Fourier transform of $s_a(\omega)$, i.e. the sequence of a_j itself, is:

$$a_0 = \frac{\sqrt{(2-2H)\gamma_0}}{1.5-H}, \quad a_j \approx \frac{a_0}{2}[(j+!)^{H+0.5} + (j-1)^{H+0.5} - 2j^{H+0.5}] \quad j > 0$$

The generation scheme of SMA with coefficients a_j can lead to a very easy algorithm for generating FGN. This method can also preserve the process skewness ξ_X by appropriately choosing the skewness of the white noise ξ_V. As for the weights a_j, there are $q+1$ in number, so that the model can preserve the first $q+1$ terms of the autocovariance γ_j of the process X_i. The relevant equations for the statistics of V_i are:

$$\left(a_0 + 2\sum_{j=1}^{s} a_j\right)E[V_i] = \mu, \quad var[V_i] = 1, \quad \left(a_0^3 + 2\sum_{j=1}^{q} a_j^3\right)\xi_v = \xi_x\gamma_0^{3/2}$$

The number q must be chosen wisely, so as to be at least equal to the desired number of autocorrelation coefficients m that are to be preserved. In addition, the ignored terms a_j beyond a_q must not exceed an acceptable tolerance βa_j. These two conditions, in combination with the terms of the sequence a_j, result in:

$$q \geq max\left[m, \left(\frac{H^2 - 0.25}{2\beta}\right)^{1/1.5-H}\right] \tag{3.47}$$

The number q can be very high (thousands or even hundreds of thousands) if H is large (e.g. $H > 0.9$) and β is small (e.g. $\beta < 0.001$). The accuracy of the method depends on q. However, even when $q \to \infty$, the method does not become exact, because of its approximate character. Despite Koutsoyiannis (2000) having introduced even more accurate estimates of the a_j series, which can be obtained numerically, the given estimates are sufficiently accurate for the purpose of this study. This is verified by the following figure, where theoretical and approximate autocorrelation functions are almost indistinguishable for all H-coefficients.
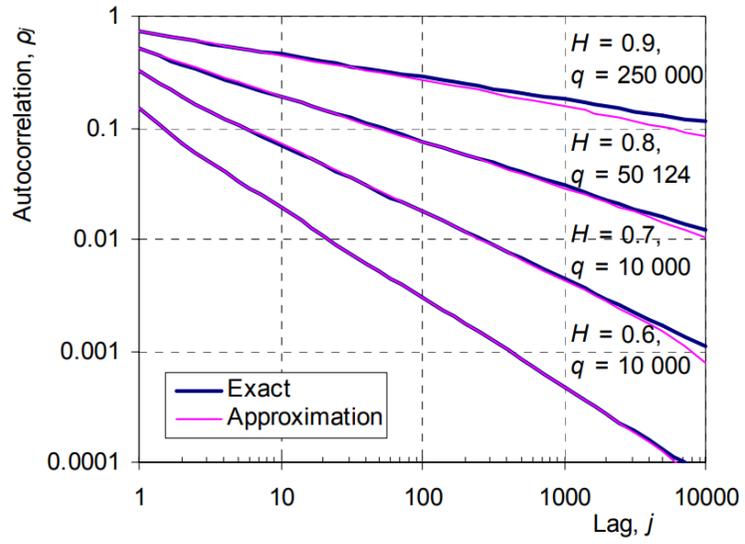
Figure 3.3 Approximate autocorrelation functions based on equations of SMA scheme versus the exact autocorrelation functions of Fractional Gaussian Noise for various values of the Hurst exponent H and the number of weights q. | Source: Koutsoyiannis (2002)

4. Computational tools

4.1 MathWorks Matlab

MATLAB is a programming platform designed by MathWorks specifically for engineers and scientists. It integrates computation, visualization, and programming in an easy-to-use environment where problems and solutions are expressed in familiar mathematical notation. MATLAB is an interactive system whose basic data element is an array that does not require dimensioning. This allows you to solve many technical computing problems, especially those with matrix and vector formulations, in a fraction of the time it would take to write a program in a scalar noninteractive language such as C or Fortran.

In this study we took advantage of the efficiency and array structure of MATLAB programming, in order to perform complex scientific calculations in a large amount of length air temperature time-series. Specifically, the functions of the Statistics and Machine Learning and Optimization toolboxes of the MATLAB, that we used are the following:

- beta: B = beta(Z,W) returns the beta function evaluated at the elements of Z and W. Both Z and W must be real and nonnegative.
- exp: Y = exp(X) returns the exponential e^x for each element in array X.
- factor: f = factor(n) returns a row vector containing the prime factors of n. Vector f is of the same data type as n.
- fsolve: Nonlinear system solver. Solves a problem specified by F(x) = 0 for x, where F(x) is a function that returns a vector value. and x is a vector or a matrix
  x = fsolve(fun,x0) starts at x0 and tries to solve the equations fun(x) = 0, an array of zeros.
- gamma: Y = gamma(X) returns the gamma function evaluated at the elements of X.
- gammaln: Y = gammaln(A) returns the logarithm of the gamma function, gammaln(A) = log(gamma(A)). Input A must be nonnegative and real. The

gammaln command avoids the underflow and overflow that may occur if it is computed directly using the expression log(gamma(A)).

- nanvar: y = nanvar(X) is the variance var of X, computed after removing NaN values. For vectors x, nanvar(x) is the sample variance of the remaining elements, once NaN values are removed. For matrices X, nanvar(X) is a row vector of column sample variances, once NaN values are removed. nanvar removes the mean from each variable (column for matrix X) before calculating y. If n is the number of remaining observations after removing observations with NaN values, nanvar normalizes y by either n − 1 or n, depending on whether n > 1 or n = 1, respectively.

- norminv: x = norminv(p) returns the inverse of the standard normal cumulative distribution function (cdf), evaluated at the probability values in p.

- quantile: Y = quantile(X,p) returns quantiles of the elements in data vector or array X for the cumulative probability or probabilities p in the interval [0,1]

- rand: X = rand returns a single uniformly distributed random number in the interval (0,1).

- sort: B = sort(A) sorts the elements of A in ascending order. If A is a vector, then sort(A) sorts the vector elements.

4.2 Microsoft Excel

Microsoft Excel is a software program produced by Microsoft that allows users to organize, format and calculate data with formulas using a spreadsheet system. Excel has the same basic features as all spreadsheet applications, which use a collection of cells arranged into rows and columns to organize and manipulate data. They can also display data as charts, histograms and line graphs.

Excel includes a tool called "solver" that uses techniques from the operations research to find optimal solutions for all kind of decision problems. "Solver" works with a group of cells, called decision variables or simply variable cells, that are used in computing the formulas in the objective and constraint cells. "Solver" adjusts the values in the decision

variable cells to satisfy the limits on constraint cells and produce the desirable result for the objective cell. One of the many advantages of the "solver" plug-in of Microsoft Excel is the ability to solve non-linear programming problems using a variety of solving methods, including the Generalized Reduced Gradient and the Evolutionary method.

The Excel solver has three primary components, all of whom are integral parts of the optimization process. These components are:

- Target cell: This cell represents the goal or ultimate objective of the problem expresses in mathematical formulation. As part of this study, the target cell had to be minimized as possible.
- Variable cells: These cells can and are modified, in order for the target cell to achieve its optimal values.
- Constraints: There are limitations to what values the solver can assign to the variable cells in order to optimize the solution. Most of the constraints are natural (e.g. temperature has an absolute minimum), while others are for practicality, since the approximate domain of the solution can be approximated.

It is worth mentioning, that while optimization could have been performed in MathWorks MATLAB environment, we preferred the use of spreadsheet, so as to be able to evaluate the intermediate results of the optimization procedure, before it concludes.

5. Data

In the current study we focus on temperature persistence patterns on different time scales and, in order for the study to be complete, we pursued the usage of daily temperature data, instead of hourly or monthly aggregated values. There are many databases offering the required data, but we preferred the GHCND database (Menne et al., 2012) offered by the National Oceanic and Atmospheric Administration of the Federal Government of the United States, since it offers an extended directory of very long time series from around the globe.

5.1 Database

GHCN (Global Historical Climatology Network)-Daily is a database that addresses the critical need for historical daily temperature, precipitation, and snow records over global land areas. GHCN-Daily is a composite of climate records from numerous sources that were merged and then subjected to a suite of quality assurance reviews. It contains temperature records from 106,283 stations in 180 countries and territories. Both the record length and period of record vary be station and cover intervals ranging from less than one year to perennial periods of more than 175 years.

The process, with which the data from multiple resources were integrated into the Global Historical Climatology Network-Daily dataset took place in three consecutive steps:

1. Screening the source data for meteorological stations, whose identity is unknown or questionable. In order for a station within a source dataset to be considered for inclusion in GHCND, it had to meet all of the following criteria:
   - It could be identified with a string of metadata that includes name, latitude, longitude and which accompanied the source dataset.
   - Its record included at least 100 values for more than one of the GHCND elements.

- It did not fail the interstation duplicate check, which eliminated stations with record commonality of more than 50% with any other station.

2. Classifying each station in a source dataset either as one that was already represented in GHCN-Daily or as a new site. Whenever possible, stations were matched on the basis of network affiliation and station identification number. If there was no such match, there was consultation from different networks for existing cross-referenced lists that identify the correspondence of station identification numbers.

3. Mingling the data from the different sources. The implementation of the above classification strategies yielded a list of GHCN-Daily stations and an inventory of the source datasets for integration of each station. This list formed the basis for integrating, or mingling, the data from the various sources to create GHCN-Daily. Mingling took place according to a hierarchy of data sources and in a manner that attempted to maximize the amount of data included while also minimizing the degree to which data from sources with different characteristics were mixed.

5.2 Quality control

As expected of any scientific integrated database, the National Centers for Environmental Information overlooking the gathering, edited and uploaded the GHCND and performed quality control of the data, to avoid specific types of erroneous values. During each reprocessing cycle, the data were first passed through a filter called "format checking program" that examined the date for problems, such as impossible months or days, invalid characters in data fields and so forth. In case the program dealt with such inconsistencies, the routine set the offending records to missing. The primary objective of this program was to ensure that the data integration did not either introduce or retain data records that violated the intended data format of the GHCND. In a next step, a comprehensive sequence of fully-automated QA procedures identified daily values that violated one of the predetermined quality tests. Described in detail by Durre et al. (2010), these quality

tests identified an array of data problems, such as the excessive duplication of the records; exceedance of physical, absolute or climatological limits; immoderate temporal persistence; overwhelmingly large gaps in the distributions of values; internal inconsistencies among elements; and inconsistencies with observations of neighboring weather stations.

The quality tests performed in all the temperature data of the GHCND, as part of the automated QA procedures, in order to identify inconsistencies between them are as follows:

- Naught check: Checked for days on which maximum and minimum temperature were both equal to 0 °C at stations not operated by the United States or were both equal to -17.8 °C (0 °F) at United States stations.

- Duplicate data check: Checked for duplication of the data between entire years, different years in the same calendar month, and different months within the same year.

- World record exceedance check: Identified values that fall outside the world extremes for the highest and lowest ever observed.

- Streak check: Checked for unrealistic sequences of identical values in time series of non-missing values. Flagged sequences of 20 or more consecutive identical values in time series of non-missing daily maximum, minimum, and observation time air temperature.

- Gap check: Identified unrealistic breaks in the period-of-record distribution of elements for a particular calendar month. Flagged maximum/minimum air temperatures that were at least 10 °C warmer or colder than all other corresponding maximum/minimum temperatures for a given station and calendar month.

- Z-score-based climatological outlier check: Checked for daily surface air maximum and minimum temperatures that exceeded the respective 15-day climatological means by at least six standard deviations.

- Internal temperature consistency check: Checked for consistency among maximum, minimum, and time of observation temperature within a three-day window.
- Temporal consistency check (spike or dip) - Checked whether a daily maximum (minimum) temperature exceeded the maximum (minimum) temperatures on the preceding and following days by more than 25 °C.
- Lagged temperature range check: Identified maximum temperatures that were at least 40 °C warmer than the minimum temperatures on the preceding, current, and following days as well as minimum temperatures that were at least 40 °C colder than the maximum temperatures within the three-day window.
- Spatial consistency check (regression): Checked for temperatures that differed greatly from a predicted value generated from a linear-regression-based estimate generated from neighboring values. Flagging of a target temperature was performed when the regression-based predicted value differed by more than 8 °C from the observed value, and the standardized residual of the predicted value exceeded four standard deviations on the target day.
- Spatial consistency check (corroboration of anomalies): Checked for temperatures whose anomalies differed by more than 10 °C from the anomalies at neighboring stations on the preceding, current, and following days.
- Mega consistency check: Flagged daily maximum surface air temperatures that were less than the lowest minimum surface air temperature for the respective station and calendar month; daily minimum temperatures that were greater than the highest maximum temperature for the station and calendar month; and observation-time temperatures that were higher than the highest maximum temperature or lower than the lowest minimum temperature for the station and calendar month.

5.3 Data observations and flags

Each record represents all selected observations (values) available for a given station-day. The initial section of each record is ordered as follows with the following definitions:

- STATION (17 characters) is the station identification code.
- STATION_NAME (max 50 characters) is the name of the station (usually city/airport name). This is an optional output field.
- GEOGRAPHIC_LOCATION (31 characters) is the latitude (decimated degrees w/northern hemisphere values > 0, southern hemisphere values < 0), longitude (decimated degrees w/western hemisphere values < 0, eastern hemisphere values > 0) and elevation above mean sea level (tenths of meters). This is an optional output field as well.
- DATE is the year of the record (4 digits) followed by month (2 digits) and day (2 digits).

Following this initial section of the record, all selected observations and flags are given in the following order: Observation(s) | Measurement Flag | Quality Flag | Source Flag | Time of Observation | repeat for next element (when more than one element is selected).

Observation value is related to the recorded core value. Measurement flag refers to the specific calculation of each data entry from the raw data obtained by the station, and how they were possibly aggregated in time.

Quality Flag (Attribute) of each record entry of air temperature relates to the success or failure of the data to each of the aforementioned quality assurance tests. It could take one of the following values:

Table 5.1 Quality flags (Attributes) of data

Blank	Did not fail any quality assurance check
D	Failed duplicate test
G	Failed gap check
I	Failed internal consistency check
K	Failed streak/frequent-value check
L	Failed check on length of multiday period
M	Failed mega-consistency check
N	Failed naught check
O	Failed climatological outlier check
R	Failed lagged range check
S	Failed spatial consistency check
T	Failed temporal consistency check
X	Failed bounds check
Z	Flagged as a result of an official Datzilla investigation

Source flag refers to the source of the recorded data, in the context of the participating meteorological agencies from all over the world.

Time of Observation is the (2-digit hour, 2-digit minute) 24-hour clock time of the observation given as the local time at the station of record.

For the purpose of this study, we considered useful, and actually utilizable, only blank values of quality flags, thus we dismissed all non-blank quality flagged values from the first stage of data gathering and processing.

5.4 Record data selection

For the investigation of the behavior of surface temperature, we used records of minimum, average and maximum air temperature. We chose these specific meteorological variables,

because they have the most profound impact on ecosystems and the function of human societies. Specifically:

- Minimum temperature affects to a great degree agricultural production, electricity demand for heating and correlates with frost and snow.
- Average temperature relates to the general level of ambience and is characteristic of the average climate of a region.
- Maximum temperature has a profound impact on crop yields, plant growth, forest fires and electricity demand for cooling of living spaces.

In addition, these three variables are available for long time periods, since air temperature was easy to be precisely recorded using mercury thermometers, which was invented by physicist Daniel Gabriel Fahrenheit in Amsterdam (1714).

We derived the data from the pool of 106,283 available weather stations of GHCND from all over the globe, by selecting the most old-living temperature records. Specifically, only stations, whose record starting point preceded the year 1935, were utilized, as they enabled comparison of more than fifty consecutive rolling 30-year periods. Although this limitation, made the pool of utilized temperature records less diverse, yet it enabled us to identify, at various scales, persistence patterns, which would not have been possible with the use of a constantly alternating sample of short records.

From the aforementioned limitation, the number of records that were used is as follows:

- For the study of behavior of the average land surface air temperature we used 245 stations
- For the study of behavior of the maximum land surface air temperature we used 5,006 stations
- For the study of behavior of the minimum land surface air temperature we used 5,006 stations

The following graphs depict the time evolution of the number of the selected weather stations records for each of the three studied parameters.
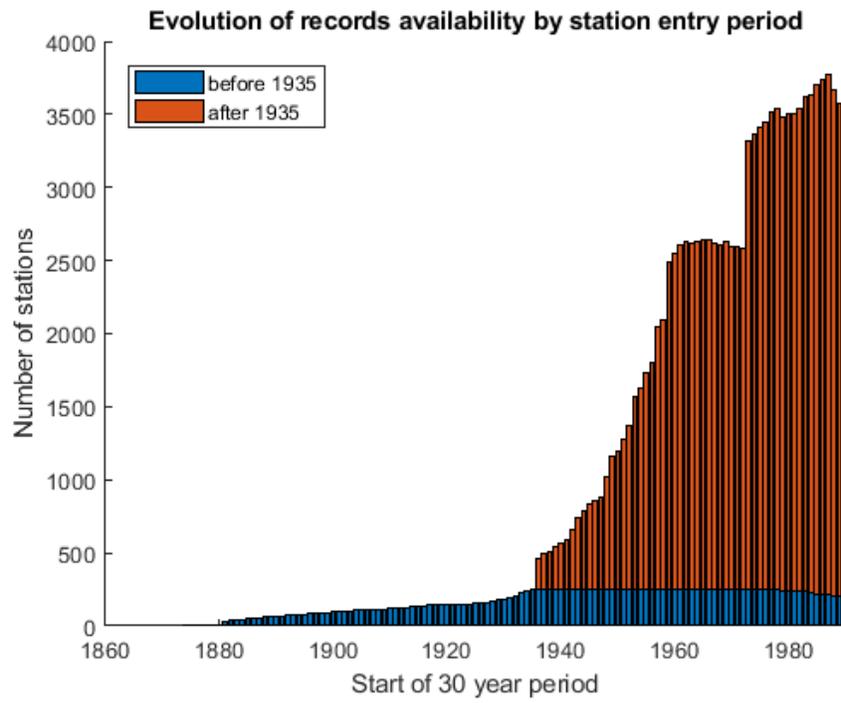
Figure 5.1 Evolution of records availability for the average temperature
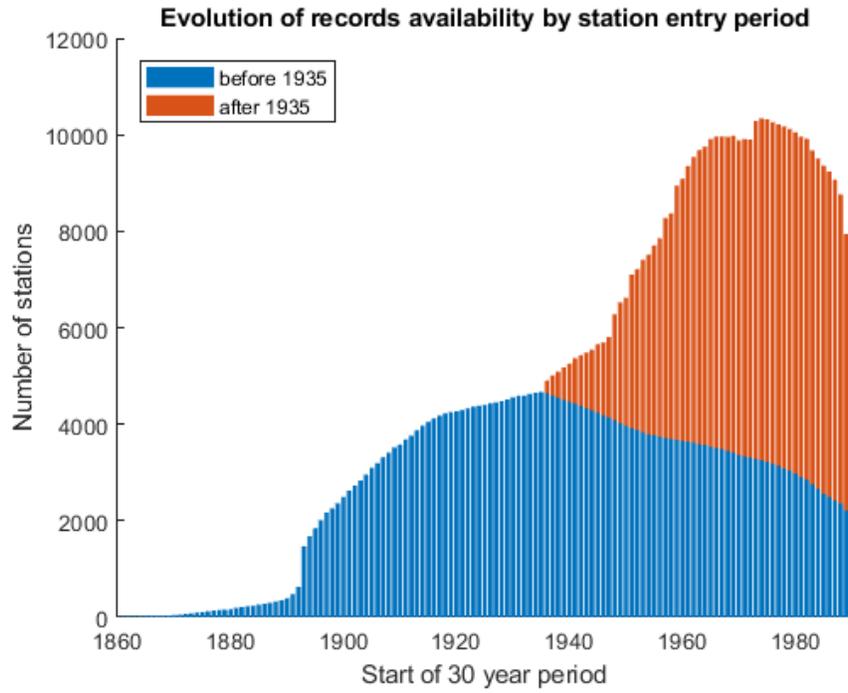
Figure 5.2 Evolution of records availability for the maximum temperature
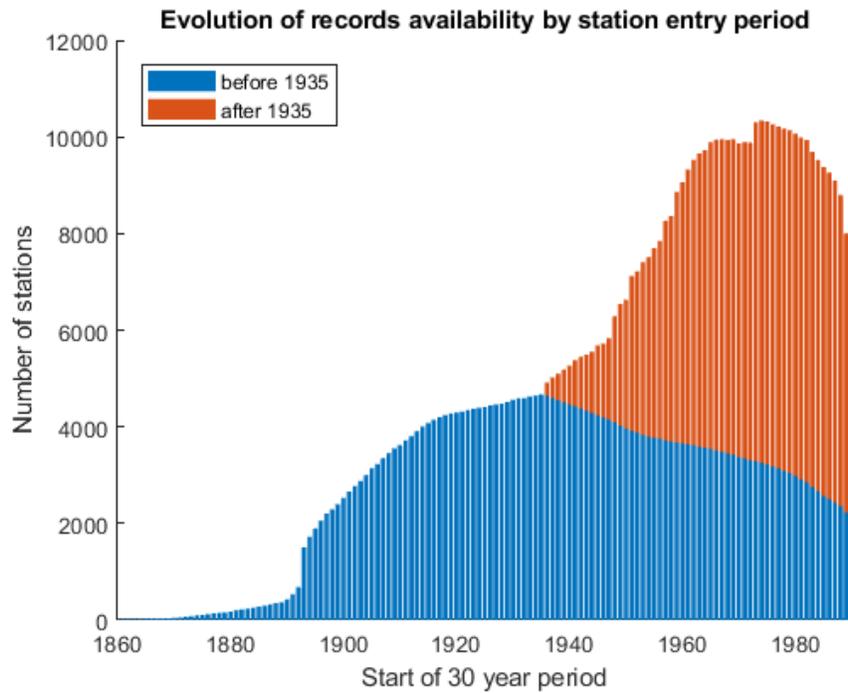
Figure 5.3 Evolution of records availability for the minimum temperature

As for the spatial distribution of the weather stations, of whom the data were utilized, it is worth mentioning that they are unevenly distributed. Weather stations with records of the average surface temperature were mainly located in Europe and Asia, while weather stations with records of the maximum or minimum surface temperature were spread across all the continents, with increased density in North America and Western Europe.

The following graphs depict the spatial variability of the selected weather stations records for each of the three studied parameters.
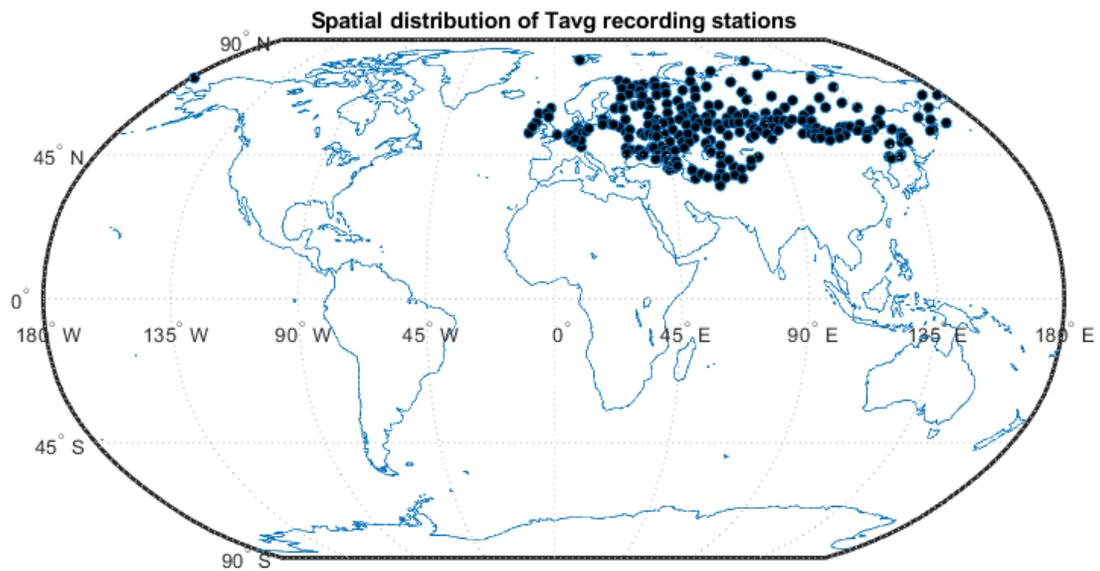
Figure 5.4 Spatial distribution of weather stations recording average temperature
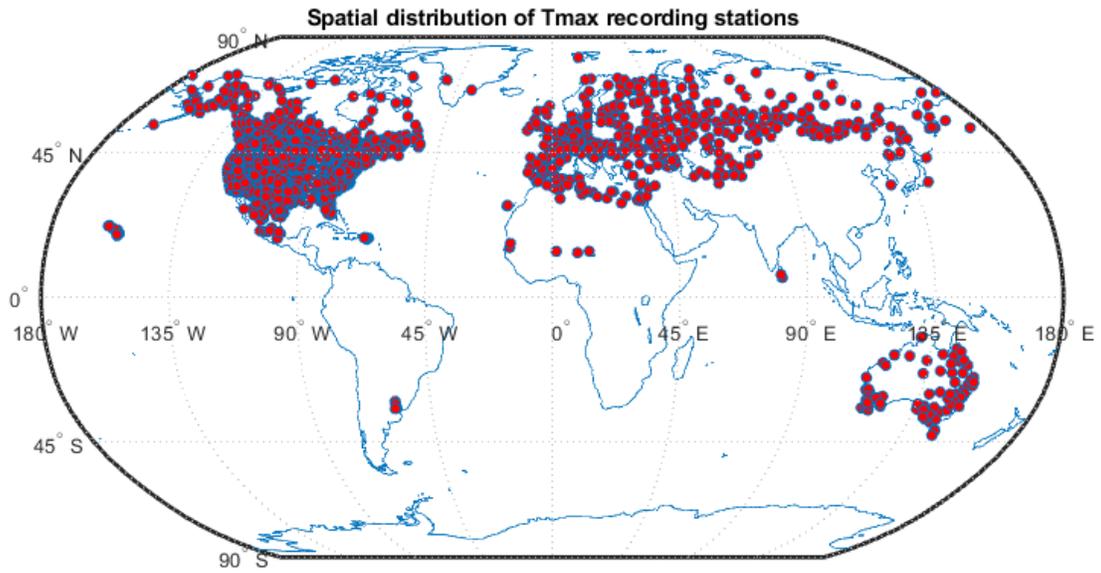
Figure 5.5 Spatial distribution of weather stations recording maximum temperature
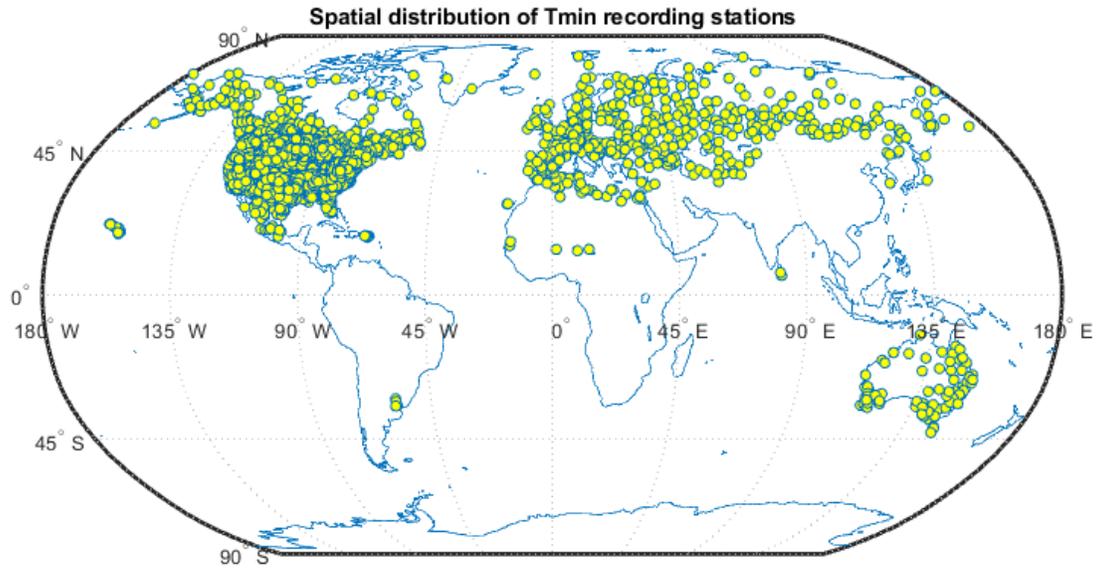
Figure 5.6 Spatial distribution of weather stations recording minimum temperature

5.5 Preliminary data processing

In order for the identification of the "suitable" weather records to be fast and efficient, we created multiple MATLAB scripts, in order to automatically accept or reject each individual station's timeseries.

The processing involved the following steps:

1. Reading of the directory, containing the files of all the records downloaded from GHCND and writing in an Excel (.xlsx) file format.
2. Calculation of the start year, end year and total length of recording period for every station.
3. For those stations with a non-zero length of record, all flagged individual entries were removed (replaced with NaN entries).
4. The stations with record beginning date before 1935 were isolated and from those, only stations with more than 30 years of recording were used.

For each weather station, which passed from all criteria 1 to 4, we isolated consecutive 30-year periods, so as to extract from them the extreme temperature events, which corresponded to specific return period levels.

6. Methodology

6.1 Methodology overview

The stages followed in the integrated study of the behavior of land surface air temperature in global scale are presented in figure 6.1 that follows. It is worth mentioning, that the procedure outlined in the figure was repeated for each of the three elements of air temperature that were studied; average, maximum and minimum temperature.

At the first stage, we downloaded the data from the GHCND database, and performed multiple quality tests and removal of flagged values and short timeseries. At the next stage, we standardized the remaining timeseries. After the standardization, we isolated rolling 30-year periods, so as to calculate the K-moments of each timeseries, that led to the quantile values selection. After this chain of actions was realized for all years, we plotted the quantile values against the starting point their respective of 30-year periods and their return period level.

In parallel with these steps, we utilized the standardized timeseries to create an aggregated Climacogram. From this Climacogram, we derived the H parameter, which was used at the next stage as an input to the Symmetrically Moving Average scheme to create synthetic timeseries. From these synthetic timeseries, we calculated K-moments, as well as selected and plotted the quantile values, as performed for the observed (real) timeseries.

```
┌─────────────────┐
│  Data collection,│
│  Quality control │
└─────────────────┘
         │
         ▼
┌─────────────────┐         ┌─────────────────┐
│ Standardization │────────▶│   Climacogram   │
└─────────────────┘         └─────────────────┘
         │                           │
         ▼                           ▼
┌─────────────────┐         ┌─────────────────┐
│   K-moments     │         │  H coefficient  │
└─────────────────┘         └─────────────────┘
         │                           │
         ▼                           ▼
┌─────────────────┐         ┌─────────────────┐
│    Plotting     │         │    SMA model    │
└─────────────────┘         └─────────────────┘
                                     │
                                     ▼
                            ┌─────────────────┐
                            │   K-moments     │
                            └─────────────────┘
                                     │
                                     ▼
                            ┌─────────────────┐
                            │    Plotting     │
                            └─────────────────┘
```
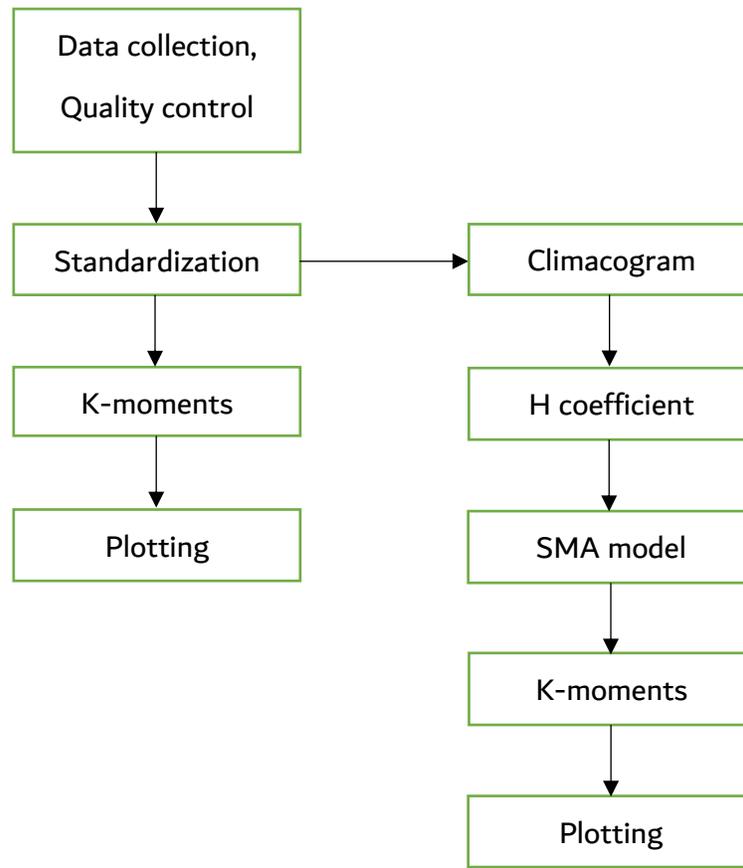
Figure 6.1 Methodology Layout

6.2 Timeseries standardization

In order for the input data, as well the results, to be comparable it was imperative to standardize the timeseries, in a way that it would be easy to identify the extreme values. Since multiple studies conclude that the distribution of the land surface air temperature closely resembles the Gaussian, it was determined to standardize the timeseries according to the Gaussian distribution.

However, since the study is focused on the behavior of the temperature in global scale, it was deemed reasonable to proceed with the standardization in a perennial time frame. This is because of the fact that so many weather stations around the world are located in climate zones with great variance of temperature among the different seasons. Had it not

been foreseen; we would have misconstrued "usual" winter temperatures as persistent low extremes and "usual" summer temperatures as long-lasting heatwaves.

In regard to the aforementioned paradox, we decided to standardized all timeseries values according to the arithmetic mean (average) and standard deviation of their specific month. Thus, only extreme, for the season, values would stand out, clearing out the extremes from the expected norm. It is worth mentioning, that we performed monthly standardization with respect to the arithmetic mean and standard deviation of each month, derived from the whole timeseries and not just the 30-year section of the timeseries, that was studied independently.

6.3 Rolling 30-year periods

A pivotal point of this study is the use of rolling 30-year periods, as independent timeseries, from which specific extreme values corresponding to pre-selected return periods were extracted. We determined that the time length of each sub-series should be 30-years long, because three decades is an adequate enough amount of time to characterize the climate of an area. Moreover, 30 years is an average time interval between generations, giving greater gravity to any changes. Longer time frames (e.g. 50 years) would significantly minimize the number of available rolling periods that could be extracted from each primary timeseries. Shorter time frames (e.g. 10 years) would inhibit the extraction of valuable extreme values occurring at larger time intervals, such as extreme values occurring once every 30 years.

The procedure with which each rolling 30-year period was isolated from the lengthy timeseries of the database is quite simple. First of all, we calculated the first and last year of each primary timeseries, and consequently the total length of it. At the next step, with the use of an iteration, using a single variable taking values ranging from the start year to the end year of the timeseries minus 29 years, we managed to identify the years, at which

each rolling 30-year period started. At this point, since the beginning of the 30-year period had been identified, and the total length of it was known, we extracted the 30-year period.

In the figure 6.2 a schematic depiction of some random, yet consecutive, 30-year periods is shown, so as to clarify the procedure.
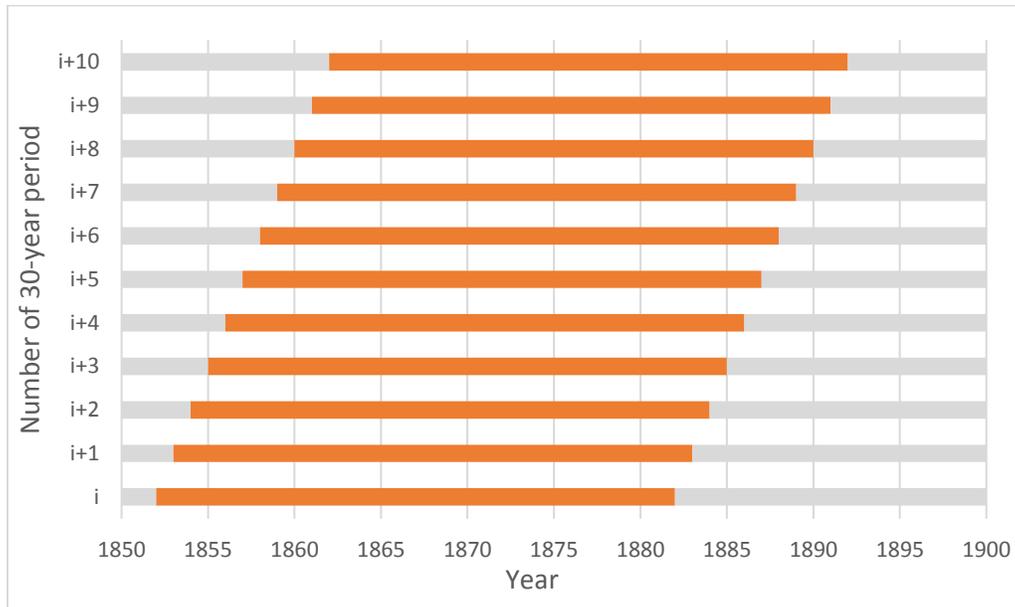
Figure 6.2 Example of consecutive 30-year periods

6.4 K-moments calculation of observed record data

After each 30-year long timeseries section had been standardized, in relation to corresponding months, we sorted the timeseries accordingly. For study of the upper tail we sorted the timeseries in ascending order, while for study of the lower tail, the timeseries was sorted in descending order.

At this point, we calculated the necessary return periods, in terms of days, not years, like the resolution of the temperature data available. The return periods, that were selected, in order to get isolated from the ensemble of K-moments are:

Table 6.1 Day intervals studied

Return period	Years	Days
T1	3	1096
T2	10	3653
T3	20	7305
T4	30	10958

However, since the exact definition of return period yields a linear relationship between T and coefficients Λ_P that depend on the distribution function (we have assumed Gaussian), the precise return period for the number of days that we selected is different, as described by the equation 6.1:

$$\frac{T(K'_{p1})}{D} = p\Lambda_p \approx \Lambda_\infty p + (\Lambda_1 - \Lambda_\infty) \tag{6.1}$$

Hence, the real return periods that we studied are:

Table 6.2 Return periods studied

Return period	Days	Years (for Gaussian distribution)
T1	1096	4.95
T2	3653	16.49
T3	7305	32.98
T4	10958	49.47

For these day intervals (shown in the second column of table 6.2) corresponding to these return periods, we used a repetition to calculate both the fixed term of each moment, which depends on only p and the length of the sample, but also the added terms, which depend on the index and the value of each specific entry, in relation to the size of the

sample. The differentiation between the fixed and the non-fixed term is apparent in the definition of the estimator of K-moments:

$$\widehat{K}'_{pq} = \frac{p-q+1}{n} \sum_{i=1}^{n} \left(\frac{i-1}{n-1}\right)^{p-q} \underline{x}^q_{(i)}$$ (6.2)

After we had calculated K-moments for the entirety of the suitable time-series and for all 30-year periods of their time span, we performed a rudimentary statistical analysis to extract valuable information from all these results. Hence, it was decided to isolate the distribution of each return period and each 30-year time-frame and extract the values corresponding to the 25th, 50th (median) and 75th percentiles.

A pivotal, yet usually underestimated, part of the results representation is the plotting of only the estimated quantile values and not of all the values calculated. Had we not isolated the quantiles, the resulting plot would have been a nebula-like shape, approximating a surface corresponding to the extremes of the average station for all time scales.

6.5 Climacogram and H coefficient

All the data, that had been standardized from the previous steps of the methodology were save in a file format, suitable for large size data. This file was read by a specifically created MATLAB script, so as to create the Climacogram for every single timeseries, for scale 1 through $n/10$, where n is the total size of each timeseries.

After this procedure was realized for all timeseries, we summed the values of respective scales of all these Climacograms, so as to produce the arithmetic mean (average) of the Climacogram for each scale. As scale of the ensemble of the timeseries was selected the arithmetic mean of the lengths n_i of all timeseries.

The resulting aggregated Climacogram was exported as an xlsx format file, so as to be read from an Excel spreadsheet. The reason, why we chose the Excel spreadsheet over MATLAB programming was the ease of use and the wide variety of optimization tools. The values of the Climacogram, that resulted from observations, were juxtaposed with the

theoretical expected values of the Climacogram for a timeseries of imaginary length n_{imag}, equal to the average of the lengths n_i of all timeseries.

The theoretical values of the Climacogram for a combined Hybrid Hurst-Kolmogorov and Markov process derive from the following equation:

$$\gamma(k) = \frac{\lambda}{2}\left(1 + (k/a)^{2M}\right)^{\frac{H-1}{M}} + \frac{\lambda}{k/a}\left(1 - \frac{1 - e^{-k/a}}{k/a}\right) \qquad (6.3)$$

We calculated the three independent parameters H, M and α in such a way, so as to create a theoretical Climacogram that coincided with the Climacogram of the observed timeseries. In order for us to perform such an optimization, a target-cell was created that represented the root mean square error (RMSE).

$$RMSE = \sqrt{\sum_{i=1}^{n_{imag}} (X_{observed} - X_{theoretical})^2} \qquad (6.4)$$

The optimization problem of minimizing the value of a RMSE was modeled in Microsoft Excel spreadsheet using a combination of the Generalized Reduced Gradient (GRG2) algorithm and the Evolutionary algorithm. We used the GRG method to quickly identify the global minimum of the domain, while the Evolutionary algorithm was used, so as to improve even further the margin of error. In order for us to avoid unnecessary time-consuming operation of the Evolutionary algorithm in finding the optimal solution, we limited the number of iterations to 100,000.

The target cell was the one containing the RMSE value between the theoretical value of the Climacogram and the expected one. The three independent parameters H, M and α were the variable parameters of the optimization process. As for the constraints, the three variable parameters were bounded as follows:

- $0.5 < H < 1$
- $0 < M < 1$
- $\alpha > 0$

It is worth mentioning that the complete range of possible values of H is [0,1]. Yet it is impossible for a natural process like temperature to present a H-coefficient value less

than 0.5, because that would mean that it is negatively correlated, which is intuitively wrong. Since temperature is actually the result of energy transfer, it cannot be negatively correlated.

From these optimizations resulted the unbiased H coefficient, indicating the degree of persistence of the three air temperature variables.

Table 6.3 H coefficient of air temperature

Air Temperature	H
Average	0.760
Maximum	0.752
Minimum	0.806

The empirical and theoretical values of the Climacogram for all three studied variables, average, maximum and minimum air temperature are being presented in figures 6.3 – 6.5.
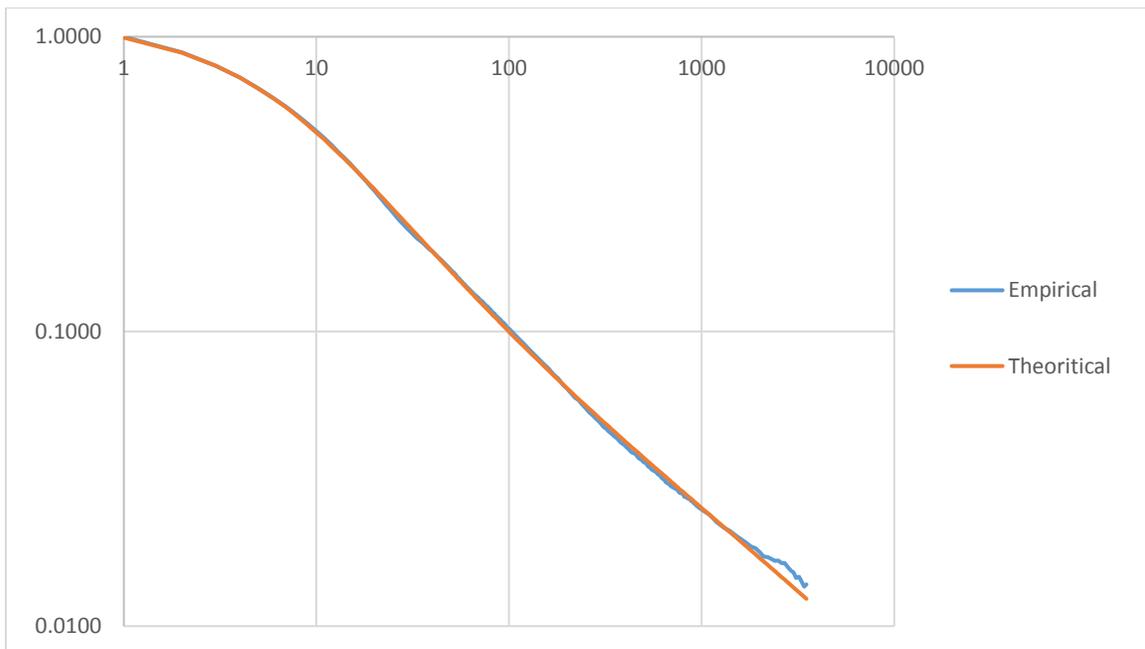

Figure 6.3 Climacogram of the average air temperature
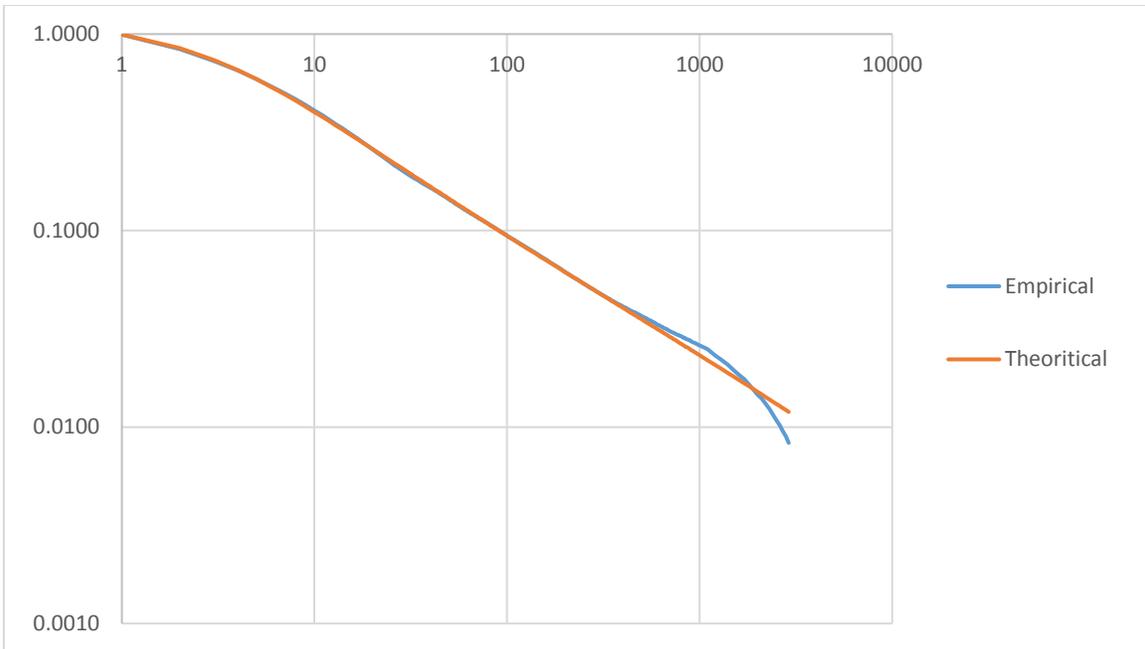
Figure 6.4 Climacogram of the maximum air temperature
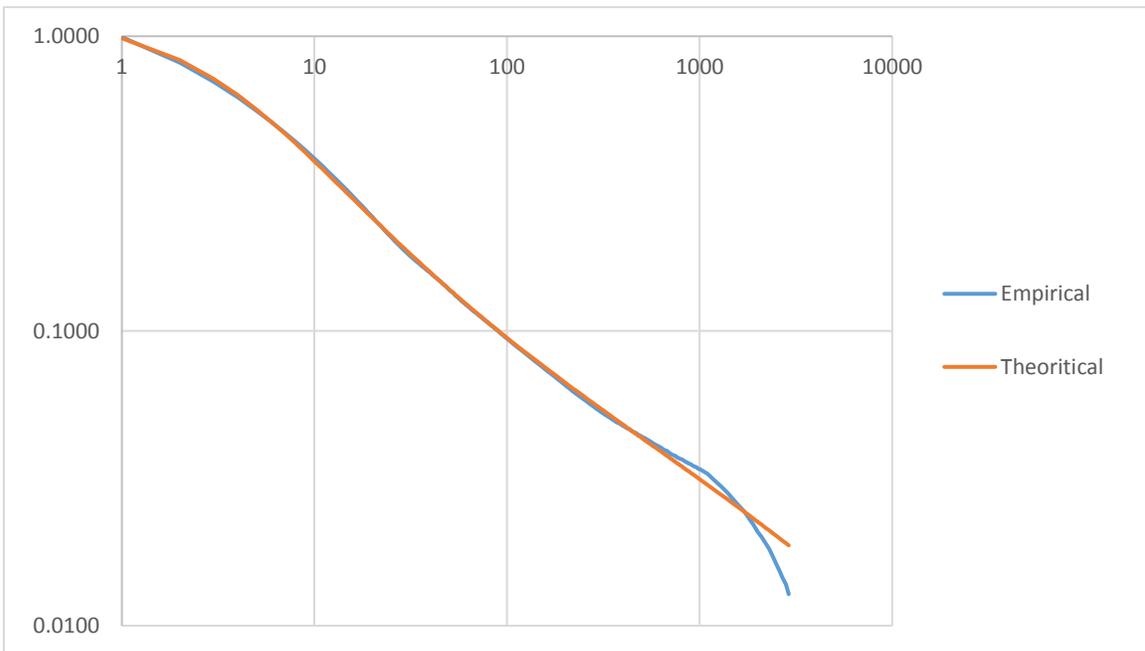
Figure 6.5 Climacogram of the minimum air temperature

6.6 Production of synthetic timeseries

A rigorous and general method for producing synthetic timeseries of a physical quantity, like temperature, by preserving its dependence structure is the symmetric-moving average (SMA) scheme introduced by Koutsoyiannis (2000), further improved by Koutsoyiannis (2016) and implemented within the Castalia computer package (Efstratiadis et al., 2014). The SMA method has the advantage of fully preserving in an exact way any second-order structure of a process and, simultaneously, the complete multivariate distribution function if it is Gaussian, like in the case of air temperature (because of the preservation of the Gaussian attribute within linear transformations). As extended by P. Dimitriadis et al. (2018), the SMA generation scheme can replicate a natural process by preserving its first four central moments, which has been found to be more-than-adequate for various distributions commonly applied in geophysical processes.

The algorithm to produce timeseries with the SMA scheme, created by P. Dimitriadis (2018), required the first four central moments, the H coefficient of each physical quantity (average, maximum and minimum temperature) and the length of the timeseries as well. For each observed timeseries that passed the multiple quality checks, we calculated the first four central moments. The H coefficient was common for all timeseries of the same physical quantity, as well as the length of the timeseries, which equaled the maximum length of all the utilizable timeseries.

Since the timeseries had been standardized according to the Gaussian distribution, the first two central moments were equal, or close to, zero and one respectively, while the latter two (third and fourth central moment) were left unchanged. In figures 6.6 – 6.11 we present the histograms of third and fourth central moments of the three studied air temperatures.
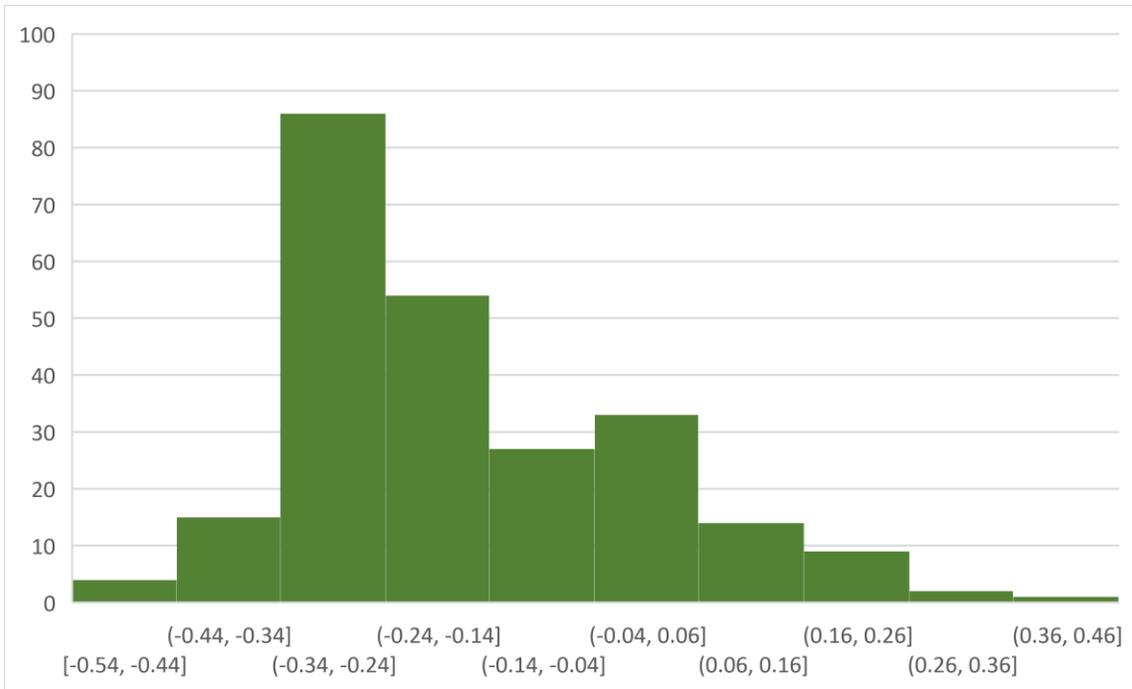
Figure 6.6 Third central moment of average temperature timeseries
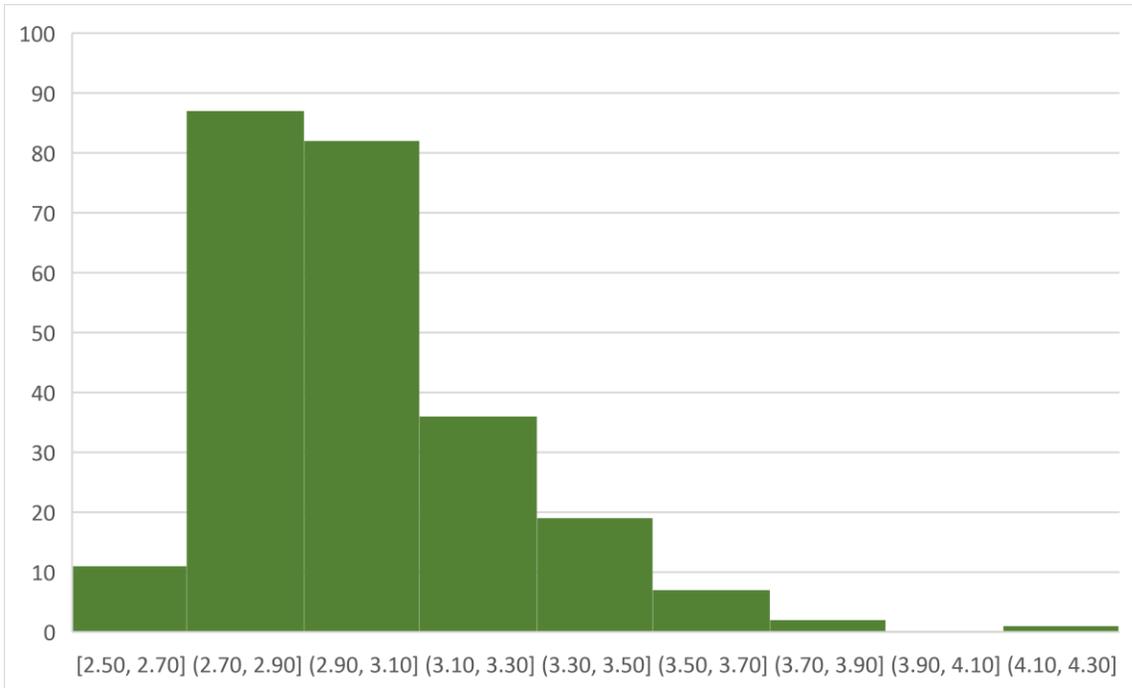
Figure 6.7 Fourth central moment of average temperature timeseries
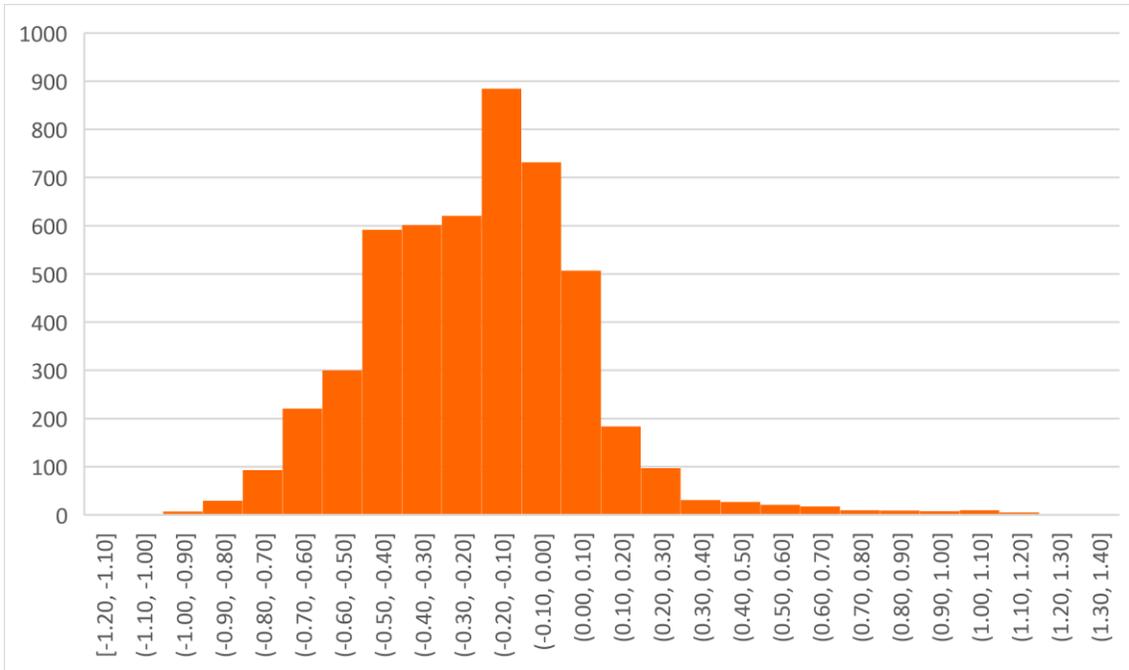
Figure 6.8 Third central moment of maximum temperature timeseries
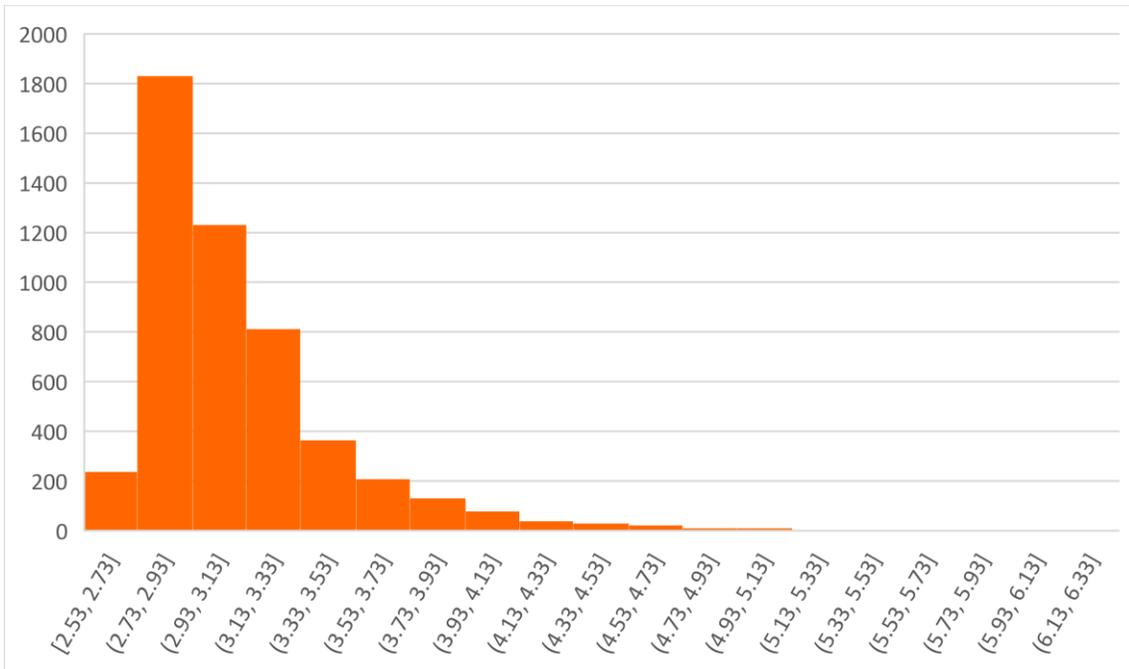
Figure 6.9 Fourth central moment of maximum temperature timeseries
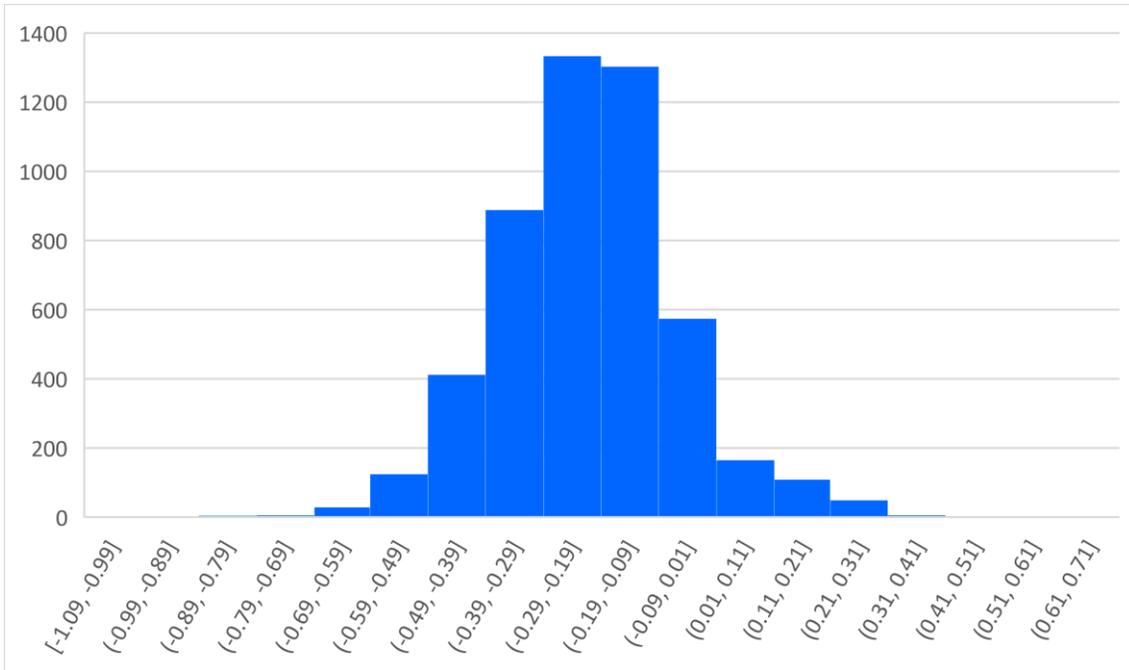
Figure 6.10 Third central moment of minimum temperature timeseries
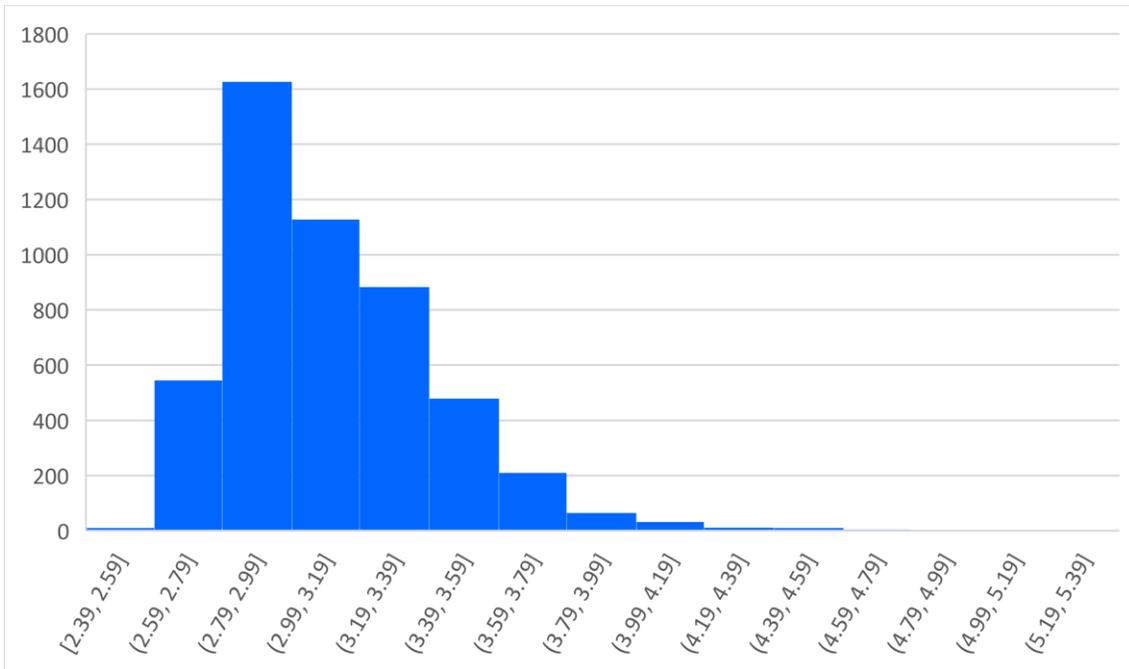

Figure 6.11 Fourth central moment of minimum temperature timeseries

Since creating a single synthetic timeseries, with respect to preserving its dependence structure, was a time-lengthy procedure, we decided to produce for each of the three physical quantities (average, maximum and minimum temperature) a fixed number of synthetic timeseries. This number of produced timeseries is equal to the least number of observed, yet utilizable, timeseries for each of the three temperature qualities. The number of observed timeseries for the average air temperature was 245, while for the maximum and minimum temperature was 5,006. Thus, 245 synthetic timeseries were created for each air temperature quality.

The fact that, for the maximum and minimum temperature, the number of synthetic timeseries was smaller than the number of the observed ones, created some concern over the unbiased selection of the central moments from the pool of the total. This was resolved by creating a random number generator, which produced 245 times an index ranging from 1 to 5,006, which corresponded to the index of an observed timeseries, whose first four central moments were to be taken as input for the production of the synthetic record.

6.7 K-moments calculation of synthetic record data

As for the observed data, we followed the same procedure for the analysis of the synthetic timeseries. For the day intervals (see Table 6.2) corresponding to the return periods that had been selected, we used a repetition to calculate both the fixed term of each moment, which depends on only p and the length of the sample, but also the added terms, which depend on the index and the value of each specific entry, in relation to the size of the sample.

After calculating the K-moments for the entirety of the synthetic time-series and for all 30-year periods of their time span, a rudimentary statistical analysis was performed to extract valuable information from all these results. Hence, as with the case of observed

data, we decided to isolate the distribution of each return period and each 30-year time-frame and extract the values corresponding to the 25th, 50th (median) and 75th percentiles.

Finally, the plotting of only the estimated quantile values and not of all the values calculated was performed. Again, had the quantiles not been isolated, the resulting plot would have been a cloud-like shape, approximating a surface corresponding to the extremes of the average station for all time scales.

6.8 Detection of the longest individual records

As part of an unbiased study of the behavior of air temperature, we considered useful to compare the aggregate behavior of all the available timeseries, with the behavior of the longest timeseries, to identify possible similarities of variations between them. In order to identify the most long-lived records, we created an algorithm for the isolation of the maximum time-length of each recording. This algorithm revealed that the most long-lived air temperature records for each aspect of land surface air temperature are as follow:

Table 6.4 Longest recording individual stations

Air Temperature	Station ID	Location	Record Length
Average	RSM00026063	St. Petersburg, Russia	136 years
Maximum	ITE00100554	Milan, Italy	246 years
Minimum	ITE00100554	Milan, Italy	246 years

6.9 K-moments calculation of individual record data

After we identified the longest records, we applied a similar procedure as the one followed in the study of the sum of observed records. First, we standardized timeseries. After the standardization, we calculated the K-moments of each timeseries, that led to the quantile values selection, that corresponded to the examined return period levels. After this chain

of actions was realized for all years, we plotted these values against the starting points of 30-year periods and their return periods.

In order for the comparison to be applicable, we depicted the length of the individual timeseries that coexisted with the time period of all the other timeseries with the same color (i.e. black) and solid line, while for the preceding time period, the data were depicted with different color (i.e. red) and dashed line.

7. Results

7.1 Observed timeseries

As resulted by the study of the actual recorded timeseries of air temperature, the behavior of the different aspects of air temperature is inconsistent when compared to each other. The irregularities are more apparent between the upper tails, while lower tails present a somewhat more expected pattern.

Upper tail of the average air temperature appears to become thicker as time progresses, with the standardized extreme values of each return period to increase by about 0.2 for the smaller return periods and about 0.4 for the larger return periods. Another interesting finding is the slight increase of variance of each return period tail progression, even though the number of the available records slowly decreases.
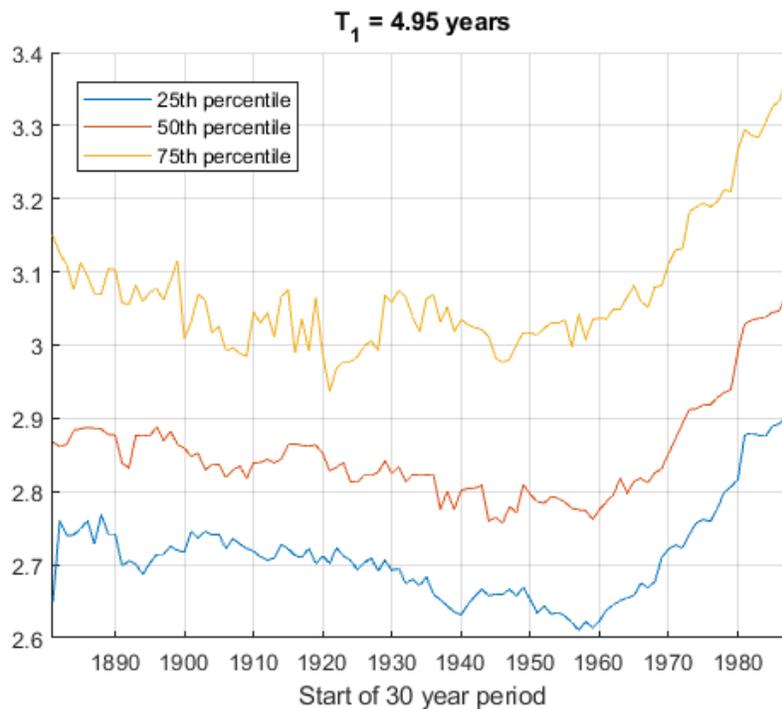
Figure 7.1 Upper tail of the observed average air temperature at return period T1
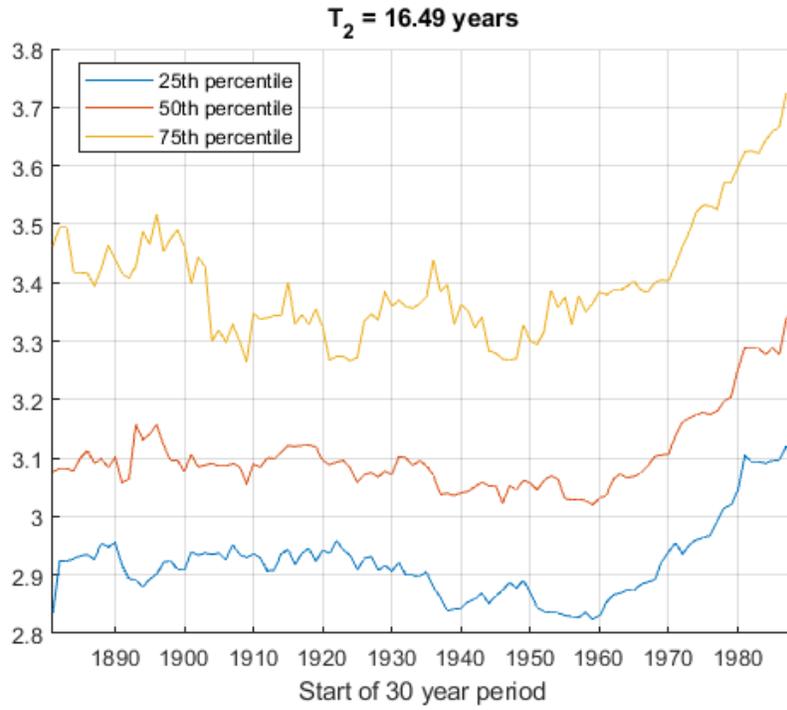
Figure 7.2 Upper tail of the observed average air temperature at return period T2
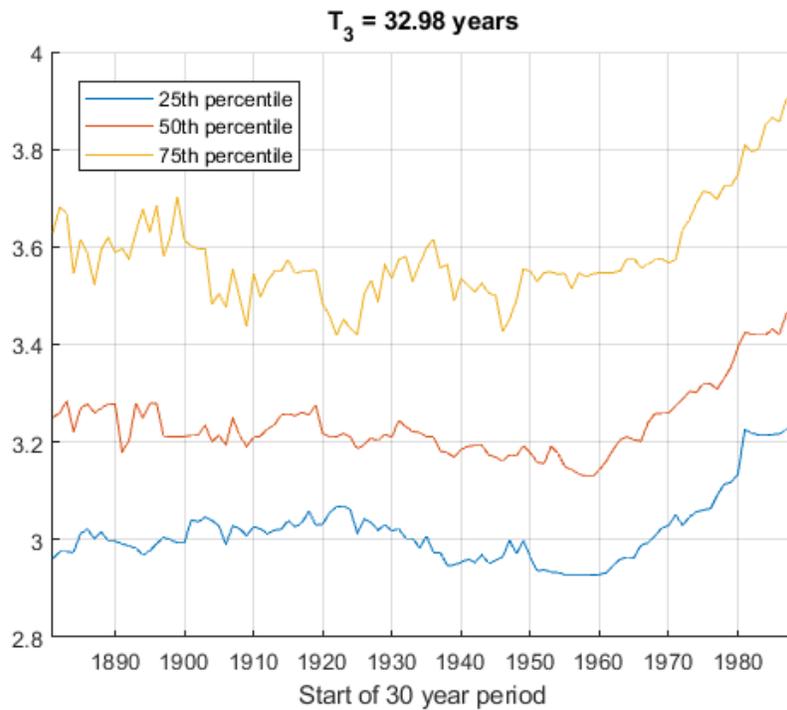
Figure 7.3 Upper tail of the observed average air temperature at return period T3
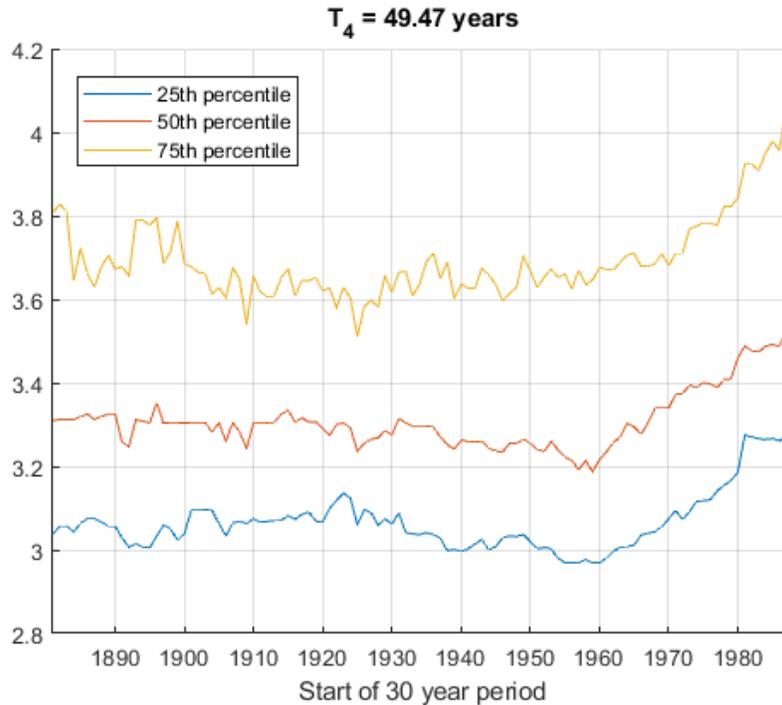
Figure 7.4 Upper tail of the observed average air temperature at return period T4

Lower tail of the average air temperature presents a more complex behavior. From 1900 until roughly 1980's it is relatively steady, yet with minor fluctuations, which probably owe their existence to the entry of more and more records as time progresses. From around the years 1980-1990 (corresponding to 30-year periods starting around 1950-1960), however, in all of the return periods, temperature appears to increase systematically. All in all, at all return periods level of the lower tail, air temperature appears to be relatively increasing, as presented by the figures 7.5 – 7.8, leading to a thinner lower tail.
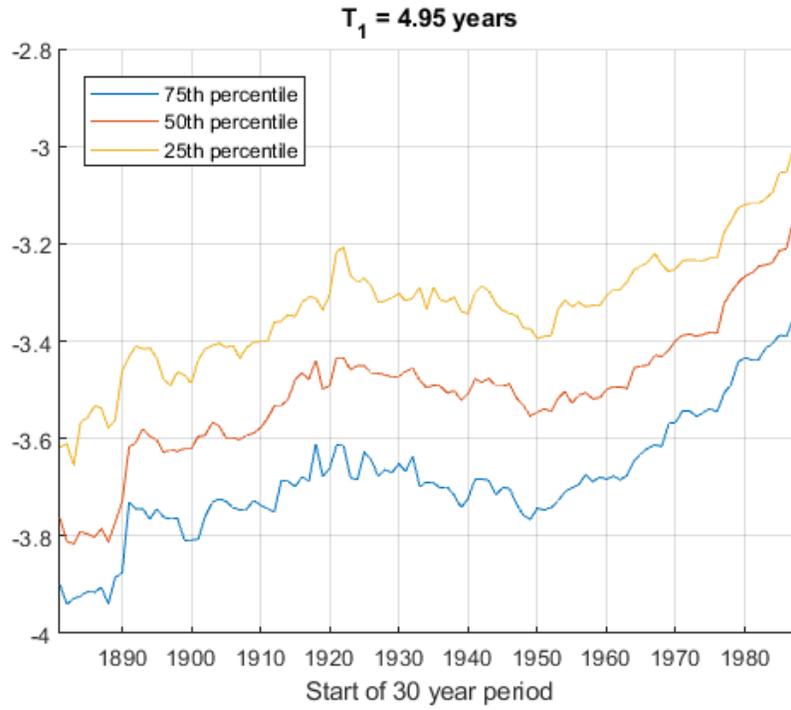
Figure 7.5 Lower tail of the observed average air temperature at return period T1
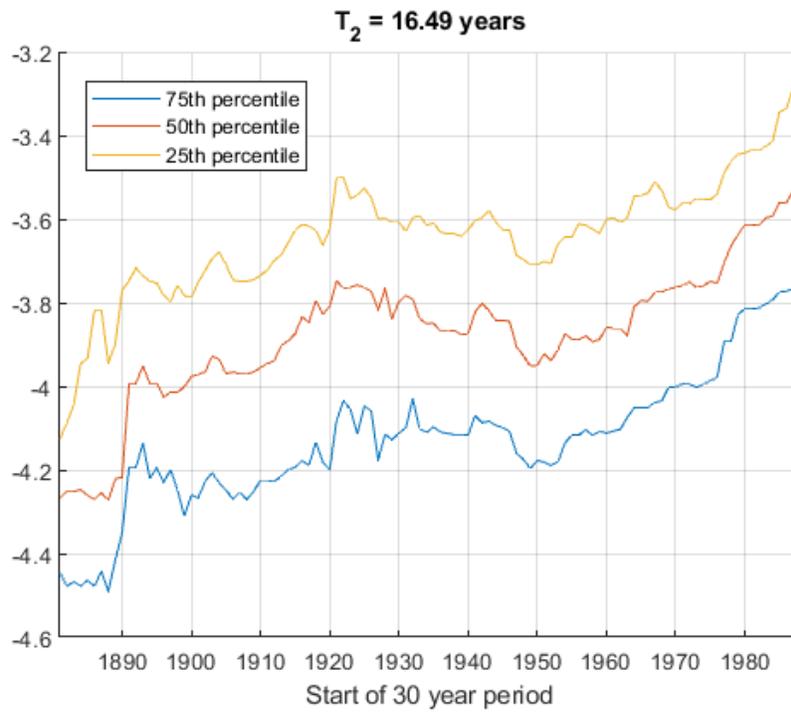
Figure 7.6 Lower tail of the observed average air temperature at return period T2
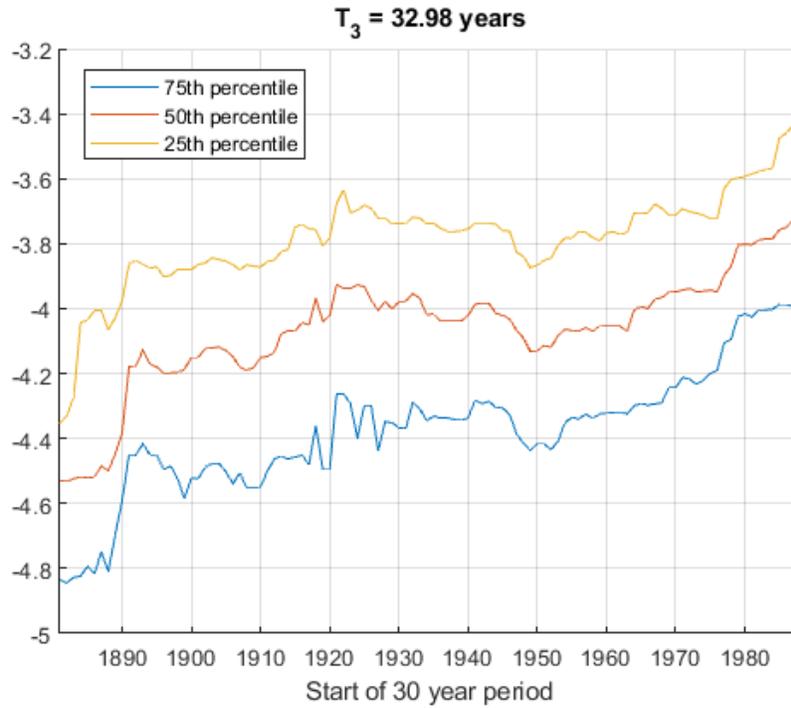
Figure 7.7 Lower tail of the observed average air temperature at return period T3
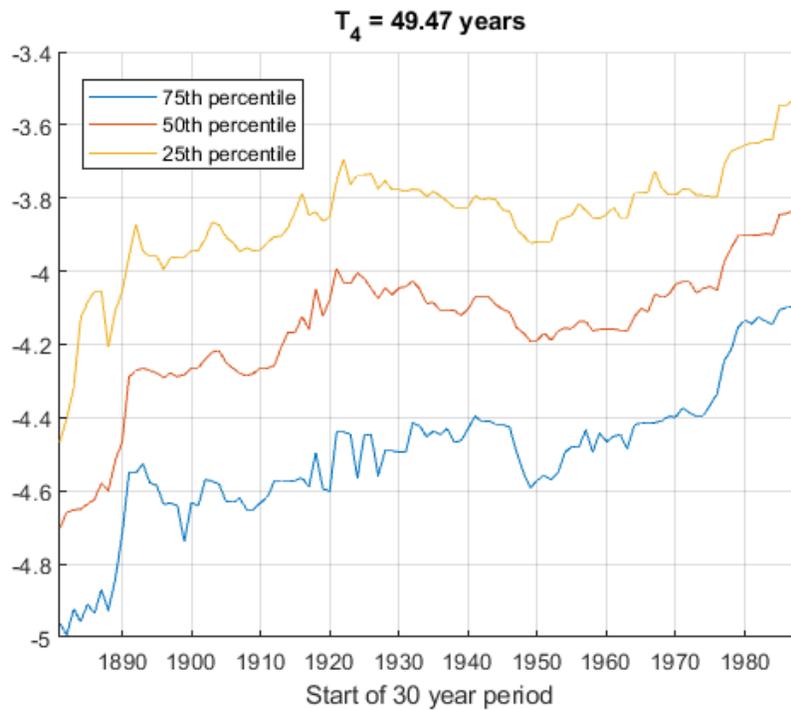
Figure 7.8 Lower tail of the observed average air temperature at return period T4

Upper tail of the maximum air temperature appears to become progressively thinner as time progresses. The general trend of each respective return period, excluding the very first years until the end 30-year periods starting up to the end of the 19th century, is slightly decreasing. Until the 1930's there is a barely noticeable thickening of the tail (in the order of 0.1), but after that time and until today there is a substantial decrease of the thickness of the upper tail of maximum air temperature by about 0.2.
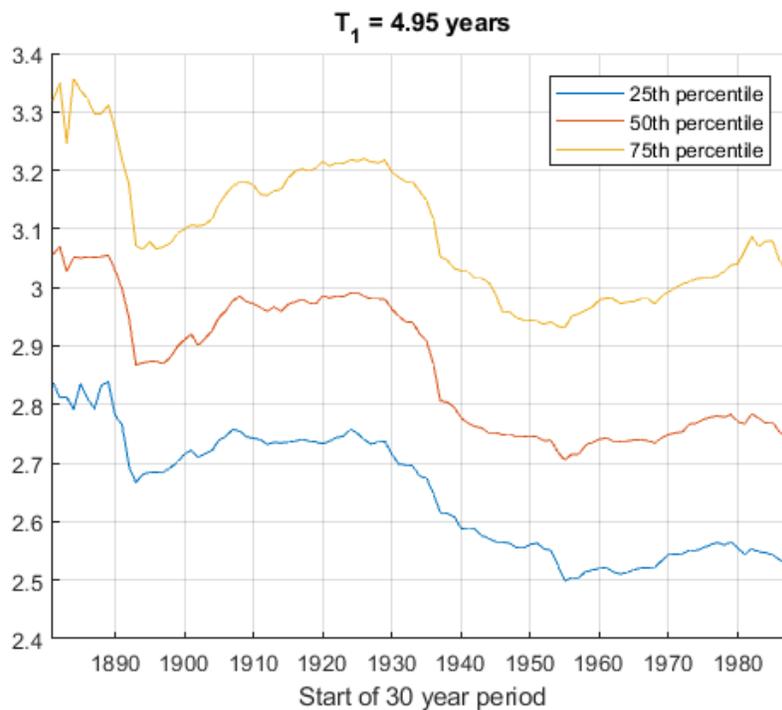

Figure 7.9 Upper tail of the observed maximum air temperature at return period T1
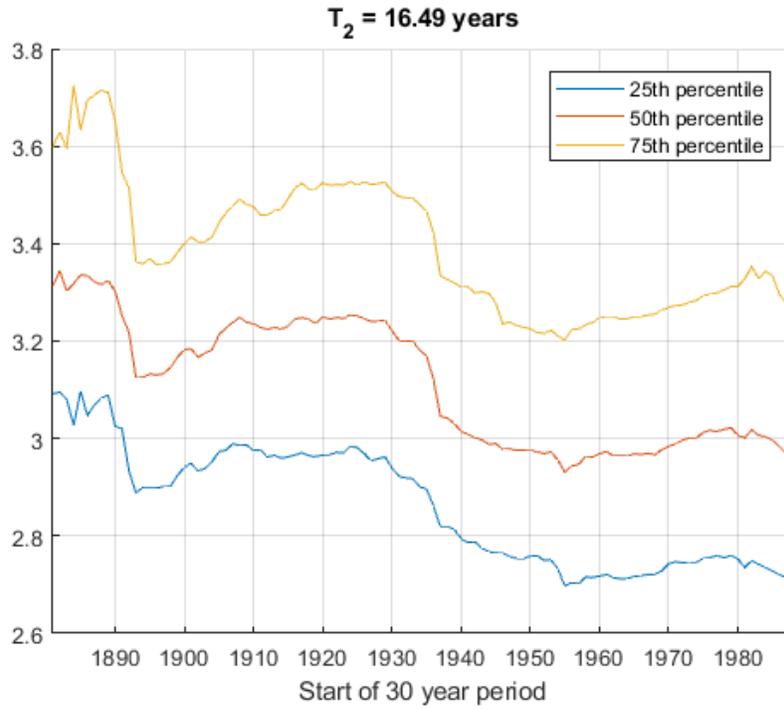
Figure 7.10 Upper tail of the observed maximum air temperature at return period T2
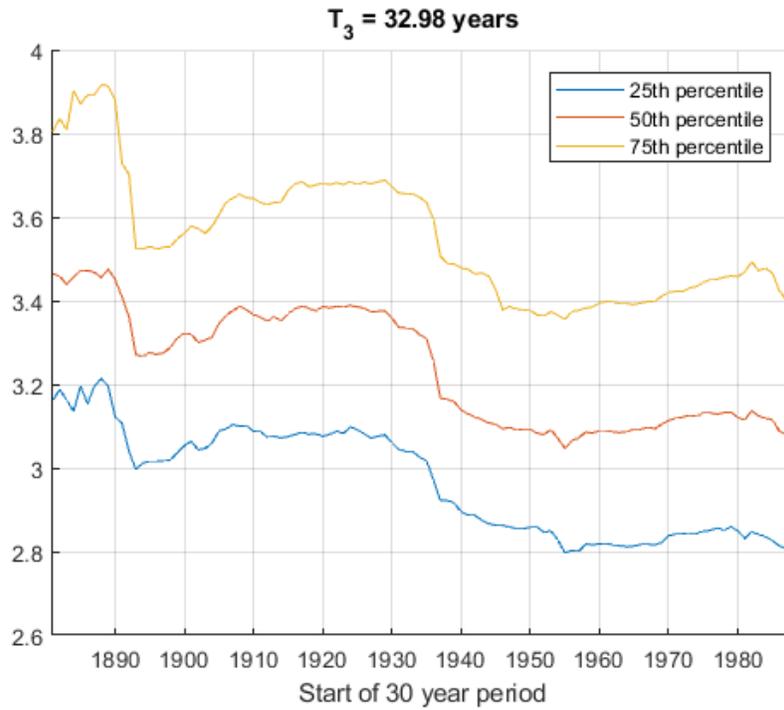
Figure 7.11 Upper tail of the observed maximum air temperature at return period T3

117
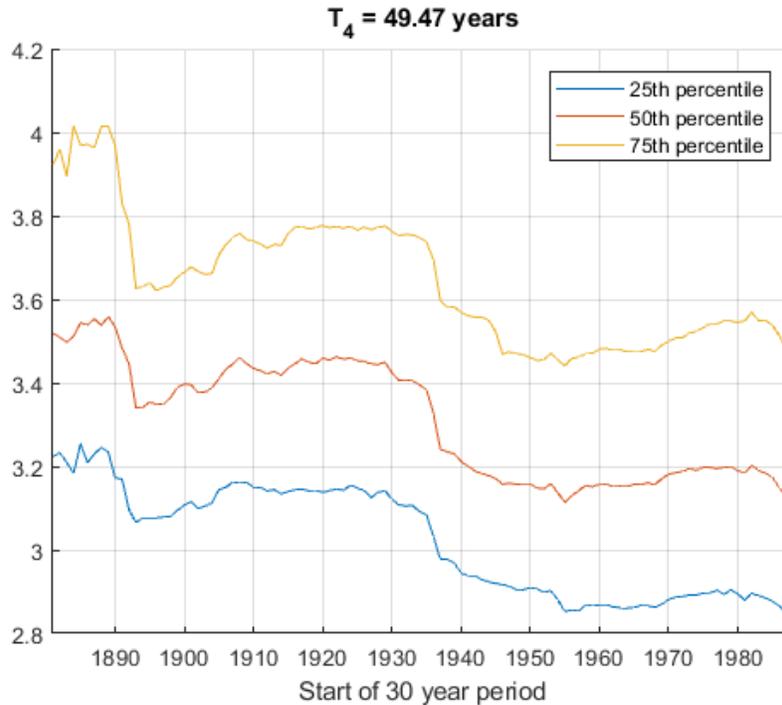
Figure 7.12 Upper tail of the observed maximum air temperature at return period T4

Lower tail of the minimum air temperature presents for the most part an astonishingly steady behavior, contrary to the upper tail of the maximum air temperature. From 1880's until 1970's there is an incredible plateau on the graph, not only in terms of the mean (50th percentile), but also of the 25th and 75th percentiles. After the 1970's though, (i.e. 30-year periods that start to include years from the 21st century) a substantial increase of the minimum temperature results in the thinning of the lower tail of minimum temperature.
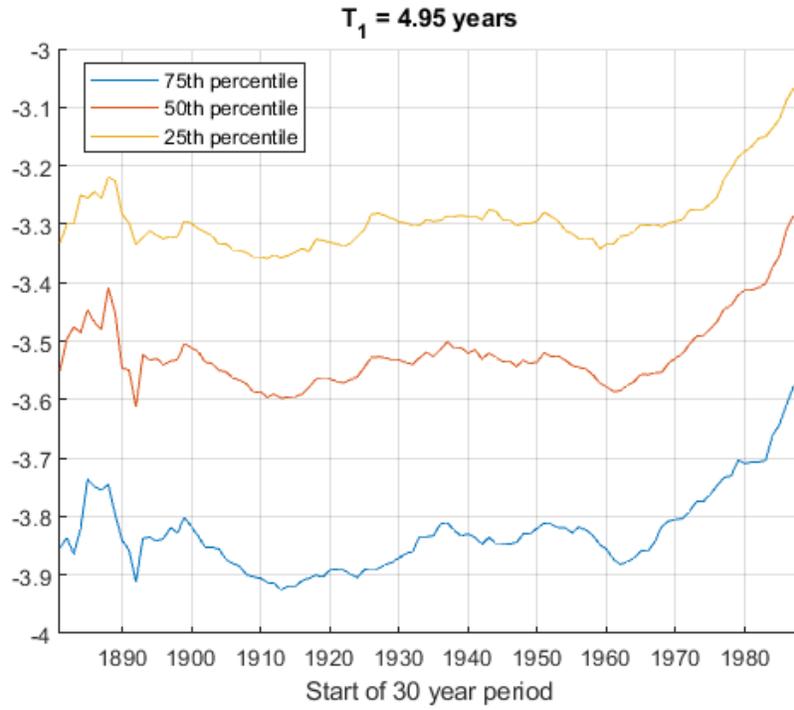
Figure 7.13 Lower tail of the observed minimum air temperature at return period T1
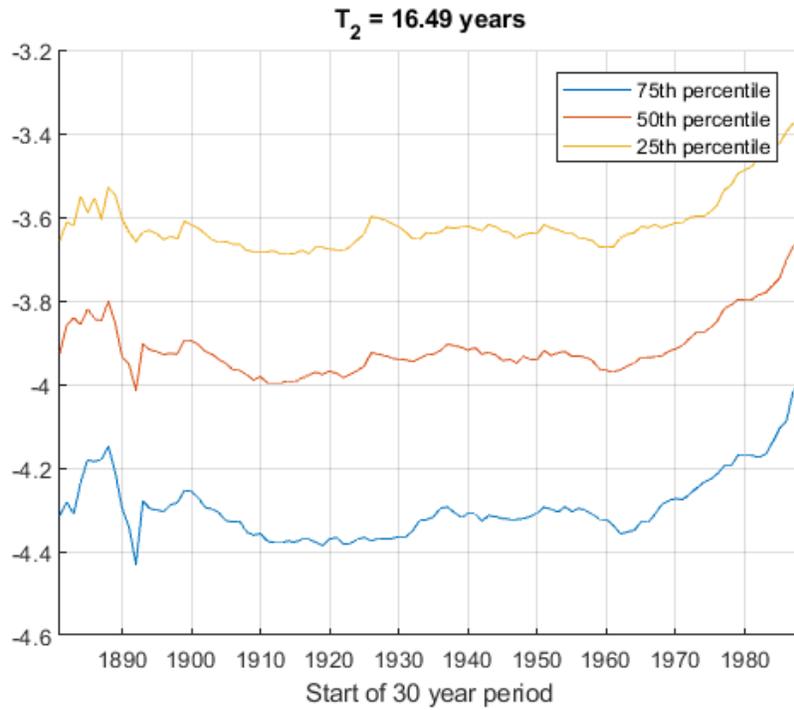
Figure 7.14 Lower tail of the observed minimum air temperature at return period T2

119
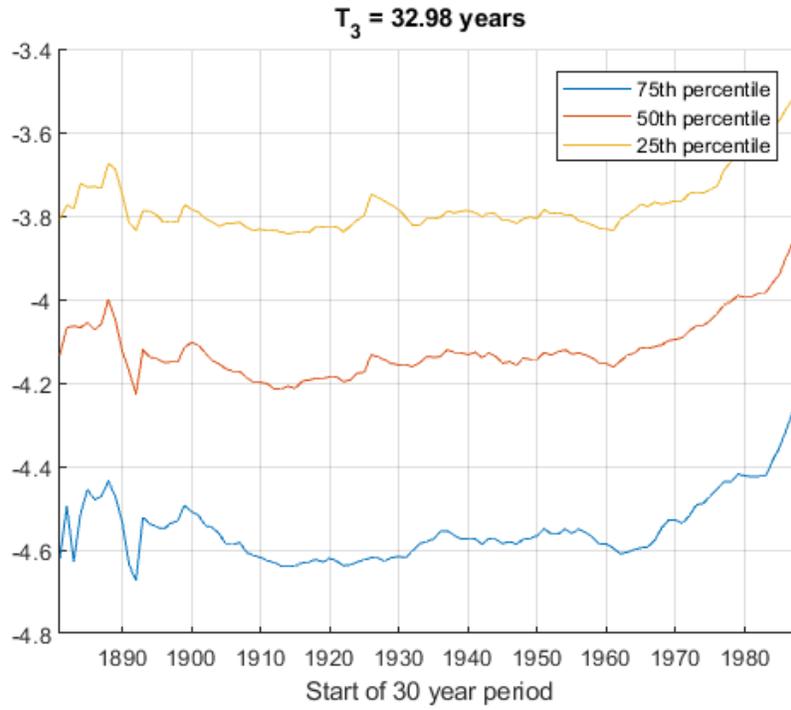
Figure 7.15 Lower tail of the observed minimum air temperature at return period T3
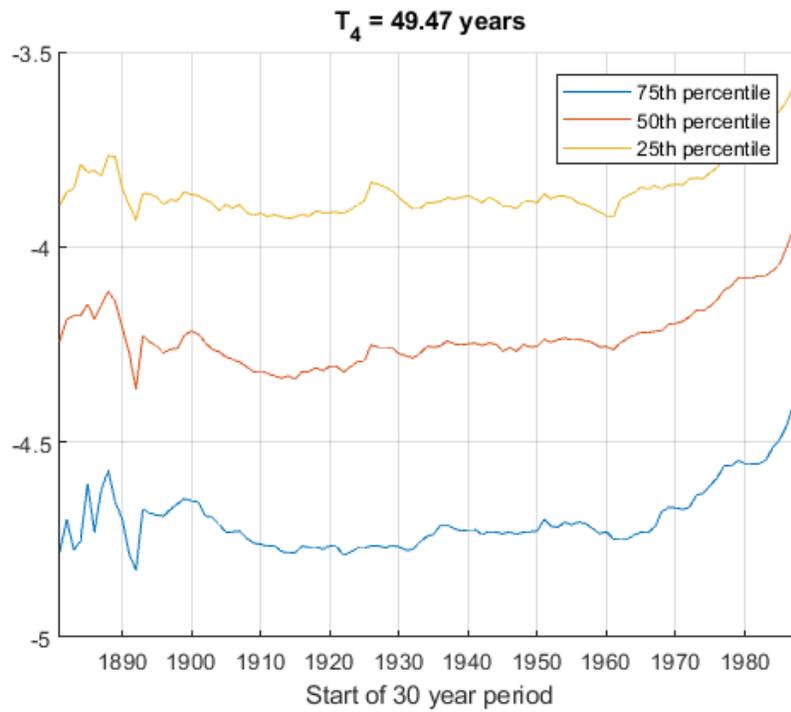
Figure 7.16 Lower tail of the observed minimum air temperature at return period T4

120

7.2 Synthetic timeseries

As expected by the production of synthetic timeseries and the quantile selection in each specific time scale, the behavior of the temperature presents homogeneity, not only in terms of variance, but also in terms of the average trend in time. A small differentiation of the synthetic timeseries compared to the observed timeseries is the slightly larger variance in each specific return period, even though the plotted quantiles are, as before, the 25th, the 50th and the 75th. In addition, the synthetic records of the lower tail of the average air temperature correspond to a thinner tail, than the one derived from the observed timeseries.
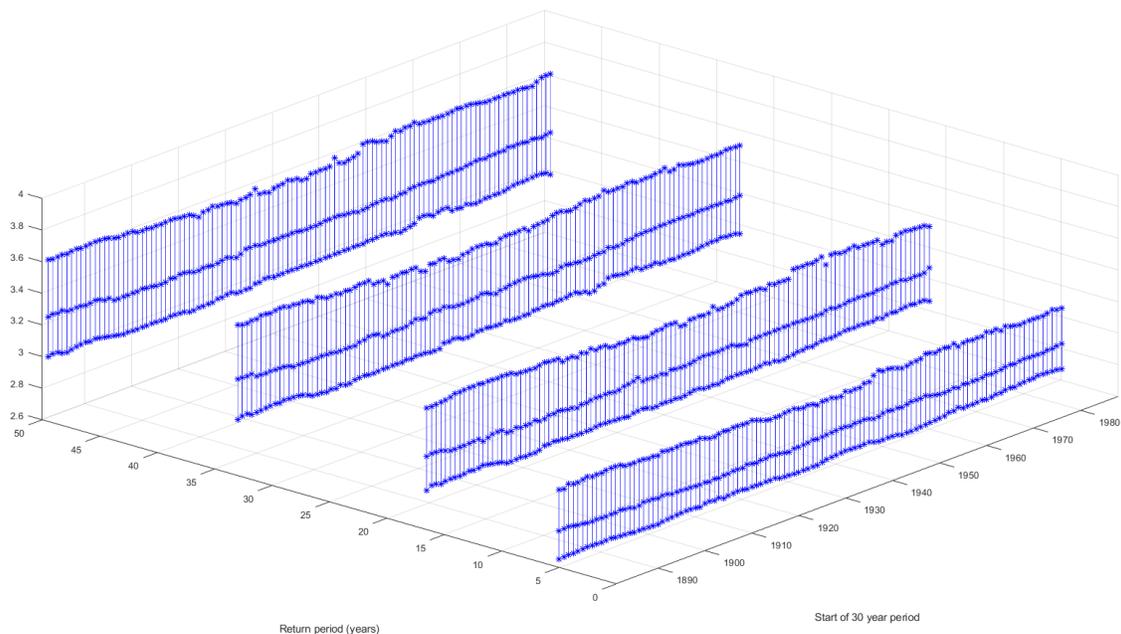
Figure 7.17 Upper tail of the simulated average air temperature behavior
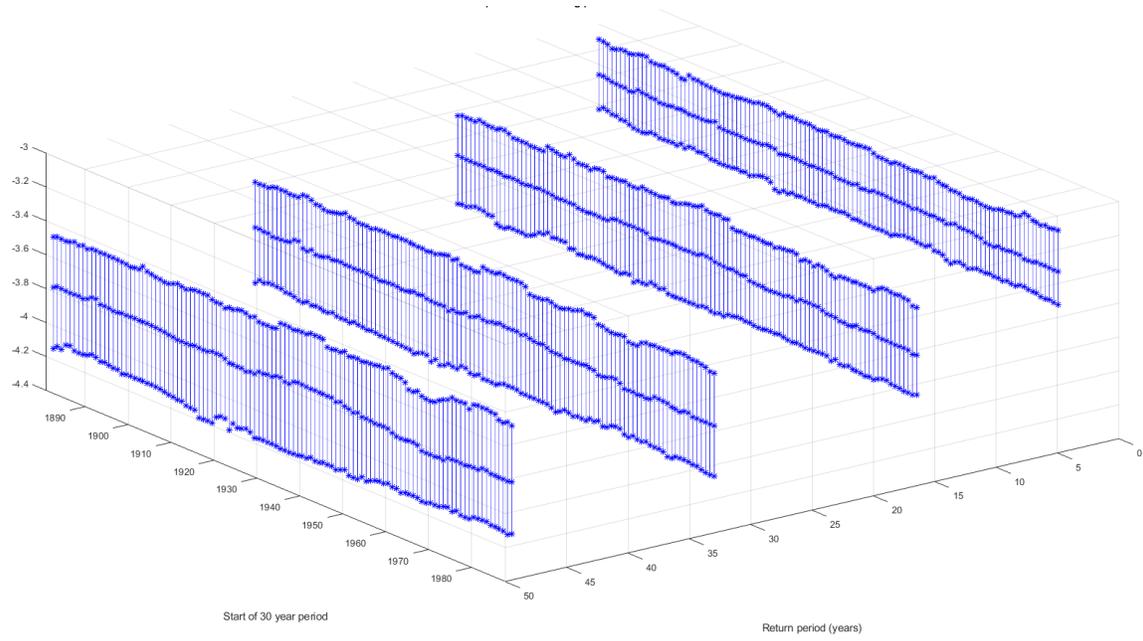
Figure 7.18 Lower tail of the simulated average air temperature behavior
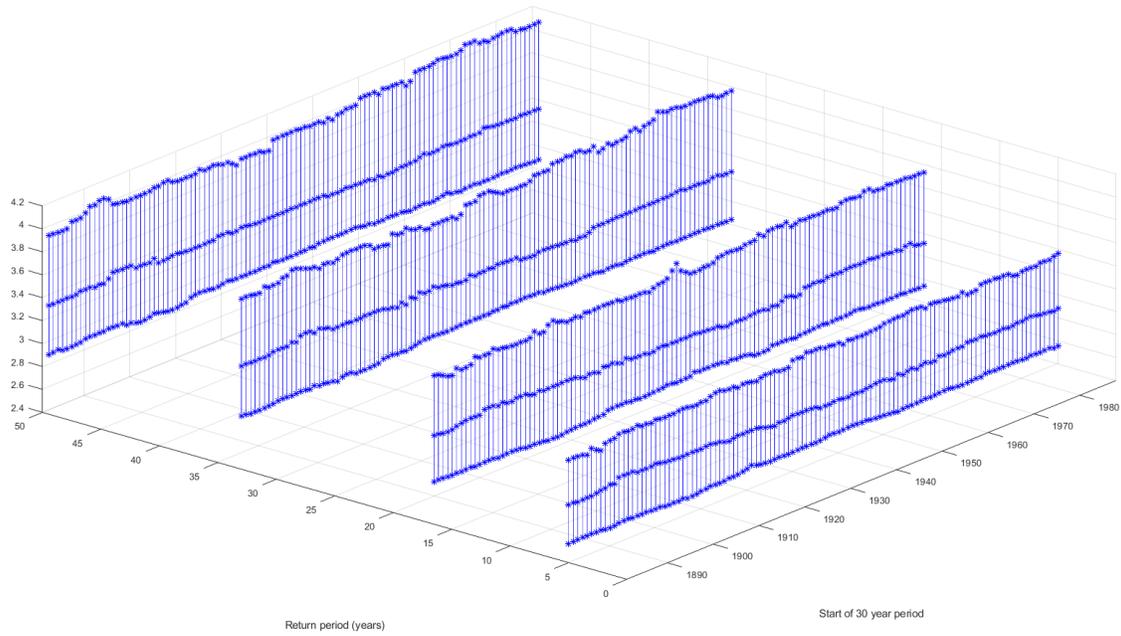
Figure 7.19 Upper tail of the simulated maximum air temperature behavior
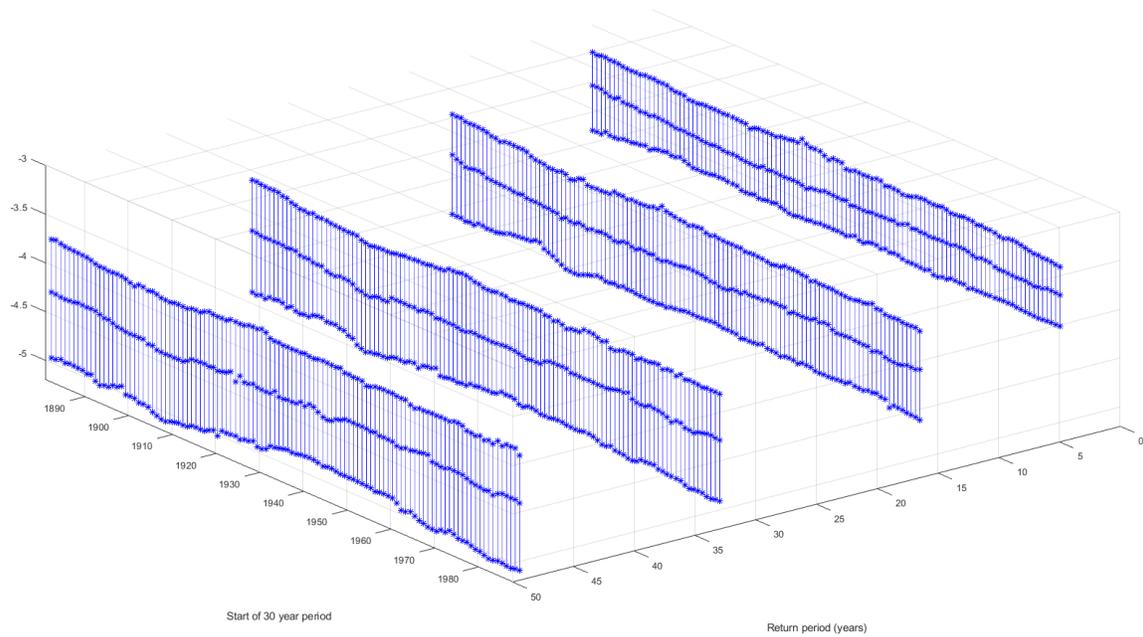
Figure 7.20 Lower tail of the simulated minimum air temperature behavior

7.3 Individual long-lived observed records

We realized this part of the study of the land surface air temperature in order to compare the general trend of the ensemble of the recorded timeseries with the longest recorded available timeseries. The individual weather stations, whose records we investigated separately are the station of St. Petersburg, Russia for the upper and lower tails of the average air temperature and the station of Milan, Italy for the upper tail of the maximum and the lower tail of the minimum air temperature.

Upper tail of the average air temperature, as presented by the data of the St. Petersburg station, corroborate the slightly increasing trend of the thickness of the tail observed from the sum of the weather stations around the globe. However, intense, yet isolated, heatwaves seem to alter substantially the stability of this trend. Specifically, in years 1972, 1986, 2010 (shown in periods starting 30 years earlier) a noticeable increase of the thickness of the tail of up to 0.6 can be observed in the larger return period. Interestingly, the latter one, corroborates the extreme heatwave experienced in the Northern hemisphere during the summer of 2010.
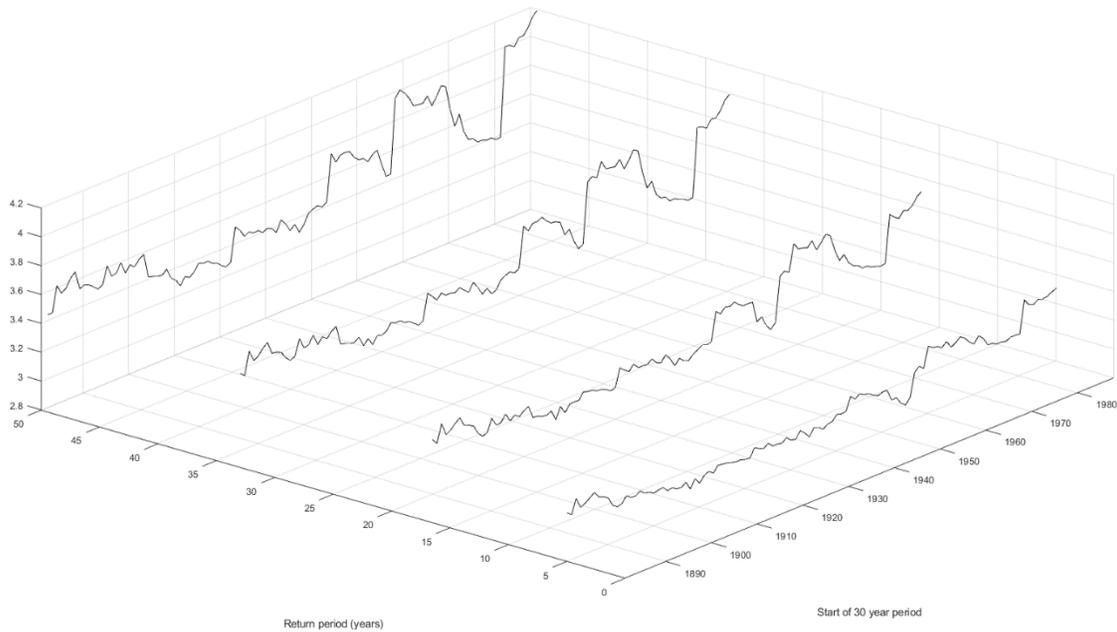
Figure 7.21 Upper tail of the average air temperature of St. Petersburg, Russia station

Lower tail of the average air temperature, as presented by the data of the St. Petersburg station, present great instability. The very first years of the record, i.e. 30-year periods starting up to 1893, show a stable behavior, but after that period and until the 30-year periods starting up to 1949, a considerable upward dislocated plateau indicate a persistent period of low average temperatures spanning for more than 50 years. After this plateau, however, a considerable plummeting of the average temperature translates to a decrease of the standardized average temperature by about 0.8 in one year and further 0.2 after 7 years, indicating persistent freezing of the region. After 2010 the effect seems to be mitigated, and the lower tail returns to an average level.
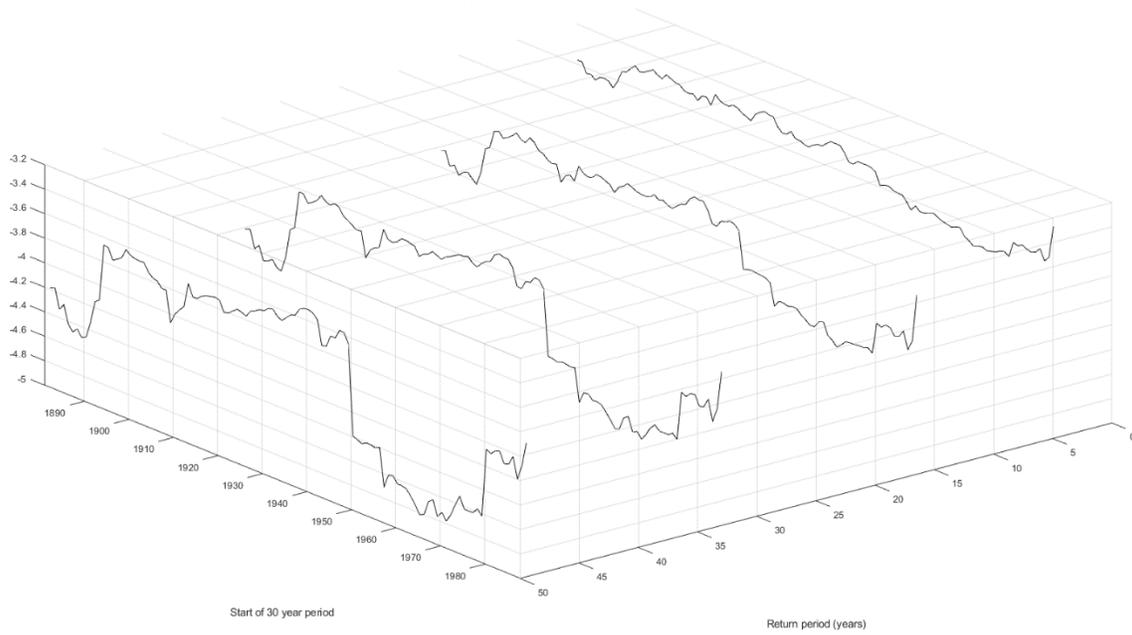
Figure 7.22 Lower tail of the average air temperature of St. Petersburg, Russia station

Upper tail of the maximum air temperature, as presented by the data of the Milan station in Italy, does not corroborate the slightly decreasing trend of the thickness of the tail observed from the sum of the weather stations. In particular, for the common record period between 1881 and 2010 an ascending trend is apparent in all the return periods. Especially in the two larger return periods, in the 30-year period starting 1955 a robust increase of about 1 (of the standardized timeseries) alter the steady behavior of the record present the previous 100 years.
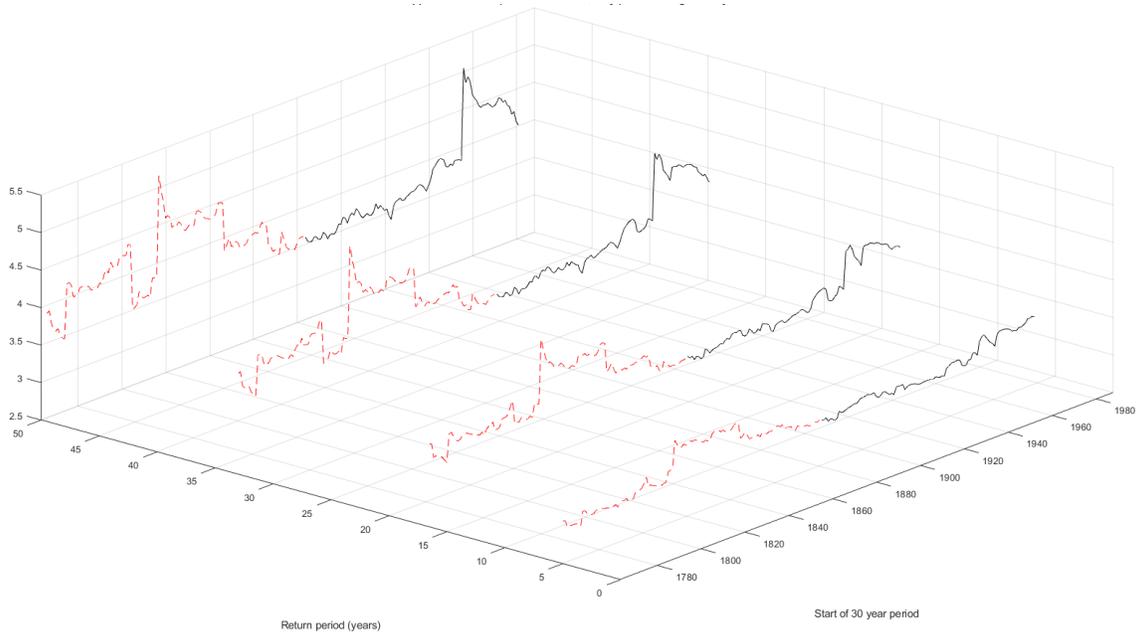
Figure 7.23 Upper tail of the maximum air temperature of Milan, Italy station

Lower tail of the minimum air temperature, as presented by the data of the Milan station in Italy, does not show to corroborate the relatively stable trend of the thickness of the tail observed from the sum of the weather stations. Specifically, for the 30 years periods starting between 1900 and 1940 a severe fall of the minimum temperature, of the scale of about 1, happens, which contradicts the general upward, i.e. thinning, of the tail of the minimum temperature.
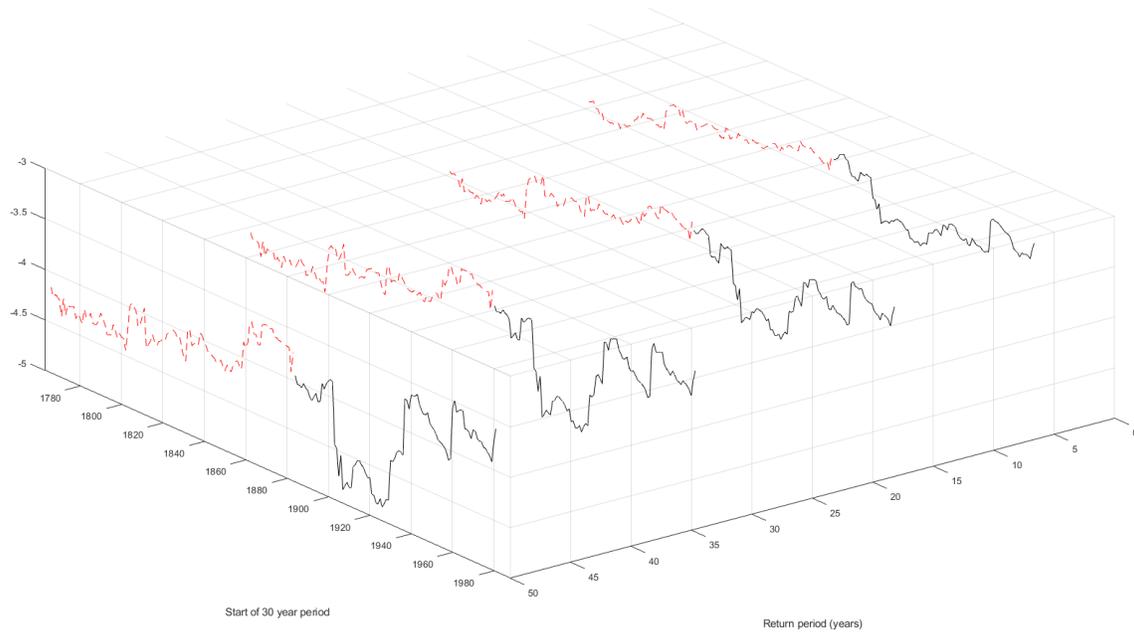
Figure 7.24 Lower tail of the minimum air temperature of Milan, Italy station

The great differences individual records present with the sum of the records from all over the globe are reasonable to appear, since aggregate behavior tends to present milder variations, thus attenuating local and isolated extreme heat or cold waves. Despite this, it is extremely useful to compare the behavior of the whole with the records that are the most long-lived, so as to identify possible baseless generalizations that may emerge from the over-focusing on individual records.

8. Conclusions

The aim of this study is to investigate the extreme land surface air temperature temporal evolution in global scale, by studying long timeseries of the average, maximum and minimum air temperature. Despite all the interest that has been given to the study of the air temperature trends in recent years, this is the first study to normalize the temperature records with respect to the respective months. Thus, statistically unimportant variations, within the scope of usual natural variation do not skew the study of the temperature in macroscopic scale, free of any microvariations bias.

First, we retrieved all the necessary timeseries data from the GHCN (Global Historical Climatology Network)-Daily database for the three studied variables; i.e. average, maximum and minimum air temperature. Then, after performing a series of quality checks, to clear out the data containing any false entries, we standardized (according to the Gaussian distribution) each timeseries, with respect to the monthly average (arithmetic mean) and standard deviation. From each standardized timeseries, consecutively rolling 30-year long sections were isolated, in order for the study of the extreme occurrence to take place.

Secondly, for each rolling 30-year section of the timeseries, we extracted, through the use of the K-moments, the extreme values corresponding to 4 pre-selected return periods, representative of the whole tail of the temperature distribution. These values were saved in a separate file, from which, after repeating this procedure for all the observed timeseries, the 25th, 50th and 75th percentile values were isolated for each year (corresponding to the start of a 30-year period) and were plotted in a boxplot.

Thirdly, and in parallel with the study of the observed timeseries, we calculated an aggregated climacogram for the ensemble of the timeseries was created, from which the persistence of the temperature variables. This was achieved through the utilization of a hybrid Hurst-Kolmogorov and Markov theoretical model being optimized, through a

Monte-Carlo analysis, to fit the Climacogram. We then used the Hurst coefficients of each temperature variable to create synthetic records with the same statistical characteristics as the observed timeseries. These synthetic timeseries were finally studied, using K-moments at specific return periods, in a similar process as the one followed in observed timeseries.

8.1 Remarks on observed record behavior

The study of the observed land surface air temperature records brought interesting facts to the surface. All three of the air temperature variables (namely average, maximum and minimum) present an unstable behavior, with fluctuations not easily negligible.

The average land surface air temperature presents the most persistent behavior, which is a progressive increase. The upper tail seems to become more and more thick, while the lower tail appears to become thinner as time progresses. This means that the average air temperature increases as a whole, with important effects on the lives of both humans and other species. Water dependence, agricultural practices and transportation of goods and people will have to adapt, in order to better cope with the change of the mean expected temperature.
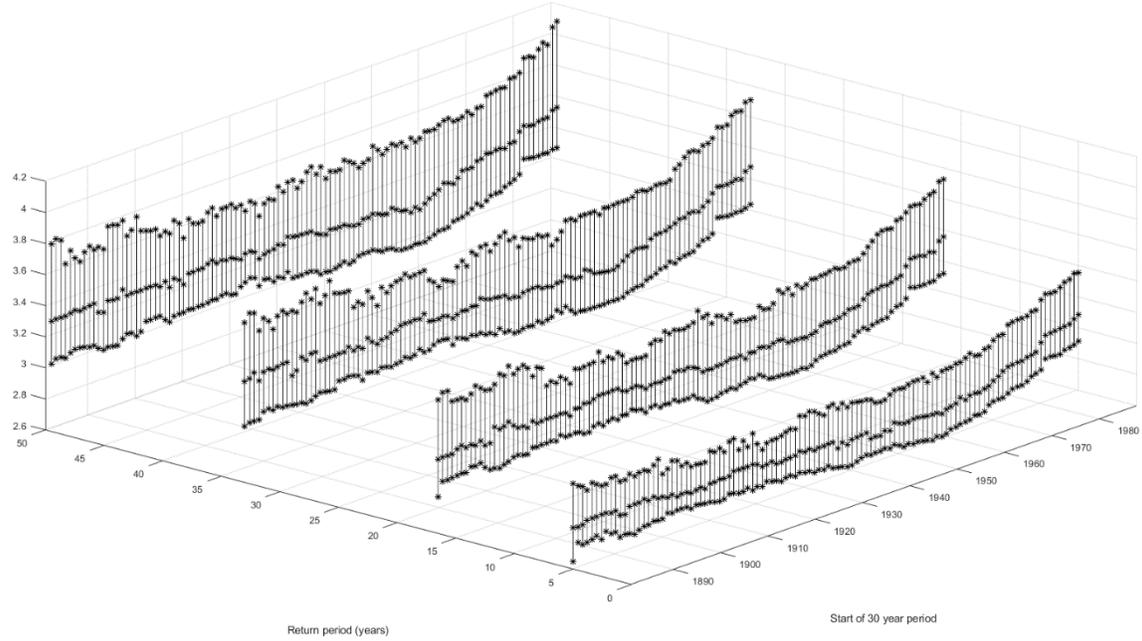
Figure 8.1 Upper tail of the observed average air temperature
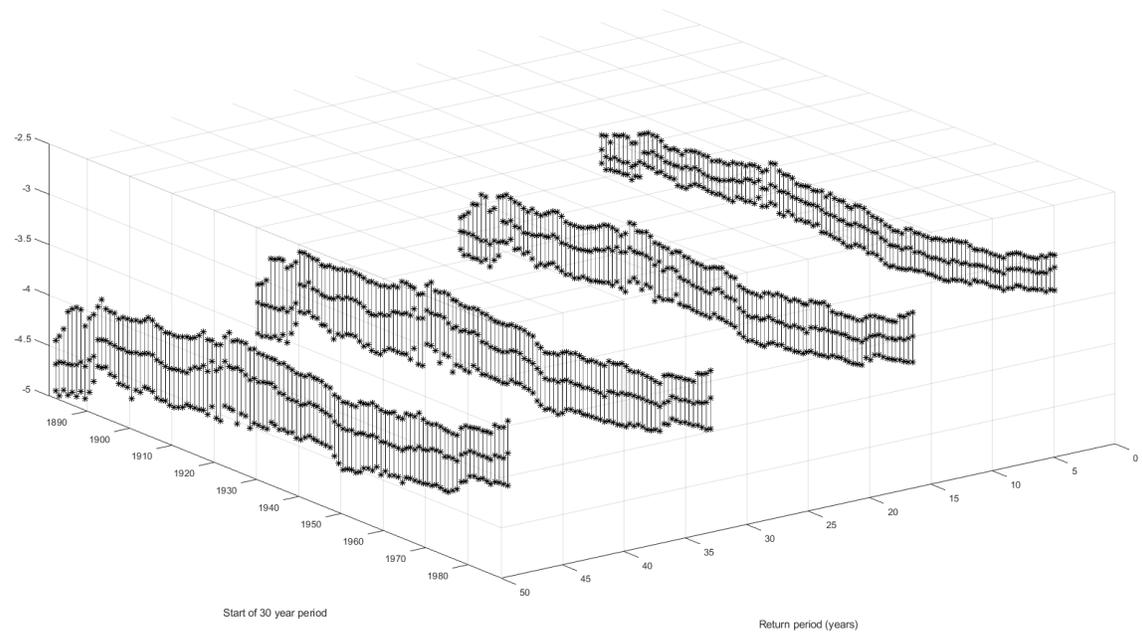
Figure 8.2 Lower tail of the observed average air temperature

An interesting and, quite frankly, unexpected finding is the thinning of the upper tail of the maximum land surface air temperature. Contrary to our expectations, it appears that the behavior of the maximum temperature does not necessarily follow that of the average, meaning that temperature is a more complex climatic variable than previously thought. Even though, the maximum recorded temperature is an integral part of the set of data from which the average temperature derives, it appears that its effect is not so intelligible. From a statistical point of view, it would be reasonable to assume that an increase of the upper extreme of a finite set would increase its expected mean. Yet the case is that the intermediate values of temperature are what affect the average the most.
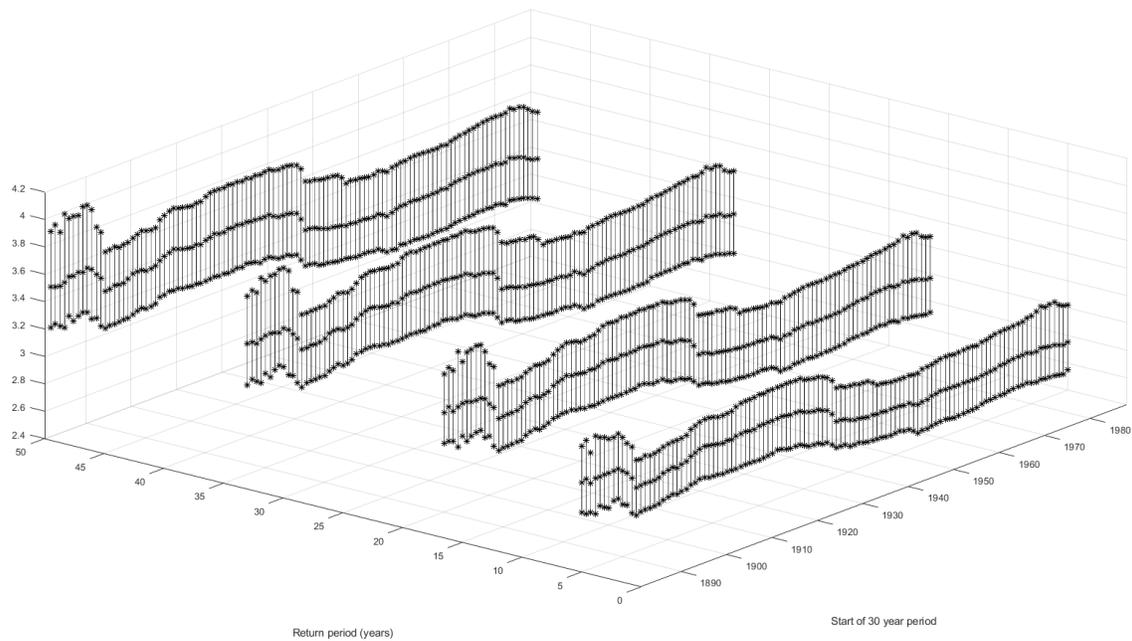
Figure 8.3 Upper tail of the observed maximum air temperature

As for the lower tail of the minimum land surface air temperature, it becomes clear that despite the increasing trend of the average air temperature (even of its lower values), it remains surprisingly steady, at all return period levels, and only in the last 10-20 years presents an increasing trend. This shows that the temperature changes are not

simultaneous through all the spectrum of the temperature variance. Thus, the climate presents stamina and is able to mitigate, to some extent, changes in factors of the energy balance of the atmosphere. The fact that almost the same level of upward trend of all the return period levels of the lower tail suggest a change of the average of the distribution is more probable than a change of standard deviation, assuming that the minimum temperature presents a Gaussian-like distribution.
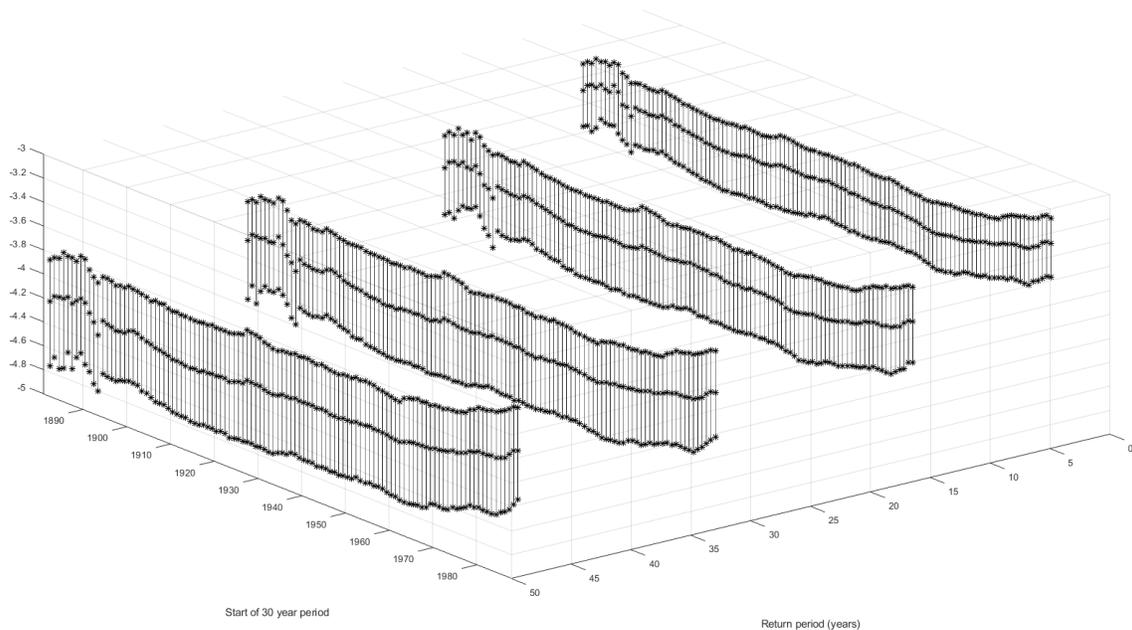
Figure 8.4 Lower tail of the observed minimum air temperature

8.2 Remarks on synthetic record behavior

The point of producing synthetic timeseries and investigating them in comparison with the observed timeseries was to identify similarities and differences between them, that would lead to a divergence of the actual natural behavior of air temperature from a simulated stochastic one.

The average land surface air temperature synthetic records produced present an ambiguous behavior. On the one hand, the upper tail presents a similar pattern as the one

of the observed data, with the exception of the increasing trend. The variance of the trend, as expressed through the interquartile range at each return period level, is almost the same, which point to "well" produced pool of synthetic data. On the other hand, the lower tail, despite having the same variance at all the return period levels, is much thinner than in reality. This could mean that the extreme cold waves, affecting the lower tail of the average temperature, are much more common than anticipated by the reproduction of the observed stochastic behavior. Despite having a uniquely fit hybrid Hurst-Kolmogorov and Markov process to estimate the persistence of the average air temperature, as witnessed by the Climacogram, it still was not enough to decipher, and consequently reproduce, the complex behavior of the average air temperature. Consequently, the selected model may not be adequate to describe such a complex behavior as the one presented by the lower tail of the average air temperature.

As for the maximum land surface air temperature synthetic records produced, the variance of the trend, as expressed through the interquartile range at each return period level, is greater than that of the observed data, hence proving that any upward trend of the upper tail of it is perfectly within the boundaries of expected. Furthermore, the slightly increasing trend of the upper end (i.e. 75th percentile) of the interquartile range present at higher return periods is completely opposite form the same limit performance of the observed data.

The minimum land surface air temperature synthetic records produced present many comparative similarities with the maximum air temperature. Specifically, the size of the interquartile range is greater than the one derived from observed data and in fact overspreads it. This means that any changes present in the observed timeseries are perfectly explainable from the study of the statistical behavior. Moreover, the slightly increasing trend of the extreme values of the lower tail may suggest a return to normality and not a spiraling towards global overheating.

8.3 Remarks on individual long-lived record behavior

Individual long-lived observed records were studied individually, in order to compare the temporal evolution of the ensemble of instrumental records, with those individuals that have the longest length. This enables us to assess the land surface air temperature evolution unbiased from differentiations on the number of temporally co-existing instrumental records. However, it has the disadvantage of local bias, thus making risky any generalization to the global scale.

The longest-lived instrumental records of the average land surface air temperature are those of Saint Petersburg, Russia. As shown from the analysis made, the upper tail presents a systematically thickening, across all levels of return periods. Especially from the point where years of the 1990's and after were added to the rolling 30-year periods (i.e. 30-year periods starting after 1960's), the increasing trend of the thickness is almost free of any micro-variations. This shows that a persistent local or superregional has been affecting the climate of Saint Petersburg after the 1990's.

The lower tail of the average land surface air temperature presents a somewhat more tumultuous behavior, yet with a relatively stable general trend of thinning. At the larger return period levels, the variations of the thickness of the tail are of the order of 0.8-1.0, and are apparent from the beginning of the 20th century. At the lowest return periods, however, the variations are significantly smaller, but the latest years (i.e. 30-year periods starting after 1980) present a thinning of the lower tail of about 0.4-0.8, that cannot be ignored.

As for the maximum and minimum land surface air temperature, the longest-lived instrumental records are those of Milan, Italy. From the proceeding analysis, we understand that from the 1770's until the 1840's the maximum air temperature had a relatively stable upper tail. Yet around the end of the 1840's and beginning of 1850's a strong force caused the upper tail to thicken almost uniformly by about 1.0, which implies a displacement of the upper tail to the right (i.e. an increase of the average of the distribution and not of the variance). Then until about 1980's the behavior of the upper

tail is surprisingly stable, considering the more-than-centennial length of the period. After the 1908's, however, the upper tail follows an similar pattern as the one of the of the 1850's period, with a substantial thickening of about 1.3-1.5 across all return period levels, suggesting another displacement of the upper tail to the right (i.e. an increase of the average of the distribution and not of the variance).

The lower tail of the minimum land surface air temperature appears to have a similar behavior as the one of the lower tail of the average land surface air temperature. It is quite turbulent, with variations of about 0.6-0.8, even at the lower return period levels, but the changes seem to cancel each other, giving a stable trend up to about the 1990's. After that period, however, the lower tail seems to thin a lot, with the decreases of the respective return period values to be more than 0.5.

What we infer from these two individual long-lived instrumental records is a systematic increase of the thickness of the upper tail and a systematic thinning of the lower tail. One of the reasons that may explain this observation is the possibility that Europe may experience a general warming compared to the rest of the world.

A more potent factor for the increase of the mean land surface air temperature in both Saint Petersburg and Milan could be the increase of the population of the two cities, accompanied by a change of land cover. This could intensify the heat island effect, which would systematically affect the warming of the regions, which host the weather stations. As shown from data of the Italian National Institute of Statistics (Istat, 2014), the population of the urban center of Milan increased from 267,000 to 1,368,000 between 1861 and 2016, which indicates a five-fold increase. As for the Saint Petersburg federal subject, the resident population increased from 843,000 to about 4,597,000 between the years 1880 and 2003 (Elyseeva and Gribova, 2003). This increase is more than five-fold, thus making plausible the suspicion of severe change in land cover affecting the temperature in the city.

8.4 Implications on the land surface air temperature tails

The assessment of the changes that occur in the tails of average, maximum and minimum land surface air temperature is essential for the understanding of the exact nature of climate change. Changes in the average (arithmetic mean) of the equivalent distribution of air temperature are completely different from changes in variance. An increase of variance leads to greater instability and more frequent and intense extreme events. On the other hand, a change of the average of the distribution translates to a displacement of the whole distribution, but not of the occurrence of extremes; the only thing changing is the definition of extremes, since events of different temperature will correspond to the same probability of happening.

As shown by the investigation of the tail behavior of surface temperature on global scale using K-moments performed by Glynis et al. (2019), the tails of the temperature distribution are not exactly Gaussian. The upper tail is lighter than that of the Gaussian, while the lower is heavier. With this in mind and giving greater gravity to the results of the maximum and minimum temperature study, which incorporated data from 20 times more instrumental records than the equivalent of the average temperature (namely more than 5,000 records compared to less than 250 records), it is reasonable to deduce the following:

- The upper tail of the land surface air temperature has remained relatively unchanged throughout the past 130 years (both in terms of average and variance of its distribution).
- The lower tail of the land surface air temperature had remained unchanged until the 1990's from which point is started to become thinner, due to a change of the average and not the variance of its distribution.
- The main body of the distribution of land surface air temperature, which closely relates to the average (arithmetic mean) air temperature has moved to warmer temperatures, which was caused by an increase of the average and not the variance of its distribution.

Thus, it is valid to say that extreme heatwaves remain the same probable as in the past, extreme cold waves have become slightly scarcer. However, the expected (average) daily temperature has increased, especially in the last 30 years. One such possible explanation is the change of the air temperature density function, as shown in the figure 8.5.
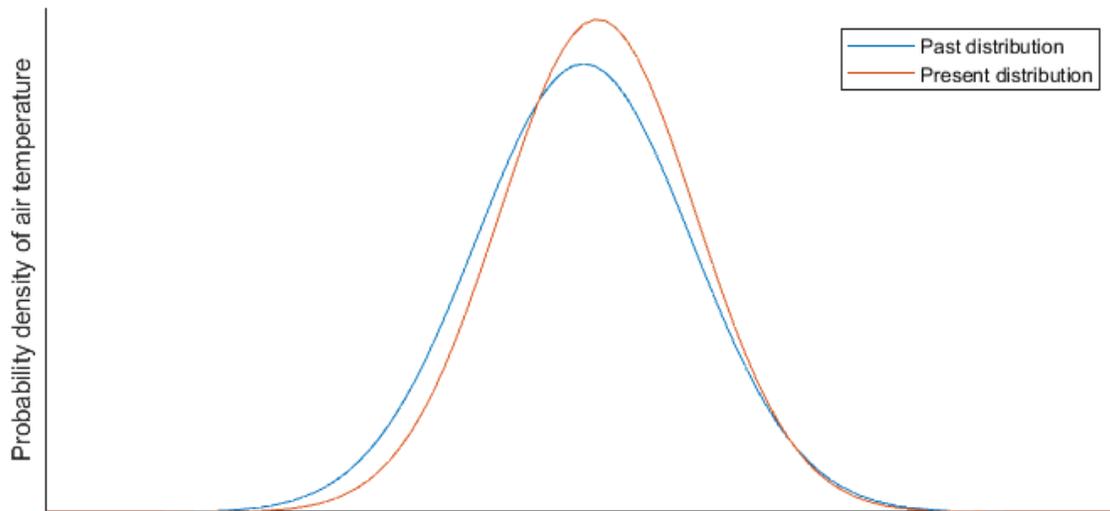
Figure 8.5 One possible historical evolution of the air temperature probability density function. Note that its purpose is purely perceptional.

This behavior strongly suggests the existence of certain physical laws that enable the Earth's climate to absorb any temperature increases by increasing the minimum temperature, but avoiding increasing the maximum temperature. This is unexpected, since the only known boundary of temperature is the absolute zero (-273.15 °C), while an upper limit does not exist.

All these changes make the land surface air temperature to have a narrower range, since the lower extremes have decreased, while the upper extremes have remained relatively

constant. However, we cannot be certain of how the internal variability of the climate is going to change, since persisting warm or cold events may increase.

8.5 Suggestions for future research

The array of possibilities that engenders the scientific methodology that we followed in this research is huge. A prime example of possible follow-up study is the implementation of K-moments and the Hurst-Kolmogorov approach on the satellite-measured surface air temperature records, which include both land and ocean areas of the planet, thus increasing significantly the spatial coverage. In such case, though, attention should be given to the time of the day at which each measurement has been taken, as well as the interference of cloud and air currents above the surface.

Another promising field of follow-up study is the spatial, and temporal of course, analysis of the temperature persistence and change. This would enable the derivation of valuable information on which climatic regions do get affected the most from the climate change and in which way. Furthermore, it could be used to correlate it with precipitation patterns alterations in order to produce a reliable model for temperature and precipitation macroscopic prediction.

Last, but not least, the same tools that we used here to assess the changes of the extreme values of land surface air temperature could be used to study the surface dew point. This would enable the understanding of how the air saturation patterns have changed in relation to the past, and what consequences this has for the precipitation. Especially in arid and semi-arid areas, the high seasonality of rainfall makes exigent the accurate prediction of how these patterns are changing, in order for the ecosystem and humans to better adapt.

References

Acker, J. G., & Leptoukh, G. (2007). Online analysis enhances use of NASA earth science data. *Eos, Transactions American Geophysical Union*, *88*(2), 14-17.

Allaby M. "Stevenson screen" A Dictionary of Plant Sciences. Retrieved October 23, 2019 from encyclopedia.com

Arum, C., & Tayo, O. A. Design Optimization of Single Span Fixed-Feet Portal Frame Using Generalized Reduced Gradient Method.

Brown, P. T., Li, W., Cordero, E. C., & Mauget, S. A. (2015). Comparing the model-simulated global warming signal to observations using empirical estimates of unforced noise. *Scientific reports*, *5*, 9957.

Butler, J. H., & Montzka, S. (2011). The NOAA annual greenhouse gas index. *NOAA Earth System Research Laboratory*.

Chang, E. K., & Fu, Y. (2002). Interdecadal variations in Northern Hemisphere winter storm track intensity. *Journal of Climate*, *15*(6), 642-658.

Charlson, R. J., Schwartz, S. E., Hales, J. M., Cess, R. D., Coakley, J. J., Hansen, J. E., & Hofmann, D. J. (1992). Climate forcing by anthropogenic aerosols. *Science*, *255*(5043), 423-430.

Claussen, E., Cochran, V. A., & Davis, D. P. (Eds.). (2001). *Climate change: science, strategies, & solutions* (Vol. 13, No. 45). Brill.

Cronin, T. M. (2009). *Paleoclimates: understanding climate change past and present*. Columbia University Press.

Dimitriadis, P., & Koutsoyiannis, D. (2015). Climacogram versus autocovariance and power spectrum in stochastic modelling for Markovian and Hurst–Kolmogorov processes. *Stochastic environmental research and risk assessment*, *29*(6), 1649-1669.

Dimitriadis, P., & Koutsoyiannis, D. (2018). Stochastic synthesis approximating any process dependence and distribution. *Stochastic environmental research and risk assessment*, *32*(6), 1493-1515.

Durre, I., Menne, M. J., Gleason, B. E., Houston, T. G., & Vose, R. S. (2010). Comprehensive automated quality assurance of daily surface observations. *Journal of Applied Meteorology and Climatology*, *49*(8), 1615-1633.

Easterling, D. R., Horton, B., Jones, P. D., Peterson, T. C., Karl, T. R., Parker, D. E., ... & Folland, C. K. (1997). Maximum and minimum temperature trends for the globe. *Science*, *277*(5324), 364-367.

Efstratiadis, A., Dialynas, Y. G., Kozanis, S., & Koutsoyiannis, D. (2014). A multivariate stochastic model for the generation of synthetic time series at multiple time scales reproducing long-term persistence. *Environmental Modelling & Software*, *62*, 139-152.

Elyseeva, I. I. & Gribova, E. I. (2003). *St. Petersburg. 1703-2003: Anniversary statistical compilation. Edition 2*,16-17.

Fall, S., Watts, A., Nielsen-Gammon, J., Jones, E., Niyogi, D., Christy, J. R., & Pielke Sr, R. A. (2011). Analysis of the impacts of station exposure on the US Historical Climatology Network temperatures and temperature trends. *Journal of Geophysical Research: Atmospheres*, *116*(D14).

Fan, J., Yuan, T., Comstock, J. M., Ghan, S., Khain, A., Leung, L. R., ... & Ovchinnikov, M. (2009). Dominant role by vertical wind shear in regulating aerosol effects on deep convective clouds. *Journal of Geophysical Research: Atmospheres*, *114*(D22).

Florescu, I. (2014). *Probability and stochastic processes*. John Wiley & Sons.

Folland, C. K., Karl, T. R., Christy, J. R., Clarke, R. A., Gruza, G. V., Jouzel, J., ... & Wang, S. W. (2001). Observed climate variability and change. *Climate change*, *2001*, 99.

Gill, P. E., Murray, W., & Wright, M. H. (1981). Practical optimization. *London: Academic Press, 1981*.

Glickman, T. S. (1995). 2000: Glossary of Meteorology.

Glynis, K. G., Iliopoulou, T., Dimitriadis, P. & Koutsoyiannis, D. (2019) Investigating the tail behaviour of surface temperature on global scale using K-moments. European Geosciences Union General Assembly 2019.

Gunning, R., & Rossi, H. Analytic functions of several complex variables, Prentice-Hall, Englewood Cliffs, NJ, 1965. *MR*, *31*, 4927.

Hansen, J., Ruedy, R., Sato, M., & Lo, K. (2010). Global surface temperature change. *Reviews of Geophysics*, *48*(4).

Hasselmann, K. (1976). Stochastic climate models part I. Theory. *tellus*, *28*(6), 473-485.

Haywood, J., & Boucher, O. (2000). Estimates of the direct and indirect radiative forcing due to tropospheric aerosols: A review. *Reviews of geophysics*, *38*(4), 513-543.

Held, I. M., & Soden, B. J. (2000). Water vapor feedback and global warming. *Annual review of energy and the environment*, *25*(1), 441-475.

Huld, T. A., Šúri, M., Dunlop, E. D., & Micale, F. (2006). Estimating average daytime and daily temperature profiles within Europe. *Environmental Modelling & Software*, *21*(12), 1650-1661.

Hurst, H. E. (1951). Long-term storage capacity of reservoirs. *Trans. Amer. Soc. Civil Eng.*, *116*, 770-799.

Huschke, R. E. (1959). Glossary of meteorology.

IPCC (2018) *Summary for Policymakers. In: Global Warming of 1.5°C. An IPCC Special Report on the impacts of global warming of 1.5°C above pre-industrial levels and related global greenhouse gas emission pathways, in the context of strengthening the global response to the threat of climate change, sustainable development, and efforts to eradicate poverty*. World Meteorological Organization, Geneva

Istat (2014) Historical population of Milan, 1861-2016 Retrieved October 23, 2019 from seriestoriche.istat.it

Jones, P. D., Lister, D. H., Osborn, T. J., Harpham, C., Salmon, M., & Morice, C. P. (2012). Hemispheric and large-scale land-surface air temperature variations: An extensive revision and an update to 2010. *Journal of Geophysical Research: Atmospheres*, *117*(D5).

Kiehl, J. T., & Trenberth, K. E. (1997). Earth's annual global mean energy budget. *Bulletin of the American Meteorological Society*, *78*(2), 197-208.

Koutsoyiannis, D. (1997). Statistical hydrology. *Edition 4*, 312.

Koutsoyiannis, D. (2000). A generalized mathematical framework for stochastic simulation and forecast of hydrologic time series. *Water Resources Research*, *36*(6), 1519-1533.

Koutsoyiannis, D. (2002). The Hurst phenomenon and fractional Gaussian noise made easy. *Hydrological Sciences Journal*, *47*(4), 573-595.

Koutsoyiannis, D. (2010). HESS Opinions" A random walk on water". *Hydrology and Earth System Sciences*, *14*(3), 585-601.

Koutsoyiannis, D. (2011). Hurst-Kolmogorov Dynamics and Uncertainty 1. *JAWRA Journal of the American Water Resources Association*, *47*(3), 481-495.

Koutsoyiannis, D. (2016). Generic and parsimonious stochastic modelling for hydrology and beyond. *Hydrological Sciences Journal*, *61*(2), 225-244.

Koutsoyiannis, D. (2018). Climate change impacts on hydrological science: How the climate change agenda has lowered the scientific level of hydrology. *School for Young Scientists "Modelling and forecasting of river flows and managing hydrological risks: Towards a new generation of methods"*

Koutsoyiannis, D. (2019). Knowable moments for high-order stochastic characterization and modelling of hydrological processes. *Hydrological sciences journal*, *64*(1), 19-33.

Koutsoyiannis, D. (2020). *Stochastics of Hydroclimatic Extremes*. (to be published).

Koutsoyiannis, D., Dimitriadis, P., Lombardo, F., & Stevens, S. (2018). From fractals to stochastics: Seeking theoretical consistency in analysis of geophysical data. In *Advances in Nonlinear Geosciences* (pp. 237-278). Springer, Cham.

Lamperti, J. (1977). Stochastic Processes, volume 23 of Applied Mathematical Sciences.

Larson, R., & Edwards, B. H. (2013). *Calculus of a single variable*. Cengage Learning.

Lawrimore, J. H., Menne, M. J., Gleason, B. E., Williams, C. N., Wuertz, D. B., Vose, R. S., & Rennie, J. (2011). An overview of the Global Historical Climatology Network monthly mean temperature data set, version 3. *Journal of Geophysical Research: Atmospheres*, *116*(D19).

Le Treut H.; Somerville R.; Cubasch U.; Ding Y.; Mauritzen C.; Mokssit A.; Peterson T.; Prather M. (2007). Historical overview of climate change. *Climate Change 2007: The Physical Science Basis. Contribution of Working Group I to the Fourth Assessment Report of the Intergovernmental Panel on Climate Change*.

Lean, J. L., & Rind, D. H. (2009). How will Earth's surface temperature change in future decades? *Geophysical Research Letters*, *36*(15).

LibreTexts library. Powered by MindTouch and supported by the Department of Education Open Textbook Pilot Project, the UC Davis Office of the Provost, the UC Davis Library, the California State University Affordable Learning Solutions Program, and Merlot. Retrieved October 23, 2019 from math.libretexts.org

Lindzen, R. S. (2010). Global Warming: How to approach the science.

Lombardo, F., Volpi, E., Koutsoyiannis, D., & Papalexiou, S. M. (2014). Just two moments! A cautionary note against use of high-order moments in multifractal models in hydrology. *Hydrology and Earth System Sciences*, *18*(1), 243-255.

Mandelbrot, B. B. (1983). *The fractal geometry of nature* (Vol. 173, p. 51). New York: WH freeman.

Marlow, W. H. (1993). *Mathematics for operations research*. Courier Corporation.

Mazzarella, A., Giuliacci, A., & Scafetta, N. (2013). Quantifying the Multivariate ENSO Index (MEI) coupling to CO 2 concentration and to the length of day variations. *Theoretical and applied climatology*, *111*(3-4), 601-607.

Menne, M. J., Williams Jr, C. N., & Palecki, M. A. (2010). On the reliability of the US surface temperature record. *Journal of Geophysical Research: Atmospheres*, *115*(D11).

Menne, M.J., I. Durre, R.S. Vose, B.E. Gleason, and T.G. Houston, 2012: An overview of the Global Historical Climatology Network-Daily Database. *Journal of Atmospheric and Oceanic Technology*, 29, 897-910.

Montanari, A., Rosso, R., & Taqqu, M. S. (1997). Fractionally differenced ARIMA models applied to hydrologic time series: Identification, estimation, and simulation. *Water resources research*, *33*(5), 1035-1044.

Morice, C. P., Kennedy, J. J., Rayner, N. A., & Jones, P. D. (2012). Quantifying uncertainties in global and regional temperature change using an ensemble of observational estimates: The HadCRUT4 data set. *Journal of Geophysical Research: Atmospheres*, *117*(D8).

Pachauri, R. K., & Reisinger, A. (2007). IPCC fourth assessment report. *IPCC, Geneva*, *2007*.

Papoulis, A. (1990). *Probability & statistics* (Vol. 2). Englewood Cliffs: Prentice-Hall.

Papoulis, A., & Probability, R. V. (1991). Stochastic process.

Parker, D. E., Jones, P., Peterson, T. C., & Kennedy, J. (2009). Comment on "Unresolved issues with the assessment of multidecadal global land surface temperature trends" by Roger A. Pielke Sr. et al. *Journal of Geophysical Research: Atmospheres*, *114*(D5).

Peterson, T. C., & Vose, R. S. (1997). An overview of the Global Historical Climatology Network temperature database. *Bulletin of the American Meteorological Society*, *78*(12), 2837-2850.

Peterson, T. C., Gallo, K. P., Lawrimore, J., Owen, T. W., Huang, A., & McKittrick, D. A. (1999). Global rural temperature trends. *Geophysical Research Letters*, *26*(3), 329-332.

Pielke Sr, R. A., Davey, C. A., Niyogi, D., Fall, S., Steinweg-Woods, J., Hubbard, K., ... & Nielsen-Gammon, J. (2007). Unresolved issues with the assessment of multidecadal global land surface temperature trends. *Journal of Geophysical Research: Atmospheres*, *112*(D24).

Prihodko, L., & Goward, S. N. (1997). Estimation of air temperature from remotely sensed surface observations. *Remote Sensing of Environment*, *60*(3), 335-346.

Rohde, R., Muller, R. A., Jacobsen, R., Muller, E., Perlmutter, S., Rosenfeld, A., ... & Wickham, C. (2013). A New Estimate of the Average Earth Surface Land Temperature Spanning 1753 to 2011, Geoinfor Geostat: An Overview 1: 1. *of*, *7*, 2.

Rohde, R., Muller, R., Jacobsen, R., Perlmutter, S., Rosenfeld, A., Wurtele, J., ... & Mosher, S. (2013). Berkeley earth temperature averaging process. *Geoinformatics & Geostatistics: An Overview*, *1*(2), 1-13.

Seneviratne, S. I., Nicholls, N., Easterling, D., Goodess, C. M., Kanae, S., Kossin, J., ... & Reichstein, M. (2012). Changes in climate extremes and their impacts on the natural physical environment. In *Managing the risks of extreme events and disasters to advance climate change adaptation: Special report of the Intergovernmental Panel on Climate Change* (pp. 109-230). Cambridge University Press.

Shindell, D., Myhre, G., Boucher, O., Forster, P., Breon, F. M., & Fuglestvedt, J. (2013). Radiative Forcing in the AR5. In *Conference Proceeding in IPCC AR5 working group I* (pp. 1-11).

Smil, V. (2003). *The Earth's biosphere: Evolution, dynamics, and change*. MIT Press.

Solomon, S., Qin, D., Manning, M., Chen, Z., Marquis, M., Averyt, K., ... & Miller, H. (2007). IPCC fourth assessment report (AR4). *Climate change*.

Stedinger, J. R., Vogel, R. M., & Foufoula-Georgiou, E. (1993). Handbook of hydrology. *Edited by*.

Stewart, J. (2008). Calculus: Early Transcendentals, volume 6E of Calculus. *Brooks Cole*.

Stocker, T. F., Qin, D., Plattner, G. K., Tignor, M., Allen, S. K., Boschung, J., ... & Midgley, P. M. (2013). Climate change 2013: The physical science basis.

Trenberth, K. E., & Caron, J. M. (2000). The Southern Oscillation revisited: Sea level pressures, surface temperatures, and precipitation. *Journal of Climate*, *13*(24), 4358-4365.

Trenberth, K. E., Caron, J. M., Stepaniak, D. P., & Worley, S. (2002). Evolution of El Niño–Southern Oscillation and global atmospheric surface temperatures. *Journal of Geophysical Research: Atmospheres*, *107*(D8), AAC-5.

Trenberth, K. E., Jones, P. D., Ambenje, P., Bojariu, R., Easterling, D., Klein Tank, A., ... & Soden, B. (2007). Observations: surface and atmospheric climate change. Chapter 3. *Climate change*, 235-336.

Twomey, S. (1977). The influence of pollution on the shortwave albedo of clouds. *Journal of the atmospheric sciences*, *34*(7), 1149-1152.

Volpi, E., Fiori, A., Grimaldi, S., Lombardo, F., & Koutsoyiannis, D. (2015). One hundred years of return period: Strengths and limitations. *Water Resources Research*, *51*(10), 8570-8585.

Vose, R. S., Easterling, D. R., & Gleason, B. (2005). Maximum and minimum temperature trends for the globe: An update through 2004. *Geophysical Research Letters*, *32*(23).

Williams, C. N., Menne, M. J., & Thorne, P. W. (2012). Benchmarking the performance of pairwise homogenization of surface temperatures in the United States. *Journal of Geophysical Research: Atmospheres*, *117*(D5).

WMO. (1992). *International Meteorological Vocabulary (WMO-No. 182)*. Geneva

WMO. (2007). *Guide to the Global Observing System (WMO-No. 488)* (3rd ed.). Geneva

WMO. (2008). *Guide to Meteorological Instruments and Methods of Observation (WMO-No. 8)* (7th ed.). Geneva

World Bank Group. Global map of direct normal irradiation. Retrieved October 23, 2019 from https://datacatalog.worldbank.org/dataset

Appendix

In this appendix we provide all the important scripts and functions, which we used (in Matlab environment) for the scientific purposes of this study.

Script 1: Search for non-zero files

```
clc; clear all; close all; tic;

%Search for non-zero data files
[~,stations] = xlsread('Data_List_Tmax.xlsx');
for i = 1:length(stations);
    filename = strcat('NOAA_GHCND_TMAX/',string(stations(i)));
    load(filename,'S'); %loading of time series
    m(i,1) = numel(find(S(:,4)))/365.25;
end
save('numyears_Tmax.mat','m');
toc;
```

Script 2: Plotting of observed timeseries

```
minimum = 30; %minimum record length
maximum = inf; %maximum record length

limit1 = 1935; %latest year of record start
tail = 1; %1 for Upper tail; 2 for Lower tail
[~,stations] = xlsread('Data_List_Tavg.xlsx');
load('numyears_Tavg.mat');
size = 245; %number of stations which entered service before 1935

start_year = 1881;
end_year = 1988;
Kp_alpha = NaN(size,end_year-start_year+1);
Kp_beta = NaN(size,end_year-start_year+1);
Kp_gamma = NaN(size,end_year-start_year+1);
Kp_delta = NaN(size,end_year-start_year+1);
temp1 = 0;
all = 106283;
for number = 1:all;
    filename = strcat('NOAA_GHCND_TAVG/',char(stations(number)));
    load(filename);
    if number == 43375;
        S = S(2273:end,:);
    end
    n=numel(S(:,4));
    if n > 0;
```

```
        years = S(n,1)-S(1,1)+1;
        S = new_cleaning(Q,S);
         if S(1,1) <= limit1;
            if and(and(years >= minimum,years <= maximum),and(n/365.25
>= minimum,n/365.25 <= maximum));
                temp1 = temp1+1;
                clear point1; clear point2; clear x; clear y;
                for j = 1:years-29 %number of distinct 30-year periods
                    point1 = min(round(1+(j-1)*365.25),n-10957); %start
point of 30-year period
                    point2 = min(point1+10957,n); %end point of 30-year
period
                    pos = S(point1,1)-(start_year-1);

[Kp_alpha(temp1,pos),Kp_beta(temp1,pos),Kp_gamma(temp1,pos),Kp_delta(te
mp1,pos)] = K_calc(S(point1:point2,:),tail);
                end
            end
        end
    end
end
y_alpha = new_organize(Kp_alpha,end_year-start_year+1);
y_beta = new_organize(Kp_beta,end_year-start_year+1);
y_gamma = new_organize(Kp_gamma,end_year-start_year+1);
y_delta = new_organize(Kp_delta,end_year-start_year+1);
years = [start_year:1:end_year];
figure(1)
hold on; grid on;
for i=1:end_year-start_year+1;
    plot3([years(i) years(i) years(i)],[4.95 4.95 4.95],y_alpha(:,i),'-
*k');
    plot3([years(i) years(i) years(i)],[16.49 16.49
16.49],y_beta(:,i),'-*k');
    plot3([years(i) years(i) years(i)],[32.98 32.98
32.98],y_gamma(:,i),'-*k');
    plot3([years(i) years(i) years(i)],[49.47 49.47
49.47],y_delta(:,i),'-*k');
end
xlim([1881 1988]);
title(['Lower tail of Tavg | Number of stations: ', num2str(temp1), ' |
Record beginning before: ', num2str(limit1)]);
xlabel('Start of 30 year period');
ylabel('Return period (years)');
hold off
```

Script 3: Aggregation of climacogram values

```
minimum = 30; %minimum record length
maximum = inf; %maximum record length
limit1 = 1935; %latest year of record start
[~,stations] = xlsread('Data_List_Tavg.xlsx');
load('numyears_Tavg.mat');
size = 5006;
start_year = 1881;
```

```
end_year = 1989;
all = 106283;
temp1 = 0;
for number = 1:all;
    filename = strcat('NOAA_GHCND_TAVG/',char(stations(number)));
    load(filename);
    n=numel(S(:,4));
    if n > 0;
        years = S(n,1)-S(1,1)+1;
        S = new_cleaning(Q,S);
        if S(1,1) <= limit1;
            if and(and(years >= minimum,years <= maximum),and(n/365.25
>= minimum,n/365.25 <= maximum));
                temp1 = temp1+1;
                for i = 1:12;
                    pos = ismember(S(:,2),i);
                    m(i,1) = nanmean(S(pos,4)); %monthly average
                    m(i,2) = nanvar(S(pos,4)); %monthly variance
                    S(pos,4) = (S(pos,4)-m(i,1))/sqrt(m(i,2)); %monthly
standardization
                end
                m_one(temp1,1) = moment(S((~isnan(S(:,4))),4),1);
                m_two(temp1,1) = moment(S((~isnan(S(:,4))),4),2);
                m_three(temp1,1) =
moment(S((~isnan(S(:,4))),4),3)/(sqrt(m_two(temp1,1))^3);
                m_four(temp1,1) =
moment(S((~isnan(S(:,4))),4),4)/(m_two(temp1,1)^2);;
                clear Scale;
                Scale = [1:100 110:10:1000 1100:100:round(n/10)];
                max_Scale(temp1) = Scale(1,end);
                length_n(temp1) = n;
                ExpectedOne(temp1,1:length(Scale)) =
pdClandHfast(S(:,4),Scale)';
            end
        end
    end
end
Moments_Tavg = [m_one, m_two, m_three, m_four];
xlswrite('Moments_Tavg.xlsx',Moments_Tavg);
ExpectedOne(:,find(ismember(Scale,100*floor(mean(length_n)/1000)))+1:en
d) = [];
clear n; clear Scale;
n = floor(mean(length_n));
Scale = [1:100 110:10:1000 1100:100:round(n/10)];
ExpectedAll = nanmean(ExpectedOne,1);
xlswrite('HHK-Markov_Tmax.xlsx',ExpectedAll');
```

Script 4: Analysis of timeseries

```
clc; clear all; close all;

minimum = 30; %minimum record length
maximum = inf; %maximum record length
limit1 = 1935; %latest year of record start
```

```matlab
tail = 2; %Lower tail

tic;
[~,stations] = xlsread('Data_List_Tavg.xlsx');
load('numyears_Tavg.mat');
size = 245; %number of stations which entered service before 1935

start_year = 1881;
end_year = 1988;
Kp_alpha = NaN(size,end_year-start_year+1);
Kp_beta = NaN(size,end_year-start_year+1);
Kp_gamma = NaN(size,end_year-start_year+1);
Kp_delta = NaN(size,end_year-start_year+1);

temp1 = 0;
all = 106283;
for number = 1:all;
    filename = strcat('NOAA_GHCND_TAVG/',char(stations(number)));
    load(filename);
    if number == 43375;
        S = S(2273:end,:);
    end
    n=numel(S(:,4));
    if n > 0;
        years = S(n,1)-S(1,1)+1;
        S = new_cleaning(Q,S);
         if S(1,1) <= limit1;
            if and(and(years >= minimum,years <= maximum),and(n/365.25
>= minimum,n/365.25 <= maximum));
                temp1 = temp1+1;
                for i = 1:12;
                    pos = ismember(S(:,2),i);
                    m(i,1) = nanmean(S(pos,4)); %monthly average
                    m(i,2) = nanvar(S(pos,4)); %monthly variance
                    S(pos,4) = (S(pos,4)-m(i,1))/sqrt(m(i,2)); %monthly
standardization
                end
                clear point1; clear point2; clear x; clear y;
                for j = 1:years-29 %number of distinct 30-year periods
                    point1 = min(round(1+(j-1)*365.25),n-10957); %start
point of 30-year period
                    point2 = min(point1+10957,n); %end point of 30-year
period
                    pos = S(point1,1)-(start_year-1);

[Kp_alpha(temp1,pos),Kp_beta(temp1,pos),Kp_gamma(temp1,pos),Kp_delta(te
mp1,pos)] = K_calc_2(S(point1:point2,:),tail);
                end
            end
        end
    end
end

y_alpha = new_organize(Kp_alpha,end_year-start_year+1);
y_beta = new_organize(Kp_beta,end_year-start_year+1);
```

```
y_gamma = new_organize(Kp_gamma,end_year-start_year+1);
y_delta = new_organize(Kp_delta,end_year-start_year+1);

years = [start_year:1:end_year];
figure(1)
hold on; grid on;
plot(years,y_alpha(1,:));
plot(years,y_alpha(2,:));
plot(years,y_alpha(3,:));
xlim([1881 1988]);
title('T_1_ = 4.95 years');
xlabel('Start of 30 year period');
legend('75th percentile','50th percentile','25th percentile')
hold off
figure(2)
hold on; grid on;
plot(years,y_beta(1,:));
plot(years,y_beta(2,:));
plot(years,y_beta(3,:));
xlim([1881 1988]);
title('T_2_ = 16.49 years');
xlabel('Start of 30 year period');
legend('75th percentile','50th percentile','25th percentile')
hold off
figure(3)
hold on; grid on;
plot(years,y_gamma(1,:));
plot(years,y_gamma(2,:));
plot(years,y_gamma(3,:));
xlim([1881 1988]);
title('T_3_ = 32.98 years');
xlabel('Start of 30 year period');
legend('75th percentile','50th percentile','25th percentile')
hold off
figure(4)
hold on; grid on;
plot(years,y_delta(1,:));
plot(years,y_delta(2,:));
plot(years,y_delta(3,:));
xlim([1881 1988]);
title('T_4_ = 49.47 years');
xlabel('Start of 30 year period');
legend('75th percentile','50th percentile','25th percentile')
hold off
```

Function 1: Calculation of unbiased K-moments

```
function [Kappa1,Kappa2,Kappa3,Kappa4] = K_calc(T,tail)

for i = 1:12;
    pos = ismember(T(:,2),i);
    m(i,1) = nanmean(T(pos,4)); %monthly average
    m(i,2) = nanvar(T(pos,4)); %monthly variance
    T(pos,4) = (T(pos,4)-m(i,1))/sqrt(m(i,2)); %monthly standardization
```

```
end
Ts = T(:,4);
if tail == 1 %Upper tail
    Ts = sort(Ts,'ascend'); %Sort in ascending order
else        %Lower tail
    Ts = sort(Ts,'descend'); %Sort in descending order
end
n = numel(Ts); %actual length of time series
temp2 = 0;
telos = min([max(find(Ts==max(Ts), 1, 'first'),find(Ts==min(Ts), 1,
'first')) n]);
for p = [1096 3653 7305 telos]
    stath = log(p)+gammaln(telos-p+1)-log(telos)-gammaln(telos);
    clear term;
    for i = 1:telos;
        if i >= p
            term(i) = exp(stath+gammaln(i)-gammaln(i-p+1))*Ts(i);
        else
            term(i) = 0;
        end
    end
    temp2 = temp2+1;
    Kp(temp2) = nansum(term);
end

if abs(Kp(1)) >= 0.5;
    Kappa1 = Kp(1);
else
    Kappa1 = NaN;
end
if abs(Kp(2)) >= 0.5;
    Kappa2 = Kp(2);
else
    Kappa2 = NaN;
end
if abs(Kp(3)) >= 1;
    Kappa3 = Kp(3);
else
    Kappa3 = NaN;
end
if abs(Kp(4)) >= 1;
    Kappa4 = Kp(4);
else
    Kappa4 = NaN;
end
```

Function 2: Removal of flagged values

```
% removes flagged values
for i=1:length(S(:,4));
    if strcmp(Q(i,2),' ') ~= 1;
        S(i,4) = NaN;
    end
end
```

```
Sout = S;
end
```

Function 3: Calculation of the climacogram for each timeseries

```
CCl=NaN(numel(k),1);
for I=1:numel(k);
    C=S;
    F=factor(k(I));
    if k(I)<50;
        for J=1:numel(F);
            if F(J)<=17;
                A=zeros(numel(C)+F(J)-1,F(J));
                for L=1:F(J);
                    A(L:end+L-F(J),L)=C;
                end
                B=nansum(A,2)/F(J);
                C=B(F(J):F(J):end-F(J)+1);
            else NN=numel(C);
                A=zeros(floor(NN/F(J)),1);
                for L=1:floor(NN/F(J));
                    A(L,1)=nansum(C(F(J)*(L-1)+1:F(J)*L,1))/F(J);
                end;
                C=A;
            end
        end
    else
        NN=numel(S);
        A=zeros(floor(NN/k(I)),1);
        for L=1:floor(NN/k(I));
            A(L,1)=nansum(S(k(I)*(L-1)+1:k(I)*L,1))/k(I);
        end;
        C=A;
    end
    CCl(I,:)=[nanvar(C)];
end
```

Function 4: Production of synthetic timeseries

```
%This is a Matlab script powered by Panayiotis Dimitriadis
(https://scholar.google.gr/citations?user=L6hWcz0AAAAJ&hl=en)
%based on the analysis of (https://www.itia.ntua.gr/el/docinfo/1656/)
%P. Dimitriadis, and D. Koutsoyiannis, Stochastic synthesis
approximating any process dependence and distribution, Stochastic
Environmental Research & Risk Assessment, 32 (6), 1493-1515,
doi:10.1007/s00477-018-1540-2, 2018. for the stochastic simulation of a
series with long-range dependence (HK model) by preserving explicitly
(i.e. in a direct way without including transformations) the first four
central moments of the target marginal distribution or of the sample
series

function [S]=SMA4_HK(Sm,Sv,Ss,Sk,H,N)
```

```
l=Sv; NA=N; MA=(1:NA)';
Ac=sqrt(2*gamma(2*H+1)*sin(pi*H)*l/(((gamma(H+1.5))^2)*(1+sin(pi*H))))*
(((abs([0;MA]+1)).^(H+0.5)+(abs([0;MA]-1)).^(H+0.5))/2-
(abs([0;MA])).^(H+0.5)); %Averaged Process (Kouts, 2015)
SA=[Ac(1+N:-1:2)' Ac(1) Ac(2:N+1)']; Vm=0; Vv=1;
Vs=Ss*((Ac(1)^2+2*sum(Ac(2:NA+1).^2)).^(3/2))/(Ac(1)^3+2*sum(Ac(2:NA+1)
.^3));
if Sk~=3;
SUM=0; for I=2:NA; SUM=SUM+(Ac(I)^2)*sum(Ac(I+1:NA+1).^2); end
Vk=abs(((((Ac(1)^2+2*sum(Ac(2:NA+1).^2)).^2)*Sk)-6*sum(Ac(2:NA+1).^4)-
12*(Ac(1)^2)*sum(Ac(2:NA+1).^2)-
24*SUM)/(Ac(1)^4+2*sum(Ac(2:NA+1).^4)));
else
Vk=3;
end
if (Ss==0)&&(Sk==3);
CW=1; a=Vm; b=Vv; c=0; d=0;
else
if (Vk-5/3*(Vs)^2-3<=0);
CW=2;
KKF=@(x) [Vs-(2*(abs(x(2))*beta(1+1/abs(x(1)),abs(x(2))))^3-
3*abs(x(2))*beta(1+1/abs(x(1)),abs(x(2)))*abs(x(2))*beta(1+2/abs(x(1)),
abs(x(2)))+abs(x(2))*beta(1+3/abs(x(1)),abs(x(2))))/(abs(x(2))*beta(1+2
/abs(x(1)),abs(x(2)))-(abs(x(2))*beta(1+1/abs(x(1)),abs(x(2))))^2)^1.5;
Vk-(-
3*(abs(x(2))*beta(1+1/abs(x(1)),abs(x(2))))^4+6*(abs(x(2))*beta(1+2/abs
(x(1)),abs(x(2))))*(abs(x(2))*beta(1+1/abs(x(1)),abs(x(2))))^2-
4*abs(x(2))*beta(1+1/abs(x(1)),abs(x(2)))*abs(x(2))*beta(1+3/abs(x(1)),
abs(x(2)))+abs(x(2))*beta(1+4/abs(x(1)),abs(x(2))))/(abs(x(2))*beta(1+2
/abs(x(1)),abs(x(2)))-(abs(x(2))*beta(1+1/abs(x(1)),abs(x(2))))^2)^2];
opt=optimset('Display','off'); warning('off','all');
[KKF,~]=fsolve(KKF,[1 10^2],opt);
a=abs(KKF(1)); b=abs(KKF(2)); d=sqrt(Vv/(b*beta(1+2/a,b)-
(b*beta(1+1/a,b))^2)); c=Vm-b*d*beta(1+1/a,b);
else
CW=3;
c=sqrt(3/Vv/(Vk-5/3*(Vs)^2-3));
b=(c^2)*Vs*sqrt(Vv)/3;
d=(c^3)*Vv/(b^2+c^2);
a=Vm-b*d/c;
end
end
if CW==1; V=norminv(rand(N+2*NA,1),a,sqrt(b)); end
if CW==2; V=d*(1-(1-rand(N+2*NA,1)).^(1/b)).^(1/a)+c; end
if CW==3;
V1=norminv(rand(N+2*NA,1),0,1); V2=V1.^2; V3=d/c+V2/2/c^2-
sqrt(4*V2*d/c+(V2/c).^2)/2/c; V4=rand(N+2*NA,1);
Z=V3; Z(V4>1./(1+V3*c/d))=((d/c)^2)./V3(V4>1./(1+V3*c/d));
V=a+b*Z+sqrt(Z).*norminv(rand(N+2*NA,1),0,1);
end
S=zeros(N,1); if H~=0.5; for J=1:N; S(J,1)=SA*V(J:2*NA+J,1); end; else
S=V(1:NA,1); end
S=S/sqrt(l)*sqrt(Sv)+Sm;
```